DECOUPLING ENZYME CATALYSIS FROM THERMAL DENATURATION

THE UNIVERSITY OF
WAIKATO
Te Whare Wānanga o Waikato

A thesis

submitted in partial fulfilment

of the requirements for the degree

of

Master of Science in Biological Sciences

at

The University of Waikato

by

ASHLEY DAVYS EASTER

The University of Waikato

2010

HC SVNT DRACONES

Abstract

The equilibrium model (EM) (Daniel et al., 2001) postulates two forms of a folded enzyme, one catalytically active (E_{act}) and the other inactive (E_{inact}), which interconvert via a fast thermal equilibrium (K_{eq}) (Figure A). This model for enzyme catalysis accounts for experimentally observed time and temperature profiles of enzyme/substrate systems more accurately than the classically derived, single folded-species, model (Figure B). In both models, the denatured species (X) is formed via the k_{inact} process, which is temperature and time-dependent.

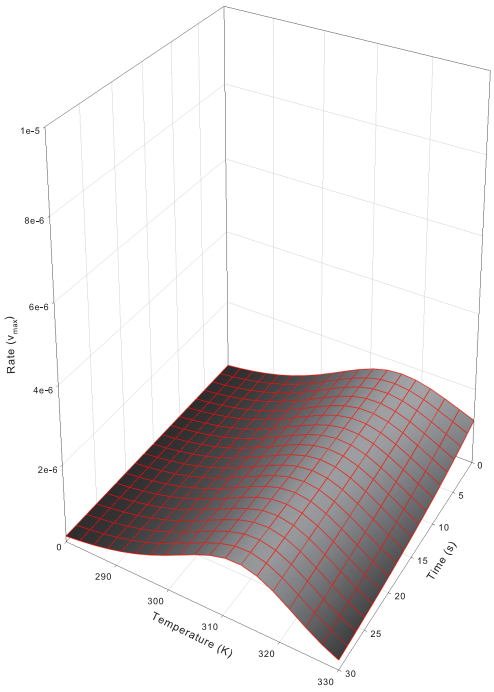

$$E_{act} \underset{}{\overset{K_{eq}}{\rightleftharpoons}} E_{inact} \xrightarrow{k_{inact}} X$$

Figure A – The equilibrium model

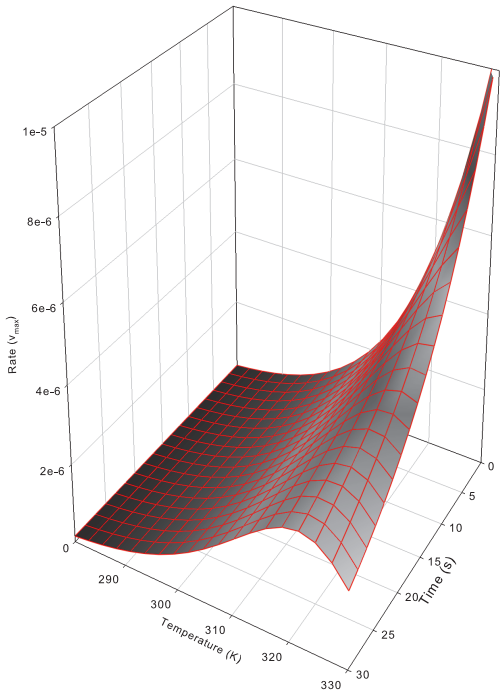

$$E \xrightarrow{k_{inact}} X$$

Figure B – The classical model

Comparison between the equilibrium model and classical model for enzyme catalysis. For both, the vertical axis is catalytic rate (M s^{-1}), the left-right axis is increasing temperature (K) and the back-front axis is assay duration (s).

The physical basis for the E_{act}/E_{inact} equilibrium is unknown. To study the equilibrium, the temperature midpoint of the E_{act}/E_{inact} transition (T_{eq}) has to be separated from the thermostability of the enzyme (T_m) to allow the E_{inact} species to exist in measurable concentrations without exhibiting denaturation.

Mutations were made in a well-studied and NMR-accessible ribonuclease, barnase, to alter the thermostability and/or the T_{eq} of the enzyme activity. The stability properties of each mutant were measured and the activity against two substrates assayed. New models were derived and fitted against wild-type barnase, and an ideal data set, to give insight into alternative irreversible and reversible denaturation pathways. Simulations of these models were developed to benchmark potential dynamics work and explain the movements of species within each model's framework.

Assay data fits to the EM and alternative models show a preference for irreversible denaturation pathways via the E_{inact} species. A mathematically simplified model was also found that accounts for data and could provide an alternative method for determining EM parameters. Although fits of barnase to the EM were statistically good, the denaturation properties could not be reconciled with the literature or experimentally determined values for stability and unfolding. Simulations illustrating how the E_{act}, E_{inact} and denatured (X) species interact also corroborate this finding.

Despite this discrepancy (in fitted parameters to the EM), it is hypothesised that the T_{eq} and T_m of a disulphide-bridged mutant of barnase have been successfully decoupled. This mutant has been ^{15}N-labelled for future NMR dynamics measurements. New approaches to the EM model are proposed where the separate determination of enzyme thermodynamic properties (e.g., rate and free energy of denaturation) would allow other EM parameters to be fitted independently to each data set.

Acknowledgements

I would like to thank first and foremost my supervisor Associate Professor Vickery Arcus for the opportunity to work on this project. Thank you for encouraging me into the kinetics/maths side of this thesis, as it has ultimately been the most fulfilling part, and for taking my questions and requests for scholarship references so graciously.

Secondly, to my fellow Equilibrium Modelers at Waikato; Professor Roy Daniel, Colin Monk, Dr Jo Hobbs and the others from the TRU. Thanks to Jo for keeping me on track, listening to my ramblings and kindly critiquing this thesis. Colin, your expertise has been invaluable, especially in getting me started with assays and the fitting procedures. The technical support of Dr F. Grant Pearce (CD & DSC, Canterbury) and Jonathan Puddick (mass spectrometry) is also greatly appreciated, along with important mathematical assistance from Associate Professor Stephen Joe.

To all the others, past and present, in the C.2.10 lab who have helped me out over the past year-and-a-bit (hopefully I have everyone): Dr Jo H, Jo M, John S, Emma S, Emma L, Dr Emma D, Marisa T, Matt C, Line H, Dr Svend H, Dr Randal W, Dr Judith B, Dr Ian M, Ali R, Kevin L and Tammy W – thank you all for help, advice, conversation and time-wasting. John deserves special mention for being my lab buddy for those first few months and putting up with my inane and sometimes stupid questions.

I must thank those across the hall in C.2.03 for the help they have given, and the numerous beers shared on Fridays: Professor Dick W, Dr Ray C, Dr Dave M, Dr Greg J, Olivia P, Raewyn T, Talia S, Niharika S, Helen M, Richard L, Jo D, Rebecca W, Claire M and Harriet F.

Lastly (but never least) I'd like to thank my flatmates, family & friends for putting up with me. Mum (who kindly proof-read this thesis), Dad & Caitlin, you have supported me in every way possible, thanks so much.

This project is supported by the Royal Society of New Zealand Marsden Fund.
A.D.E. received a University of Waikato Masters' Research Scholarship.

MARSDEN FUND
TE PŪTEA RANGAHAU A MARSDEN

Table of Contents

List of Figures

List of Tables

List of Equations

List of Abbreviations

A_{xxx}	Absorbance at xxx nm wavelength
ACN	Acetonitrile
CCD	Charge-Coupled Device
CD	Circular Dichroism spectroscopy
CEC	Cation Exchange Chromatography/Column
CO	Carbonyl Oxygen
C_p	Heat Capacity at constant Pressure
$\Delta G^{\ddagger}$	Change in Gibbs free energy for the transition state
ΔH_{eq}	Enthalpy of the E_{act}/E_{inact} Equilibrium
ΔH_{VH}	Van 't Hoff enthalpy
ΔS_{eq}	Entropy of the E_{act}/E_{inact} Equilibrium
ΔT_m	Change in Temperature Midpoint of denaturation
Da	Dalton(s)
DEPC	Di-Ethyl Pyro-Carbonate treated water (RNAse free)
DLP	Double-Layered (Rotovirus) Particle
DM	Refer to S80C/A43C
dNTP	di-Nucleotide Tri-Phosphate
DSC	Differential Scanning Calorimetry
E_{act}	Active Enzyme
EDTA	Ethylene Diamine Tetra-acetic Acid
E_{inact}	Inactive Enzyme
EM	Equilibrium Model (usually the established model)
em.	Emission
ex.	Excitation
$Fl._{xxx}$	Fluorescence at xxx nm wavelength
FLD	Formamide Loading Dye
FrG	Florescent substrate for barnase assays
GpUp	Dinucleotide substrate for barnase assays

GTE	Glucose Tris EDTA
HWHM	Half-Width Half-Maximum
I51V	WT barnase residue 51 replaced with valine
I88V	WT barnase residue 88 replaced with valine
K	Degrees Kelvin
K_d	Affinity constant
K_{eq}	Equilibrium constant for the E_{act}/E_{inact} Equilibrium
K_M	Michaelis-Menten constant
k_{xxx}	Rate constant for the xxx process
L89V	WT barnase residue 89 replaced with valine
LB	Luria-Bertani media / Luria Broth
MALDI-TOF	Matrix-Assisted Laser Desorption Ionisation – Time of Flight mass spectrometry
MQ	Mili-Q water
MS	Mass Spectrometric
MW	Molecular Weight
NH	Amino Hydrogen
NMR	Nuclear Magnetic Resonance spectroscopy
OD_{600}	Optical Density (absorbance) at 600 nm wavelength
[P]	Concentration of Product
PAGE	Poly-Acrylamide Gel Electrophoresis
PCR	Polymerase Chain Reaction
PDB	Protein Database
PMT	Photo Multiplier Tube
pMT1002	Expression plasmid
QX4	4 x SDS loading buffer / "Quench"
R^2	R-Squared value (coefficient of determination)
RAM	Random Access Memory
RMS	Root Mean Square
RO	Reverse Osmosis water
RT-PCR	Real-Time Polymerase Chain Reaction

S80C/A43C	WT barnase residues 80 & 43 replaced with cysteine
SDS	Sodium Dodecyl Sulphate
SEC	Size Exclusion Chromatography/Column
SOC	Super Optimal broth with Catabolite repression
SSE	Sum of Squared Errors
t_0	Fit of the EM at $t = 0$ using maximum initial rates
$t_{1/2}$	Half-life for a process
TB	Terrific Broth
TBE	Tris Borate EDTA
T_{eq}	Temperature midpoint of the E_{act}/E_{inact} Equilibrium
TFA	Tri-Fluoro Acetic acid
T_{growth}	Growth Temperature of enzyme source organism
T_m	Temperature Midpoint of denaturation
TEMED	TEtra-Methyl Ethylene Diamine
T_{opt}	Temperature at $t = 0$ of maximum catalytic rate
TS	Transition State
UV/Vis	Ulta-Violet/Visible spectrum
V_{max}	Maximum rate of catalysis
WT	Wild-Type enzyme
X	Denatured enzyme
Y78F	WT barnase residue 78 replaced with phenylalanine

1 Introduction

1.1 Catalysis and Kinetics

1.1.1 General Catalysis and Kinetics

Chemical reactions can spontaneously occur on time-scales with half-lives ($t_{1/2}$) of millions of years, to those that are almost instantaneous (Fersht, 1999). When another entity – be it another molecule in solution or a rare-metal/carbon composite – speeds up a chemical reaction, but is not itself consumed, that entity is called a catalyst.

To briefly illustrate how catalysts work, we can consider a simple chemical-reaction; the hydrolysis of an ester molecule by a water molecule:

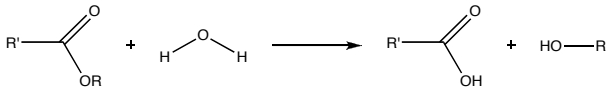

Figure 1.1 – Ester hydrolysis in neutral aqueous solution

The transition state (TS) for the spontaneous uncatalysed reaction is highly unstable due to the formation of negative and positive partial charges on the ester's carbonyl oxygen and the water's oxygen, respectively:

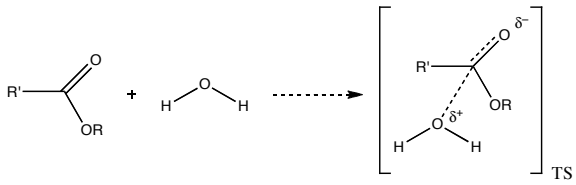

Figure 1.2 – Transition state for uncatalysed ester hydrolysis (Fersht, 1999)

If, for example, an acetate ion was in solution, the negative charge on the acetate carboxylate group could partially stabilise the δ^+ on the water, lowering the overall free energy of the TS. In this case, the effect is known as general-base catalysis. It can be shown that the Gibbs free energy barrier from the ground state (reactant) to the TS is therefore less (by $\Delta\Delta G^{\ddagger}$), and due to the laws of mass action, the reaction proceeds at a faster rate (Fersht, 1999) (Figure 1.3).

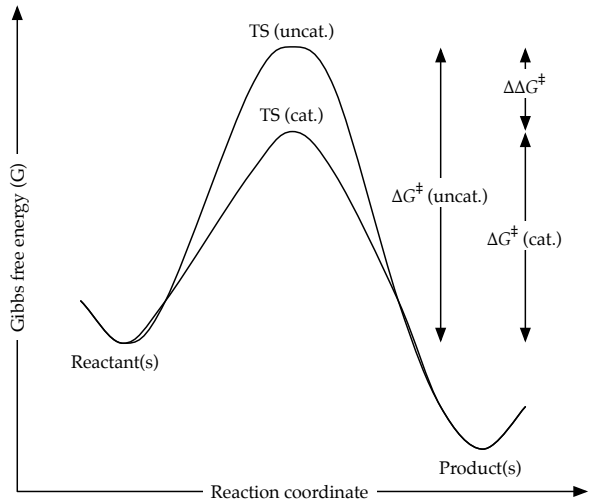

Figure 1.3 – Gibbs free energy diagram for uncatalysed and catalysed reactions

$\Delta\Delta G^{\ddagger}$ is the difference between $\Delta G^{\ddagger}$ for the uncatalysed reaction (uncat.), and $\Delta G^{\ddagger}$ for the catalysed reaction (cat.). The rate constant for the reaction (k) can be described in terms of $\Delta G^{\ddagger}$ using transition state theory and the Eyring equation (Laidler & King, 1983):

$$k = \frac{k_B \cdot T}{h_P} \cdot \exp\left(\frac{-\Delta G^{\ddagger}}{R \cdot T}\right)$$

Equation 1.1 – The relationship between rate constant and $\Delta G^{\ddagger}$

where k_B is Boltzmann's constant, h_P is Planck's constant, R is the gas constant and T is the temperature in Kelvin. Linus Pauling, amongst others, hypothesised that enzymes might work as catalysts by similarly lowering the $\Delta G^{\ddagger}$ of a reaction (Pauling, 1948).

1.1.2 Enzyme Catalysis and Kinetics

Catalysts are ubiquitous; it has been suggested that life itself has arisen from autocatalytic processes, where inorganic precursor molecules were arranged into basic building blocks of many enzymes – porphyrins chelating iron, for example, mediating reaction redox properties – and that these processes have been refined in the RNA- and DNA-based organisms present today (Johnson et al., 2008; Miller & Urey, 1959). Some proteins are the most efficient catalysts known and are called enzymes (Fersht, 1999).

Given that organisms produce metabolically costly enzymes, from an evolutionary standpoint they must gain an advantage from doing so. In an

extreme example, the decarboxylation of orotidine 5'-monophosphate to 5'-uridylic acid has a $t_{1/2}$ of 78 million years in neutral aqueous solution, but with orotidine 5'-phosphate decarboxylase present as a catalyst this drops to 18 milliseconds, a ~10^{17} rate increase (Miller & Wolfenden, 2002). The benefit in terms of higher (faster) rate constants is clear, as at 298 K (25 °C), this equates to a $\Delta\Delta G^{\ddagger}$ advantage of ~98 kJ mol^{-1}.

So, how do enzymes achieve such rate increases? The components that make up $\Delta G^{\ddagger}$ itself give insight:

$$\Delta G^{\ddagger} = \Delta H^{\ddagger} - T \cdot \Delta S^{\ddagger}$$

Equation 1.2 – The relation between Gibbs free energy, enthalpy and entropy

where $\Delta H^{\ddagger}$ is the enthalpy change and $\Delta S^{\ddagger}$ the entropy change in going from the substrate to the TS structure. Hence, smaller enthalpy changes and more positive entropy changes will result in a lower $\Delta G^{\ddagger}$ overall. Equation 1.1 can be modified:

$$k = \frac{k_B \cdot T}{h_P} \cdot \exp\left(\frac{-\Delta H^{\ddagger}}{R \cdot T}\right) \cdot \exp\left(\frac{\Delta S^{\ddagger}}{R}\right)$$

Equation 1.3 – The relationship between rate constant, $\Delta H^{\ddagger}$ and $\Delta S^{\ddagger}$ (Fersht, 1999)

Simplistically, enzymes are scaffolds made up of amino acids that maintain an environment (the active site) with several properties that aid in catalysis (Benkovic & Hammes-Schiffer, 2003). Firstly, the TS of the reaction is stabilized by the active site (by straining the shape of a substrate towards the TS conformation shape, it reduces the amount of activation energy, a kind of enthalpy, required to complete the reaction) (Pauling, 1948). Secondly, the pocket in which the substrate binds is complementary to the properties of the substrate, e.g. in terms of shape, charge, polarity and hydrophobicity. Hence, the fit of the substrate is induced; binding gets tighter as more favourable contacts are made (Tsou, 1995). A major related effect involves reducing the entropy change of catalysis by bringing substrate(s) and the enzyme together in the correct orientation to react (Daniel et al., 2003; Garcia-Viloca et al., 2004).

Lastly, enzymes can provide an alternative pathway. Reactions under uncatalysed "normal" conditions may have alternative pathways via

enzyme catalysis. These pathways can be of significantly lower $\Delta G^{\ddagger}$, and hence have faster rate constants. The variance in enzymatic pathways is large (Fersht, 1999). For example, covalent catalysis involves the formation of temporary chemical bonds between enzyme and substrate, allowing a more energetically favourable series of reactions than the uncatalysed pathway. Alternatively, electrostatic effects that polarise bonds or stabilise charges on intermediates can enhance the reactivity of substrate groups (Warshel et al., 2006).

1.1.3 Michaelis-Menten Kinetics

The previous section suggests that the binding of the substrate is a major force in enzymatic catalysis. Leonor Michaelis and Maud Menten developed a general model for the binding of an enzyme to its substrate in 1913 to explain the saturation kinetics seen experimentally with enzyme rate and substrate concentration (Michaelis & Menten, 1913). Such behaviour (Figure 1.4) is seen with all enzymes that follow the Michaelis-Menten model (Equation 1.4) (Briggs & Haldane, 1925; Fersht, 1999).

$$E + S \underset{}{\overset{K_M}{\rightleftharpoons}} ES \xrightarrow{k_{cat}} E + P$$

Equation 1.4 – Illustration of substrate binding and catalysis from the enzyme-substrate complex

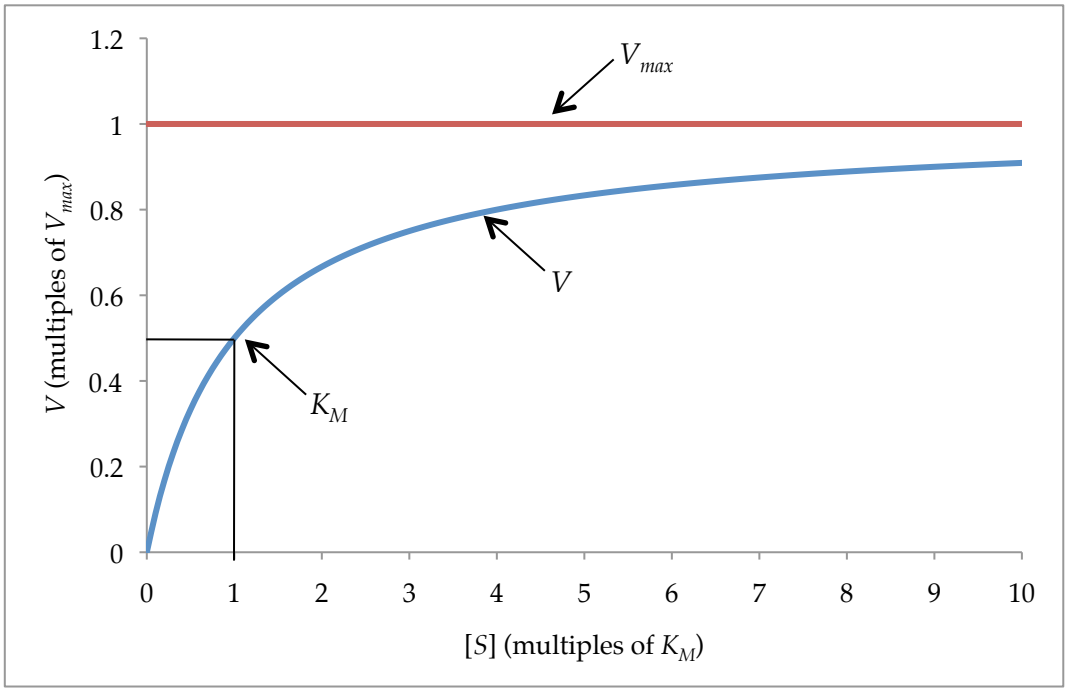

Figure 1.4 – Plot of the Michaelis-Menten equation for enzyme kinetics

$$V = \frac{k_{cat} \cdot [E] \cdot [S]}{K_M + [S]} \quad \text{and} \quad V_{max} = k_{cat} \cdot [E]$$

Equation 1.5 – (Left) Michaelis-Menten equation for enzyme kinetics (V)

Equation 1.6 –(Right) The general case for maximum enzyme velocity (V_{max})

In Equation 1.5 and Equation 1.6 V, the reaction velocity, is expressed as a function of $[S]$, the concentration of substrate. K_M is the concentration of substrate at which $V=V_{max}/2$; k_{cat} is the rate constant for catalysis and $[E]$ is the concentration of active enzyme in the assay. V_{max} is the velocity of the reaction if no product inhibition is observed and $K_M \approx 0$ (or $[S]$ is $>> K_M$).

1.2 Time, Temperature and the Equilibrium Model

1.2.1 Time and Temperature

Michaelis-Menten kinetics are time-independent; for example, in Equation 1.5, k_{cat} varies with temperature (as in Equation 1.1), but not assay duration. This assumption holds only if the enzyme is not inhibited by product formation and the temperature is well below that where the enzyme denatures – both conditions that lead to $[E]$ decreasing and hence, a reduction in the observed rate. The Michaelis-Menten equations can be modified to account for enzyme denaturation, a generally slow thermodynamic process, assuming the following scheme:

$$E \xrightarrow{k_{denat}} X$$

Equation 1.7 – Irreversible denaturation in the classic enzyme kinetics model

where E is the active enzyme available for catalysis, X is the denatured form of the enzyme and k_{denat} is the rate constant for the denaturation process. Hence, the amount of active enzyme available to catalyse the reaction at any point in time, $[E]$, is given by:

$$[E] = [E]_0 - [X] \quad \text{and therefore} \quad [E] = [E]_0 \cdot \exp(-k_{denat} \cdot t)$$

Equation 1.8 and Equation 1.9 – Expressions for the amount of active enzyme present in assays according to classical enzyme kinetics

where t is time and $[E]_0$ is the amount of active enzyme added to the assay at $t = 0$. Therefore, the equation for V_{max} (Equation 1.6) can be modified to allow for denaturation (Daniel et al., 2001):

$$V_{max} = k_{cat} \cdot [E]_0 \cdot \exp(-k_{denat} \cdot t)$$

Equation 1.10 – Maximum enzyme velocity allowing for denaturation in the classical kinetics

1.2.2 The Equilibrium Model Concept

Equation 1.10 can be analysed to understand why Figure 1.6 shows high rates at short assay duration and high temperature. The rate constants for catalysis and denaturation (k_{cat} and k_{denat} respectively) are both relatively high (due to the high T term in Equation 1.1), but the high k_{denat} is compensated for by the small t term. Thus, the rate of catalysis according to Equation 1.10 is much higher than that seen experimentally (Figure 1.5) for these conditions (Daniel et al., 2001). This flaw was ignored until the last ~15 years, as most enzyme assays were performed under "ideal" conditions away from denaturing temperatures and over longer time periods (Daniel & Danson, 2001).

The equilibrium model (EM) was conceived to reconcile experimentally observed enzyme rates (with respect to time and temperature) with the kinetics (Daniel et al., 2001). The classical Michaelis-Menten kinetics approach, even when corrected for non-V_{max} conditions (Equation 2.5), fails to adequately explain the high temperature/short timescale portion of the profile observed (vertical axis is V_{max}):

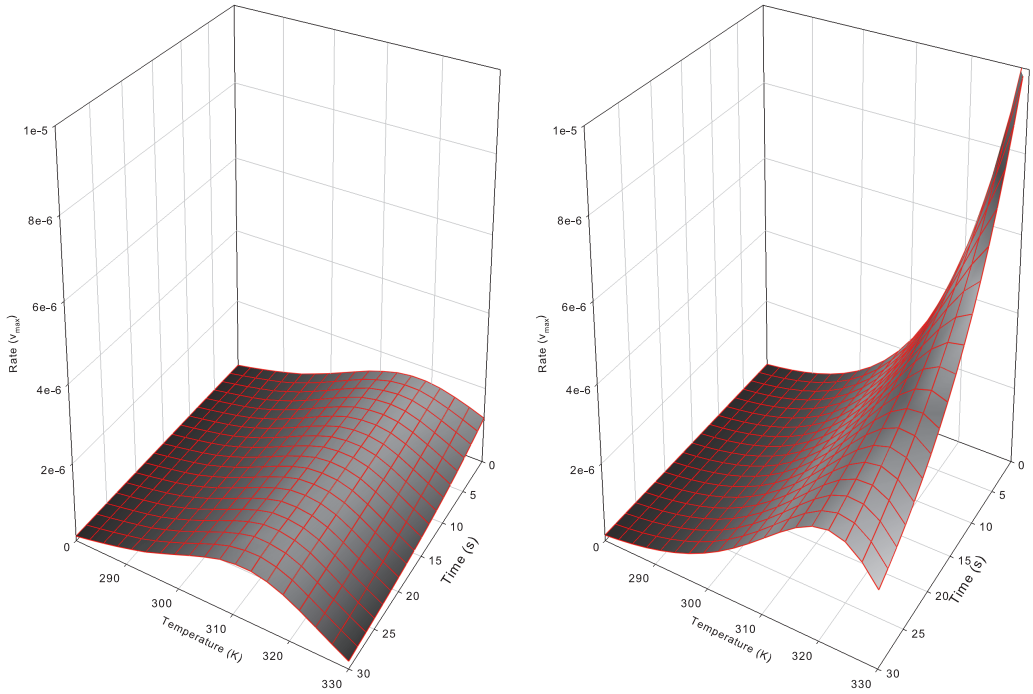

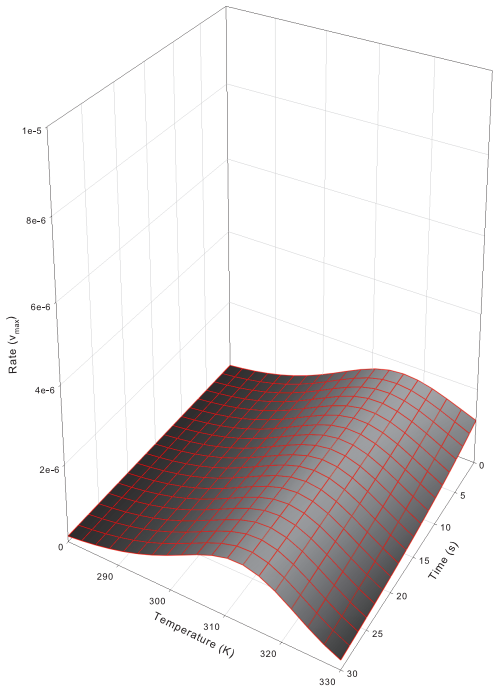

Figure 1.5 – (Previous Left) Smoothed experimental data for a model enzyme (collected as per Section 2.6.1)

Figure 1.6 – (Previous Right) Simulated rate profile for the same enzyme using classical kinetics (Equation 1.10)

Figure 1.7 – (Immediate Left) Simulated rate profile for the same enzyme using the equilibrium model kinetics (Equation 1.15)

To account for the low experimentally-observed rates at short time scales and high temperatures, something other than denaturation must be occurring. The classical Michaelis-Menten equations only adequately describes experimental data when temperatures are significantly below the denaturation temperature of the enzyme being studied (the thermal midpoint of denaturation being T_m), and the assay duration is long (on the order of tens of seconds and greater) (Daniel et al., 2001).

1.2.2.1 Initial Postulate

It was proposed that, with increasing temperature, the active enzyme (E) was being inactivated in a reversible way that was separate from denaturation (Daniel et al., 2001; Thomas & Scopes, 1998). This was because denaturation, as shown in Section 1.2.1, is not a fast enough process to counteract the high rate of catalysis at higher temperatures (Fulton et al., 2005). Hence, the inactivation process has to be very fast (cf. denaturation) to account for the lower-than-expected rates of activity at high temperatures. This concept has existed since 1944 in various guises, but never explicitly as an enzymatic thermal equilibrium (Sizer, 1944).

If two folded forms of the enzyme are allowed for, one form being catalytically active and one catalytically inactive (E_{act} and E_{inact}

respectively), and they are in fast thermal equilibrium with one another, then we can use Equation 1.11 to describe their relationship:

$$E_{act} \overset{K_{eq}}{\rightleftharpoons} E_{inact}$$

Equation 1.11 – The E_{act} to E_{inact} equilibrium

where K_{eq} is the equilibrium constant. The thermal interconversion can be explained using a modified Van 't Hoff equation (Daniel et al., 2001; Fersht, 1999):

$$K_{eq} = \exp\left(\frac{\Delta H_{eq}}{R} \cdot \left(\frac{1}{T_{eq}} - \frac{1}{T}\right)\right)$$

Equation 1.12 – The dependence of K_{eq} on ΔH_{eq} and T_{eq} for thermal equilibrium

Here T_{eq} is the midpoint of the transition (in Kelvin) between the two forms and ΔH_{eq} is the Van 't Hoff enthalpy for the interconversion process. It then follows that instead of V_{max} being in terms of E (Equation 1.5), it must be in terms of E_{act}:

$$V_{max} = k_{cat} \cdot [E_{act}]$$

Equation 1.13 – The rate of enzyme catalysis according to the equilibrium model

If Equation 1.11 is expanded to include a version of Equation 1.7, the manner in which two folded and one denatured forms of the enzyme might interact is obtained:

$$E_{act} \overset{K_{eq}}{\rightleftharpoons} E_{inact} \xrightarrow{k_{inact}} X$$

Equation 1.14 – The interconversion between forms in the equilibrium model

k_{inact} is the rate constant for denaturation from the E_{inact} form. The authors of the EM saw that a thermal equilibrium between E_{act} and E_{inact} would lead to E_{inact} being the dominant folded species at high temperatures and short timescales (Daniel et al., 2001). This implies that it is on-path to denaturation, as illustrated above in Equation 1.14.

All that remains is for the scheme in Equation 1.14 to be described kinetically in terms of K_{eq}, k_{inact} and k_{cat}, which defines the rate profile (V_{max}) in terms of assay time (t) and temperature (T). By expanding Equation 1.13, the full rate equation is obtained in terms of constants describing

rates for catalysis, denaturation and the E_{act}/E_{inact} thermal equilibrium (Equation 1.15). For a full derivation of the EM, see Appendix B.1.

$$V_{max} = \frac{k_{cat} \cdot [E]_0}{1 + K_{eq}} \cdot \exp\left(\frac{-k_{inact} \cdot K_{eq} \cdot t}{1 + K_{eq}}\right)$$

Equation 1.15 – The full equilibrium model rate equation for V_{max}

1.2.3 Building Evidence for the Equilibrium Model

1.2.3.1 Work up to 2009: Proof, Validation and Key Points

The basis of the theory for the EM has been discussed above, and was first published in 2001 (Daniel et al., 2001). The concept was initially tested against phosphoglycerate kinase from mesophilic and thermophilic sources, and found to qualitatively account for the lack of enzyme activity at temperatures lower than where significant denaturation occurs. Prior research on other enzymes also agreed, showing zero-time plots similar to the model (Arnott et al., 2000; Buchanan et al., 1999). An alternative strategy allowing denaturation through the E_{act} form in addition to E_{inact} was found to have a similar fit to the original EM (Equation 1.15). Hence, the original model, specifying that E_{inact} alone is on path to denaturation, was used exclusively in all future work (Daniel et al., 2001).

The methodology for fitting experimental data to model equations was first cited in 2004, where individual experimental time/temperature/rate data sets were fitted to Eyring and Arrhenius plots (see Equation 1.1 & Equation 1.12) (Peterson et al., 2004). The data was smoothed in the time dimension before fitting. This allowed for the determination of ΔH_{eq}, T_{eq}, $\Delta G^{\ddagger}_{cat}$ and $\Delta G^{\ddagger}_{inact}$ parameters, but not an overall model fit that would minimise the residual error between the model and the entire experimental data set. Four more enzymes (acid & alkaline phosphatases, an aryl-acylamidase and a ß-lactamase) were trialed against the model. Observations were made that the model was not restricted to purely monomeric enzymes and that the T_{opt} (T at t = 0 where maximum V is reached) for the enzymes was ~20-40 °C above the ideal growth temperature of the organism (Peterson et al., 2004; Thomas & Scopes, 1998).

It was also observed that the E_{act}/E_{inact} equilibrium process was at least two orders of magnitude faster than thermal denaturation (Fulton et al., 2005; Peterson et al., 2004). Plots extrapolated back to the assay start, at $t = 0$, showed drops in activity at high temperatures that could not be ascribed to denaturation. For example, in the case of aryl-acylamidase, at 5 °C higher than the T_{opt} the activity was ~40% lower than maximum, yet 40% denaturation at that temperature was known to take ~60 seconds (Peterson et al., 2004). Hence, the EM accounted mathematically more accurately for what was seen experimentally, compared with the classical model (Equation 1.10).

By 2006, 30 enzymes had been studied in detail and all adhered to the EM, having a distinctive "tent shape" three-dimensional rate profile (Figure 1.7). The equilibrium process was shown to be reversible as enzymes could be taken past their apparent T_{opt} (as above), but not their T_m, and regain lost activity once cooled (Eisenthal et al., 2006). This kind of reactivation is assumed to be disallowed in the classical kinetic situation, where denaturation is irreversible and is the only process leading to loss of enzyme activity (Section 1.2.1). The effects of a stabilising agent (betaine) and a destabilising agent (guanidinium hydrochloride) on T_{eq} were also explored and found to have no effect on T_{eq}, providing initial evidence that T_{eq} is a distinct and decoupled property from T_m (Eisenthal et al., 2006).

Alternative substrates were tested on enzymes, and it was found that different substrates gave different experimental values for ΔH_{eq}, T_{eq}, $\Delta G^{\ddagger}_{cat}$ and $\Delta G^{\ddagger}_{inact}$ (the output parameters) (Peterson, 2005). From this, the molecular difference between E_{act} and E_{inact} was hypothesised to be a change at the active site, seeing as T_{eq} was substrate-specific. It was suggested that NMR would be a possible method to investigate the molecular basis for the K_{eq} equilibrium change, as long as T_{eq} was sufficiently below the enzyme T_m that a population of E_{inact} could be maintained for NMR timescales (~24 hours).

The extensive data gathered by 2007 (for ~40 enzymes) provided a large data set with not just ΔH_{eq}, T_{eq}, $\Delta G^{\ddagger}_{cat}$ and $\Delta G^{\ddagger}_{inact}$ for each enzyme, but also

data on enzyme size, quaternary structure, growth temperature and other derivations from the output parameters. Hence, a correlation analysis was performed to see if any significant trends could be observed (Lee et al., 2007). Correlations between ΔH_{eq}, HWHM (the temperature difference at $t = 0$ between T_{opt} and the temperature at which activity is half-maximal, on the high-temperature side of the curve), and the difference between T_{eq} & T_{opt} were observed. As these parameters are linked mathematically, it is unsurprising that they are correlated (Daniel et al., 2008; Lee et al., 2007; Peterson et al., 2004). Growth temperature was shown to have a strong positive correlation with T_{eq} however, backing up inferences made earlier about the relationship between T_{eq} and optimal temperatures for enzymes based on their environments (Daniel et al., 2008; Peterson et al., 2004; Thomas & Scopes, 1998).

Now that the model had been established, the methodology behind gathering experimental data was explored to ensure valid determination of parameters. As the rate equation described V_{max}, yet most measurements were not made under saturated conditions (due to substrate expense, solubility or other considerations), most gathered V data had to be corrected for K_M influences (see Equation 1.5 and Equation 2.5). Other considerations, such as product inhibition and the minimal amount of data points required for fitting of data to the model, were also explored (Daniel et al., 2007). Fitting was automated by a stand-alone MATLAB run-time program, which takes matrices of data and fits the model via a least-squares residual minimisation approach (Section 2.7.2) (Daniel et al., 2007). The validation culminated in a full analysis of the required conditions for reliable determination of EM parameters (Peterson et al., 2007).

The fitting of enzyme assay data was further streamlined by integrating the rate equation for the model (Equation 1.15 and Section B.1.6) which enabled processing using raw product concentration data (Peterson et al., 2007). This removed the steps of smoothing raw product data runs (in the time dimension) and then deriving the rate from the manipulated data. Although only minimal differences in output parameters were observed, this gave more confidence in the parameter derivations. The use of initial rates (called t_0 runs) found linearly over the first few seconds of an assay

also gave valid parameters, useful for non-ideal enzymes. However, this excluded determining the time-dependent $\Delta G^{\ddagger}_{inact}$ parameter. It was also shown that discontinuous assays could be used for model data collection by reducing data sets to discontinuous points (Peterson et al., 2007).

Lastly, circular dichroism (CD) work was performed on the α-glucosidase from *Saccharomyces cerevisiae* to probe the molecular basis for the E_{act}/E_{inact} species equilibrium. It was found that E_{inact} is not significantly unfolded and is structurally more similar to E_{act} than the denatured form (X) or a molten-globule state (Daniel et al., 2009).

1.2.3.2 The Current State of the Model

As of 2009, the EM had been tested against nearly 50 different enzyme/substrate combinations. Extremophile enzymes from the Pomeii worm (*Alvinella pompejana*) and its episymbionts have even been fitted to the model (Lee et al., 2008). All systems, "monomeric to hexameric, and including a citrate synthase where the active site is at a subunit interface" (Daniel et al., 2009) follow the model rate profile much more closely than that of the classical model, but the molecular basis for the E_{act}/E_{inact} equilibrium is still unknown (Daniel et al., 2008; Weinberg et al., 2008).

Value	$\Delta G^{\ddagger}_{cat}$	$\Delta G^{\ddagger}_{inact}$	ΔH_{eq}	ΔS_{eq}	T_{eq}	T_{growth}	Sub-units	Sub-unit MW	$\sum$ MW
Units	kJ mol^{-1}	kJ mol^{-1}	kJ mol^{-1}	kJ mol^{-1} K^{-1}	(°C)	(°C)	#	(kDa)	(kDa)
Av.	68	96	213	638	58	40	2.0	46	91
Std. Dev.	9	5	177	517	15	19	1.6	21	89

Table 1.1 – Average values for enzyme/substrate systems fitted to the equilibrium model

The range of output parameters for 28 model enzyme/substrate systems is shown (Table 1.1) (Daniel et al., 2009). ΔS_{eq} is the entropy of equilibrium, T_{growth} is the optimum growth temperature for the source organism, sub-units is the number of monomers in the enzyme complex and MW is the molecular weight of each monomer or complex (∑). There is relatively little variance in the free energies of catalysis and inactivation, but large variance in the enthalpy change of equilibrium. This reflects how ΔH_{eq}

describes the broadness or sharpness of the K_{eq} transition. The range of T_{eq} is from ~18-90 °C, with the T_{growth} ranging from ~2-75 °C, mirroring earlier work showing a ~20°C increase in T_{eq} over T_{growth} (Daniel et al., 2008; Peterson et al., 2004; Thomas & Scopes, 1998).

1.3 Barnase

1.3.1 Structure and Expression

Barnase is a small 110-residue RNase produced by *Bacillus amyloliquefaciens* that has been studied since the early 1980s (Mauguen et al., 1982). It has a major helix consisting of residues 6-18 ($helix_1$), two smaller helices to complete the first half of the sequence, then five antiparallel strands making up the ß-sheet. The packing of $helix_1$ onto the ß-sheet creates the first of three hydrophobic cores (Fersht, 1999). As barnase is such a small ($M_r \approx 12383$ Da) functional enzyme, it has been the focus of many studies over the past ~25 years. A cartoon representation of wild-type (WT) barnase (Figure 1.8) with the helices in blue and sheets in red is taken from a 1.7 Å-resolution crystal structure deposited in the PBD (1BRN) (Buckle & Fersht, 1994) and ray-traced using PyMol 1.2r1 (DeLano Scientific LLC, USA) (DeLano, 2002).

Barnase was first expressed, with its structure and properties also determined, in 1982 (Mauguen et al., 1982). In its natural operon, barnase is expressed with its inhibitor, barstar, which is an 89-residue protein of mixed α- and ß-structure – both proteins are expressed together to ensure non-toxicity to the expression cell (Hartley, 1988). The complex has an affinity (K_d) of ~ 10^{-14} M, one of the tightest known (Wang et al., 2004), and the two bind fast with a rate (k_{on}) of 10^8 M^{-1} s^{-1}. Both barnase and barstar fold alone in solution, reversibly denature, and neither has any post-translational modifications or disulphide bonds (Paddon et al., 1989).

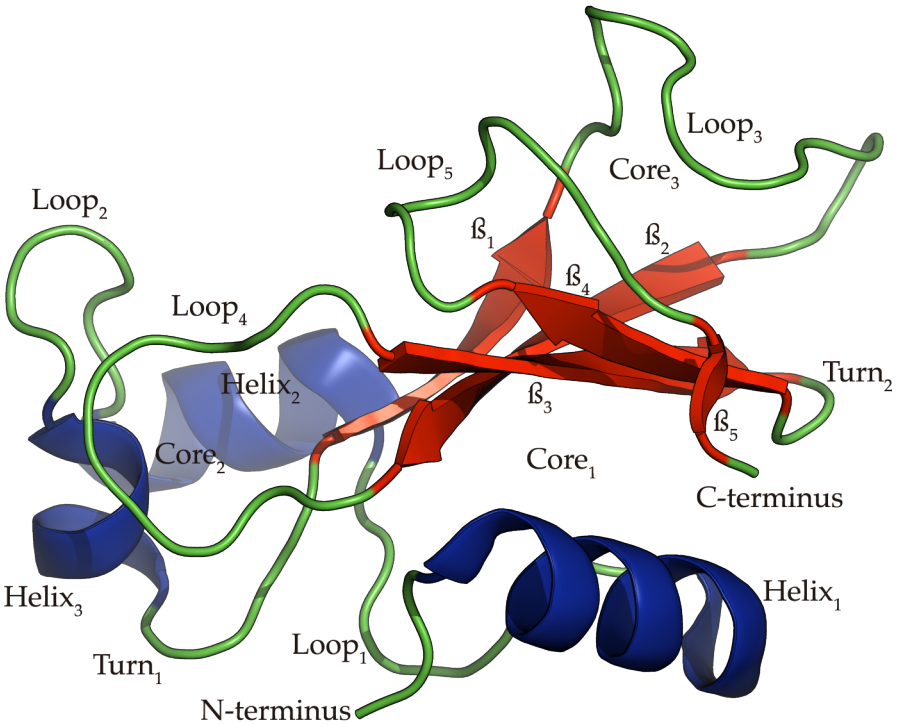

Figure 1.8 – Cartoon representation of WT barnase from PBD 1BRN

1.3.2 Substrates and Activity

Barnase cleaves RNA via a two-step hydrolysis; firstly, cleaving the phospho-ribose bond via internal 2,3'-cyclisation to the sugar (transesterification), then (via a much less rapid reaction using the same catalytic residues in reversed roles) the hydrolysis of that bond (Day et al., 1992). Several studies have shown that the active site of barnase consists of subsites with strong preferences for certain nucleotides. Generally, a GpN motif is required for activity, with A > G > C > U in terms of activity at position N, where p is the phosphodiester bond. This is shown by the preference of barnase for GpN dinucleotides (Day et al., 1992). The pH profile for short (e.g. di-,tri-,tetra-nucleotide) substrates has a maximum at approximately pH 5-6, whereas longer substrates are favoured at higher pHs (~ 8-9) (Mossakowska et al., 1989).

Figure 1.9 shows another PyMol rendering of Figure 1.8, this time with a DNA substrate analogue (CGAC, GAC shown) fragment co-crystallised into the active site. Glu-73 and His-102, the general base and acid respectively, are shown in yellow carbons and the substrate in white carbons with orange for phosphorus. Day et. al (1992) showed that substrates of the type $Zp_0Gp_1Xp_2Y$ were favoured as before, but that

occupation of the p_2 site led to a 1000-fold increase in k_{cat}/K_M. This means that GpUp, with its low K_M and single cleavage site is ideal for EM data acquisition (Section 2.6.1) (Kippen et al., 1994).

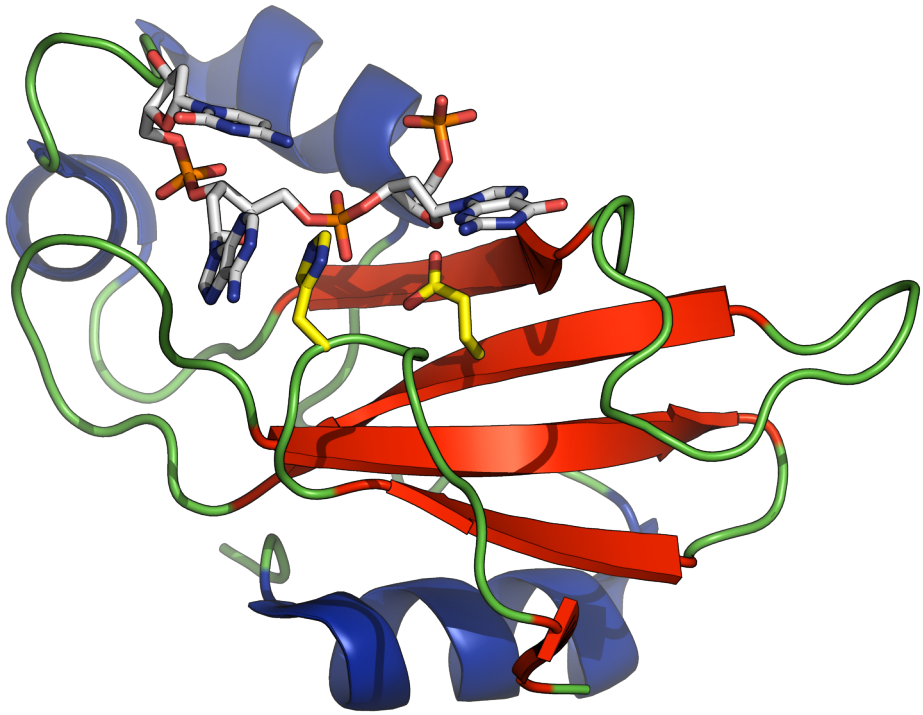

Figure 1.9 – Barnase complexed with CGAC tetranucleotide (PDB 1BRN)

1.3.3 Barnase and the Equilibrium Model

Barnase has been used extensively as a model protein, with >800 articles including "barnase" in their topic since 1989 in the ISI Web of Science database (Thomson Reuters, USA). This means that there is a wealth of information available on the folding and unfolding processes for barnase, the effects of many different point mutations (and x-ray and/or NMR structures of most of these) and extensive structural and functional data. It was hoped that this large reference set of data could go some way towards explaining the molecular basis of the EM if suitable barnase mutants were identified.

1.3.3.1 Protein Folding Studies

Studies on the folding of barnase were first published in 1989, with the bulk of the work available in 1992. Early work (Matouschek et al., 1989) showed, using amino-acid point mutations and urea denaturation studies, that ϕ-values (Fersht et al., 1992) could be used to approximate the

structure of the transition state and pathway of folding (and hence unfolding). The transition state ensemble for barnase was closely related to the folded form, with most secondary structure formed and only hydrogen bonds and loop docking to be completed (Serrano et al., 1992). The effect of temperature on the transition state has also been probed (Dalby et al., 1998).

The half-life for refolding of barnase ($t_{1/2}$) is about 30 ms in the most favourable conditions (Fersht, 1999). This is within the range (from tens of μs to tens of seconds) usually seen for WT proteins (Kubelka et al., 2004). Interactions were found to be synergistic, meaning that the sum of the ΔG terms for each interaction was greater than each interaction alone (Horovitz & Fersht, 1992). This body of evidence means that the molecular basis for the E_{act}/E_{inact} transition can be distinguished from processes that are on-pathway to denaturation – for example, it is known that the docking of α-helix$_1$ to the ß-sheet is preceded by secondary structure formation in folding (Matouschek et al., 1989; Sancho et al., 1992).

1.3.3.2 Mutations of Barnase

As part of the folding work, many mutations were made for ϕ-value analysis and other experimental techniques. In 1991, for example, 64 mutations were characterised for their effects on stability (Serrano et al., 1992a). These were also characterised via x-ray structures etc. for their effects on hydrogen bonding, torsion angles, solvation and sidechain ordering in the folded protein. The following mutations were selected for this thesis research due to their minimal effects on active site residue ordering and sidechain ordering, meaning that T_{eq} changes can be attributed to changes in dynamics, not physical interactions.

The I51V mutation (replacing isoleucine 51 with valine) was found to delete van der Waals' interactions with two helices and three loops (Serrano et al., 1992a), decreasing stability by 7.53 kJ mol^{-1}. The mutant is shown superimposed on the WT (Martin et al., 1999), from PDB structure 1BSA. I51V, on ß-strand$_1$, has a solvent-accessible surface area of 2 Å^2, making it almost completely buried within hydrophobic core$_2$ (Buckle et al., 1993) (see Figure 1.10).

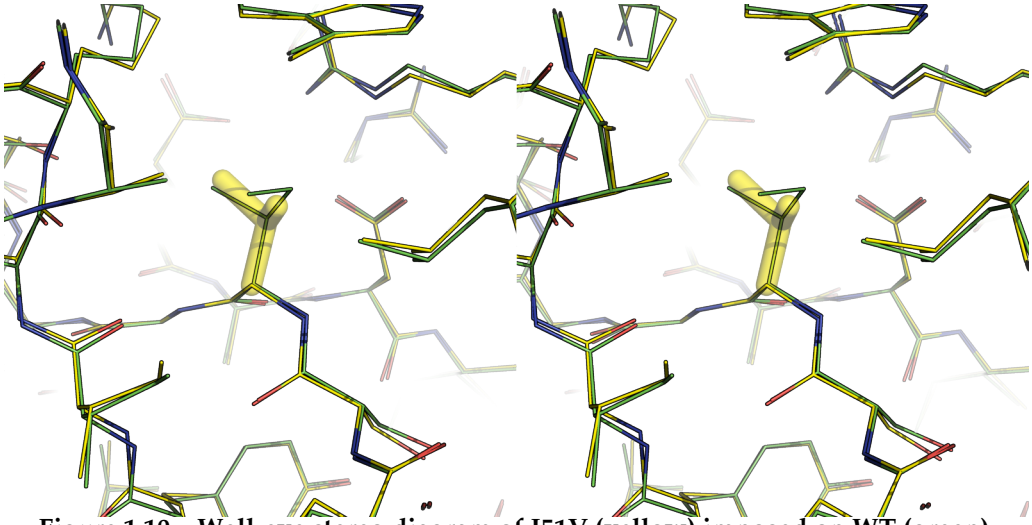

Figure 1.10 – Wall-eye stereo diagram of I51V (yellow) imposed on WT (green)

I88V and L89V are mutations either side of ß-strand$_3$, with residue 88 pointing down into the middle of core$_1$ and residue 89 the opposite way into core$_3$ (Serrano et al., 1992a). Both are completely buried; I88V deletes the sidechain interaction with helix$_1$ and L89V only causes minor rearrangements of close residues with very little destabilisation of the protein as a whole (Buckle et al., 1993). Stereo views are presented below for I88V and L89V from PDBs 1BSC and 1BSE respectively (as above):

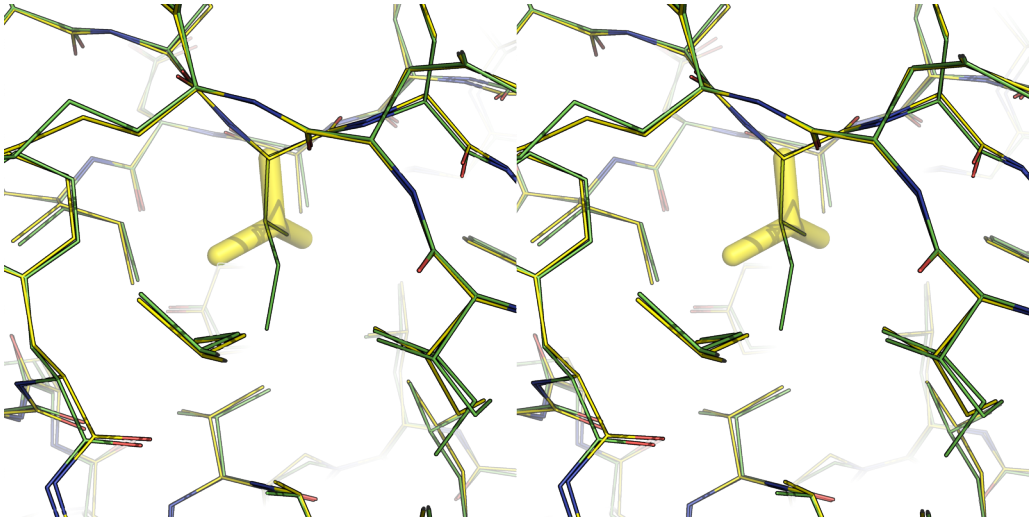

Figure 1.11 – Wall-eye stereo diagram of I88V (yellow) imposed on WT (green)

Rate constants of folding/unfolding for I51V, I88V and L89V are known (Matouschek et al., 1992), meaning that the shape of the three-dimensional EM rate profiles may be reconcilable with the relative speeds of refolding.

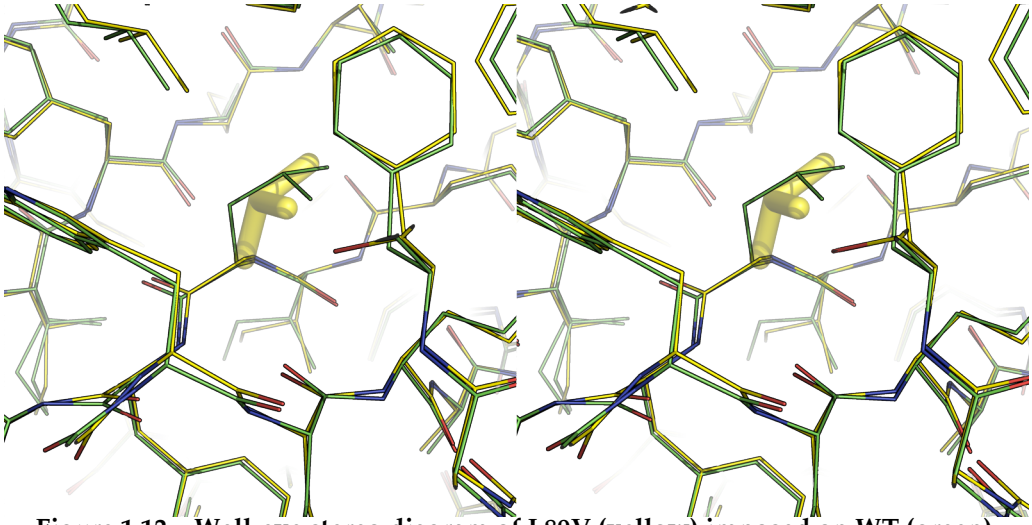

Figure 1.12 – Wall-eye stereo diagram of L89V (yellow) imposed on WT (green)

In 1993 the effect of buried hydrogen bonds on the stability of barnase was investigated (Chen et al., 1993). Removing the hydroxyl group of tyrosine via a Y78F mutation, two hydrogen bonds (to the chain CO and NH at G81, shown with black dashed lines) stabilising $loop_4$ are deleted, destabilising the structure to a similar amount as in I88V. The side chain van der Waals' interactions to nearby residues were also altered slightly as they moved to compensate for the cavity, which was not filled with water (Chen et al., 1993). Refolding constants are also known (Chen et al., 1993).

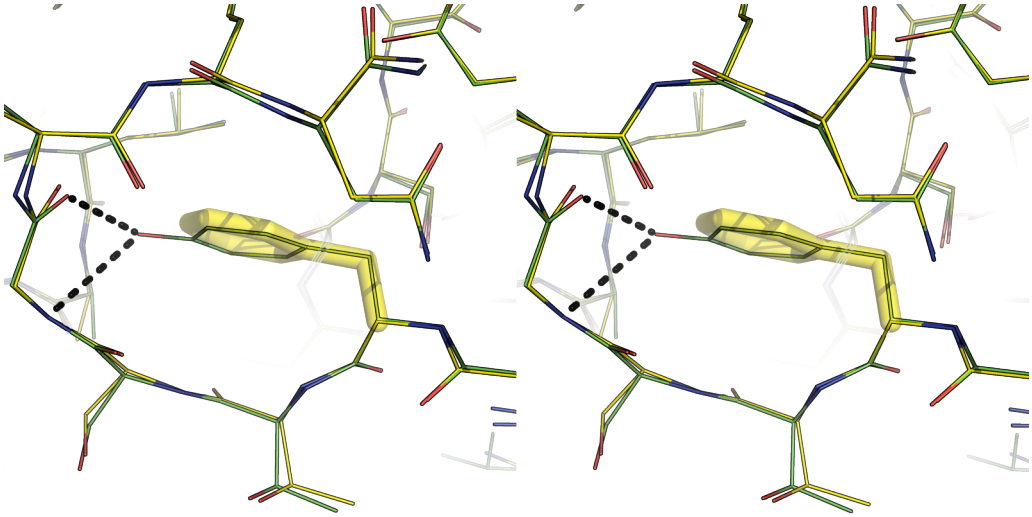

Figure 1.13 – Wall-eye stereo diagram of Y78F (yellow) imposed on WT (green)

The above mutations all destabilise barnase and, hence, would also have to drop T_{eq} by a large margin compared with T_m in order to have an accessible E_{inact} population (Section 1.2.3.1). In case this did not occur, a significantly stabilised mutant was needed that was far enough from the

active site as to not affect substrate binding or active site residue configurations. Hence, if T_{eq} did not change, at least the T_m would be significantly higher. Clarke and co-workers (Clarke & Fersht, 1993; Clarke et al., 1995a; Clarke et al., 1995b) have made several disulphide mutants of barnase, probing the effects on folding and stability. In the S80C/A43C double mutant (DM), a disulfide bridge was made between two residues known to pack together only *after* the rate limiting step for folding. Therefore, the structure was stabilised against unfolding which occurs ~20 times slower than in WT barnase (Clarke & Fersht, 1993). This was due to the covalent bonding between $helix_3$ and $loop_4$, where normally they are not in contact.

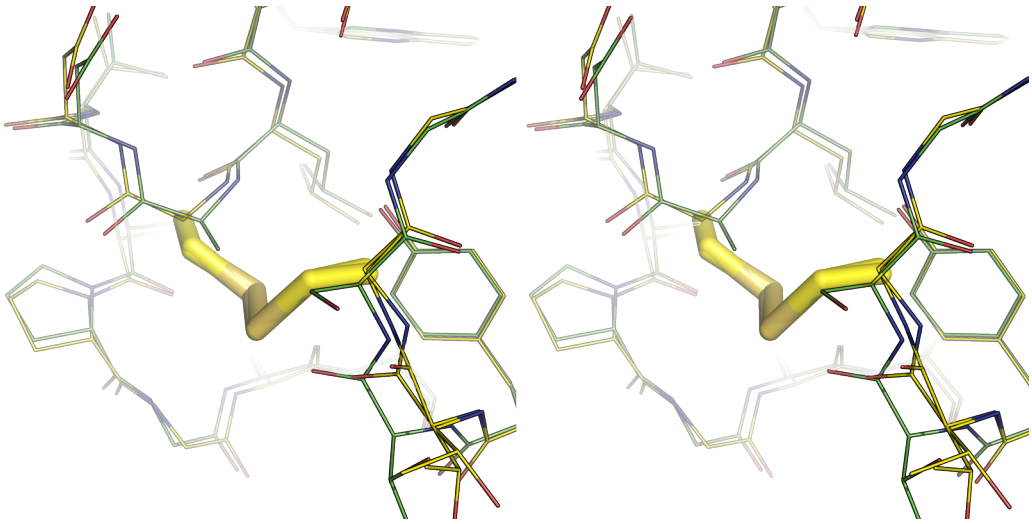

Figure 1.14 – Wall-eye stereo diagram of S80C/A43C (yellow) imposed on WT (green)

It was shown, however, that the disulphide linkage induces slight disorder and rearrangement in nearby residues, with only T79 being severely disordered (Clarke et al., 1995a). This means that the DM is not as stable as could be predicted. Note that root mean square (RMS) values for the main chain showed that the majority of the structure, including the active site, was very close in structure to the WT (Clarke et al., 1995b).

In conclusion, one mutant is significantly stabilised (DM), one significantly destabilised (I51V), one similar to the WT (L89V), and two of equal destabilisation through different means (I88V & Y78F). These properties are summarised in Table 1.2. The overlaid PDB files of the structures above (as PyMol session files) are in Appendix C.

Mutation	I51V	I88V	L89V	Y78F	S80C/A43C
$\Delta\Delta G_{U\text{-}F}^{D50\%}$ (kJ mol^{-1})	7.53	5.61	1.26	5.65	-8.79
Side-chain solvent exposure (Å)	2	0	0	12	–

Table 1.2 – Thermodynamic and solvation properties of selected barnase mutants

$\Delta\Delta G_{U\text{-}F}^{D\,50\%}$ is the difference in the $\Delta G_{U\text{-}F}^{D\,50\%}$ from WT to mutant (e.g. negative values are stabilising). $\Delta G_{U\text{-}F}^{D\,50\%}$ is the change in free energy associated with unfolding the WT or mutant at 50% [denaturant]. All values are from Serrano et. al (1992a) except for S80C/A43C (Johnson et al., 1997).

1.3.3.3 Reversible Denaturation

A special property of barnase, and all mutants of barnase that fold spontaneously, is that they renature and do not appreciably aggregate (hence, do not form a kinetic "sink" for the denatured species *X*) (Sali et al., 1988). If a population of barnase is equilibrated at a temperature close to its T_m, there is an equilibrium between the folded and unfolded forms (Matouschek et al., 1992). The EM for activity was expected to either a) not fit the data well or b) not fit the data at all, as it cannot account for renaturing (the one-direction k_{inact} implies irreversible denaturation) (Equation 1.14).

1.3.3.4 NMR Accessibility of Mutants

Barnase is small enough (~12 kDa) that it is NMR-accessible. Sizes greater than ~50 kDa (the EM average being 91 kDa (Table 1.1)) have been inaccessible or problematic with traditional NMR experiments, although complexes of 300 kDa and 14 subunits have now been used successfully (Mittermaier & Kay, 2009). Proteins in complex with GroEL (~900 kDa) have also been studied (Fiaux et al., 2002). NMR has been performed on barnase extensively: structure determination (Bycroft et al., 1991), denatured structure studies (Arcus et al., 1995), pKa titrations (Loewenthal et al., 1992; Tan et al., 1995), catalysis (Meiering et al., 1993), hydrogen-exchange (Clarke et al., 1995b) and even real-time folding (Killick et al., 1998). Hence, probing the dynamics change in the E_{act}/E_{inact} equilibrium

with a suitable mutant would be viable and comparable to a large body of previous work.

1.4 Research Objectives

The overall goal of this thesis was to identify and characterise either the wild-type or a mutant of barnase that would allow insight into the structural changes occurring over the E_{act}/E_{inact} equilibrium. A major contribution towards this goal would be decoupling the thermal stability of an enzyme from its thermoactivity through mutation(s) that either lower T_{eq} or raise T_m. This would allow the E_{inact} species to predominate at temperatures lower than the T_m if the separation of T_m and T_{eq} was sufficient and the magnitude of ΔH_{eq} for the enzyme was sufficient. The following objectives make up this overall goal.

1.4.1 Experimental

As elaborated in Section 1.2.3.2, the current EM only considers irreversible denaturation and the exact changes associated with T_{eq} are currently unknown. Therefore, the objectives for this research were to:

- generate mutants of barnase (Section 1.3.3.2) then express and purify them;
- determine T_m values and enthalpies of unfolding (ΔH_{VH}) determined under the conditions used to assay the enzymes, using circular dichroism (CD), differential scanning calorimetry (DSC) and other appropriate techniques;
- acquire data for fitting to the EM, using previously characterised substrates (Section 1.3.2) and moving on to others if unsuccessful;
- assess the experimental data to see if the interesting properties of barnase (Section 1.3.3) fit to the model, or if barnase is an exception; and
- prepare barnase for NMR dynamics measurements (e.g. ^{15}N labelling, preliminary testing etc.).

1.4.2 Theoretical

The theory behind the EM has been explained in introductory detail (Section 1.2). The mathematics, however, is not trivial and understanding the derivation of the full rate and product equations was important. For the purposes of NMR dynamics measurements, new mathematical derivations that describe EM species concentration changes with time and temperature were also required.

It was also investigated to see if a simpler model could be derived and checked against the data to adequately describe the observed kinetics. In addition, alternative derivations of equal complexity to the EM were investigated to see if they too could account for the observed rate profiles, or shed light on the movements of species within the EM. Lastly, to explore the full compliment of possible scenarios, a general model that could account for every possible instance of renaturation was developed and fitted against data.

2 Materials and Methods

2.1 Reagents and General Methods

Unless otherwise stated, all chemicals were purchased from Merk KGaA (Germany), BDH Chemicals Ltd (UK), Sigma-Aldrich Chemicals (USA), Applichem (Germany), Invitrogen (USA), Bio-Rad Laboratories (USA), Scharlau Chemie (Spain) or Fluka Biochemica (Switzerland). All percent values are in weight/volume unless noted otherwise. Details of reagents and buffers referred to below are given in Appendix A.

2.2 DNA, Transformation and Sequencing Methods

2.2.1 Plasmids

Plasmid pMT1002 was obtained from Professor C. Nick Pace (Center for Advanced Biomolecular Research, Texas A&M University). pMT1002 (Addgene plasmid 8621) (Hartley et al., 1996) was synthesised by the Hartley group, based primarily on pMT416 (Addgene plasmid 8607) (Hartley, 1988).

Both plasmids require bacterial strains with the $lacI^q$ gene (such as DH5-α, XL1-blue, SURE or HB107). pMT1002, which was used for all work in this thesis, has a temperature sensitive repressor gene (CI157) from lambda phage, followed by its own promoter and, in the forward direction, the PR promoter from λ phage (Okorokov et al., 1994) for barnase (Hartley, 1988). Only a partial sequence of pMT1002 was available (see Section 2.2.4). pMT1002 was resuspended in 50 μL Tris buffer.

2.2.2 Nucleic Acid Concentration Determinations

The Nanodrop ND-1000 Spectrophotometer (Nanodrop Technologies, USA) was used to measure the concentration of DNA/RNA samples via extinction coefficients.

2.2.3 General Electroporation Methodology

The following was used for the transformation of WT pMT1002 plasmid into *E. coli* DH5-α cells (Appendix A.5.1) and mutant pMT1002 plasmids (Section 2.3) into *E. coli* XL1-blue cells (Appendix A.5.2 and A.5.3).

A Bio-Rad Gene Pulser™ (Bio-Rad Laboratories, USA) with Pulse Controller was used, following the procedure in the manual. An aliquot of 1 μL rehydrated plasmid DNA or mini-prep DNA (Appendix A.6) was added to 50 μL freshly thawed (on ice) electrocompetent cells from a 10% glycerol stock. The mixture was placed between the electrodes in a 0.2 cm electroporation cuvette (Bio-Rad Laboratories, USA) and electroporated with 2.5 kV at 25 μF capacitance and 200 Ω resistance. The electroporated cells were immediately pipetted into 1 mL of SOC media pre-equilibrated at 37°C, and shaken at that temperature for 1 hour at 200 rpm in a 1.5 mL tube for cell recovery.

2.2.3.1 Agar Plating of Freshly Transformed Cells

50 μL of recovered SOC culture (Section 2.2.3) was spread on LB-agar plates with ampicillin at 100 μg/mL. Plates were grown at 37 °C until optimal colony formation (generally overnight, 16 hours) and kept at 4 °C thereafter. Mutant plasmids were grown on plates containing X-gal as prescribed in the Stratagene QuikChange™ II-E kit manual (Stratagene, USA) revision B.01.

2.2.4 Plasmid Sequencing and Transformed Cell Stocks

DNA was prepared for sequencing using an alkaline lysis method (Appendix A.6) on cultures grown from single transformed colonies from agar plates (Section 2.2.3.1).

2.2.4.1 Sequencing Methods

pMT1002 was initially sequenced using outward primers based on the sequence of the barnase/barstar gene known from the addgene entries. Primers used were “Reverse start” and “Forward end”, see below. New primers (“Forward start” and “Reverse end”) were designed using initial results to give inward sequence overlap, confirming sequence for design

of mutagenesis primers and for confirmation of successful mutagenesis (Section 2.3) (see Appendix D for results).

Name	Sequence (5'–3')
Reverse start	ATAATCCGCAACCCCGTC
Foward end	GAGAGTGTGCTTCAGGTT
Forward start	GCACTGGCACTCTTACCG
Reverse end	CTCCCATTGATCGTATTAAG

Table 2.1 – Sequencing primers for plasmid pMT1002

12 μL plasmid DNA, prepared as in Appendix A.6, was submitted to the Waikato DNA Sequencing Facility (The University of Waikato) at concentrations of between 50-150 ng/μL with 2 μL of each required primer at 5 μM concentration. Results were obtained electronically as .ab1 files.

2.2.4.2 Alignment of Sequences

Geneious Pro (Version 4.8) (Biomatters Ltd, NZ) was used for proofing electropherograms received from sequencing and alignments of the results were performed using a cost matrix of 65% similarity (5.0/-4.0), a gap open penalty and extension penalty of 12 and 3 respectively, as a global alignment. Once the area of interest on pMT1002 was mapped, mutagenesis products were aligned to the consensus sequence, confirming the codon changes of interest.

2.2.4.3 10% Glycerol Stocks of Transformed Cells

Once plasmids were sequenced and confirmed (see Section 2.2.4), 1 mL of the culture volume from Appendix A.6 was transferred to a 2 mL cryo-tube and mixed in with 250 μL autoclaved 50% glycerol, to give a final concentration of 10% glycerol. This tube was labelled and stored at -80 °C.

2.3 Site-Directed Mutagenesis

Site-directed mutagenesis was performed using the protocol from the Stratagene QuikChange™ II-E kit (Stratagene, USA) revision B.01. All reagents used in this section are given in the kit manual.

2.3.1 DNA Preparation

WT pMT1002 plasmid DNA used in the mutagenesis reactions (template) was prepared as in Appendix A.6 and sequenced before use (Section 2.2.4.1). For the creation of S80C/A43C (DM) mutant DNA, the first mutation made was S80C. This mutant plasmid was then used as the template for the A43C mutagenesis reaction, using the same methodology. All reactions used template DNA at a stock concentration of 5 ng/μL.

2.3.2 Primer Design and Preparation

Primers were designed as suggested in the manual, using the online system (http://www.stratagene.com/qcprimerdesign). Primers in particularly GC-rich regions (e.g. for the S80C mutation) were slightly longer to stay within the other requirements. All primers were diluted to a stock concentration of 100 μM in MQ water. See Table 2.3 for codon changes.

Name	Sequence (5'–3')
A43Cfwd	GGTGGCATCAAAAGGGAACCTTTGTGACGTCGCTCCG
A43Crev	CGGAGCGACGTCACAAAGGTTCCCTTTTGATGCCACC
S80Cfwd	GCGTGAAGCGGATATTAACTATACATGTGGCTTCAGAAATTCAGAC
S80Crev	GTCTGAATTTCTGAAGCCACATGTATAGTTAATATCCGCTTCACGC
Y78Ffwd	GAACATGGCGTGAAGCGGATATTAACTTCACATCAGGCTTCAG
Y78Frev	CTGAAGCCTGATGTGAAGTTAATATCCGCTTCACGCCATGTTC
I51Vfwd	CTCCGGGGAAAAGCGTCGGCGGAGACAT
I51Vrev	ATGTCTCCGCCGACGCTTTTCCCCGGAG
I88Vfwd	CTTCAGAAATTCAGACCGGGTTCTTTACTCAAGCGACTG
I88Vrev	CAGTCGCTTGAGTAAAGAACCCGGTCTGAATTTCTGAAG
L89Vfwd	GAAATTCAGACCGGATTGTTTACTCAAGCGACTGG
L89Vrev	CCAGTCGCTTGAGTAAACAATCCGGTCTGAATTTC

Table 2.2 – Mutagenesis primers for WT barnase in pMT1002 plasmid

2.3.3 Mutagenesis Protocol

Each mutagenesis reaction used 5 μL 10 x reaction buffer, 5 μL template DNA stock, 4 μL each mutation primer stock, 1 μL dNTP mix, 1 μL

PfuUltra HF DNA polymerase and 30 μL RO water to give a final volume of 50 μL. Control reactions were as stated in the kit manual.

Thermal cycling was performed as in the kit manual, utilising an Eppendorf Mastercycler Gradient PCR machine (Eppendorf, Germany), with the number of cycles for each mutation varying depending on the number of mutated bases:

Mutagenesis	S80C	A43C	Y78F	I51V	I88V	L89V
Original codon	TCA	GCA	TAT	ATC	ATT	CTT
New codon	TGT	TGT	TTC	GTC	GTT	GTT
No. of cycles	14	16	14	14	12	12

Table 2.3 – Settings for mutagenesis thermal cycling and details of codon changes

Product DNA was *Dpn I* digested and purified using the supplied StrataClean resin as per the kit manual. Mutagenesis and transformation controls were the same as the kit method. Transformation was performed as in Section 2.2.3, with all mutations sequenced, confirmed and made into glycerol stocks as in Section 2.2.4.

2.4 Protein Expression and Purification

Expression trials were carried out using overnight cultures (see Section 2.4.2.1) and sodium dodecyl sulfate polyacrylamide gel electrophoresis (SDS-PAGE) analysis as described below to ensure barnase production. The large-scale method used for expression and purification was adapted from the work of others, with modifications for available equipment, reagents and speed (Baxa et al., 2002; Krishnaswamy et al., 2006; Mossakowska et al., 1989).

2.4.1 SDS-PAGE Methodology

Protein samples at appropriate concentrations were taken (diluted if necessary) and added to aliquots of 4 x SDS loading buffer (QX4) at a ratio of 3:1. Before running, the samples were incubated at 95 °C for 5 minutes. 18 μL of each sample was added to the appropriate well and 18 μL Precision Plus Protein™ Unstained Ladder (Bio-Rad Laboratories, USA) was added to each of the outside wells.

Gels were run using Bio-Rad PowerPac™ Basic (Bio-Rad Laboratories, USA) electrophoresis equipment in constant current mode. Samples were stacked in the gel using 10 mA/gel for the first half-hour, then run at 25 mA/gel until the dye-front had reached the bottom of the gel.

2.4.1.1 Staining and Destaining of Gels

Gels were removed from their casts and transferred to a pipette-tip box (with lid). ~75 mL coomassie stain was added and the closed box heated on high for 40 seconds in an 1100W microwave. The box was then transferred to a shaker for 30 minutes at 160 rpm. Destaining was performed in a similar manner using destain solution and microwaving, shaking overnight to fully destain. Colour scans were taken on a Canon LiDE100 scanner (Canon, USA) of each gel.

2.4.2 Large-Scale Expression Cultures

A sterile tungsten loop was heated to glowing, and dipped into the still-frozen 10% glycerol stock (Section 2.2.4.3) of the required transformant, whilst on ice. The loop was streaked on LB-agar plates with ampicillin at 100 μg/mL in a ¼-segment pattern, sterilising between each ¼. Plates were grown at 37 °C until optimal colony formation.

2.4.2.1 For WT and Mutant Protein Expression

3 mL cultures were inoculated with a colony from an agar plate and incubated overnight at 30 °C in LB media with 3 μL ampicillin stock, shaken at 200 rpm. A 1 L culture of TB media in a 2 L baffled flask was inoculated with 1 mL of the overnight culture, 1 mL ampicillin stock and the flask shaken at 200 rpm and 37 °C overnight (16-24 hours) for expression (plasmids were temperature-inducible).

2.4.2.2 ^{15}N-incorporation for NMR

10 mL cultures were incubated at 30 °C in LB media for 18 hours with 10 μL ampicillin stock, shaken at 200 rpm. Cells were pelleted at 4000 x g and 4 °C in 50 mL centrifuge for 5 minutes. Pellets were washed with 10 mL M9 media (containing $^{15}NH_4Cl$ label) and spun down again, then resuspended in 10 mL M9 media. A 1 L culture of labelled M9 media in a 5 L baffled flask was inoculated with the 10 mL resuspension, 1 mL of

ampicillin stock and the flask shaken at 200 rpm and 37 °C for 36 hours or greater.

2.4.3 Crude Isolation

Following growth, the flask was immediately placed in an ice-slurry and 55 mL glacial acetic acid added (5% of final volume), stirred, and left for 15 minutes to lyse cells. This mixture was decanted evenly into 3 x 500 mL centrifuge bottles and cells pelleted at 4500 x g for 15 minutes to remove debris. The supernatant was decanted and then stirred into 560 g of $(NH_4)_2SO_4$ in a 2 L beaker stirrer on a 40 °C hotplate, precipitating protein. After 30 minutes, 50 mL aliquots of MQ water were added until all salt was dissolved. This solution was decanted into 4 x 500 mL bottles and pelleted at 11000 x g.

The resulting protein pellets, which were tacky and brown (from TB media; clear from M9 media), were collected into a 50 mL falcon tube and redissolved into a minimal volume of MQ water (approx. 15 mL). This volume was dialysed twice against 1 L of buffer A (20 mM Na Citrate, pH 5.5) for ~8 hours initially, then overnight against fresh buffer, using 14.6 mm diameter Spectra/Por® 6-8 kDa cut-off dialysis membrane tube (Spectrum Laboratories, USA). This step raises the pH and lowers the salt content, refolding the protein. Immediately before any column steps, the contents of the dialysis were transferred to 15 mL falcon tubes and centrifuged at 26000 x g for 30 minutes. The pH was checked to be 5.5 ± 0.1, and if not was dialysed further still.

2.4.4 Cation Exchange Chromatography

The centrifuged supernatant was applied at 5 mL/minute to a HiTrap™ SP FF cation exchange column (GE Healthcare Life Sciences, UK) pre-equilibrated in buffer A. If more than 10 mL of supernatant was available, multiple column runs were needed as the capacity of the column was exceeded (i.e. protein flowed through).

The column was placed inline on an Äkta™ Basic or Prime system (GE Healthcare Life Sciences, Sweden). 35 mL of buffer A was washed through before a 50 mL gradient to 100% buffer B (200 mM NaCl, 20 mM K-phosphate, pH 8.0) eluted barnase. 2 mL fractions were collected. A

further 5 mL of buffer B was washed through and the Äkta system used to manually re-equilibrate the column into buffer A for further runs.

Fractions showing barnase on the UV trace (confirmed by SDS-PAGE analysis (Section 2.4.1)) were pooled and concentrated at 3500 x g and 4 °C using 20 mL Vivaspin-2 5 kDa cut-off concentrators (GE Healthcare Life Sciences, UK) to a final volume of approx. 3 mL.

2.4.5 Size Exclusion Chromatography

An additional size-exclusion step was added to the methods used previously (Baxa et al., 2002; Krishnaswamy et al., 2006). This was to ensure completely clean protein for sensitive enzyme assays.

2.4.5.1 Small Scale S75 10/300

Multiple 300 μL aliquots of the concentrate from cation exchange were injected into a 500 μL loop and applied to a Superdex™ 75 10/300 GL size exclusion column (GE Healthcare Life Sciences, UK). Buffer B was the pre-equilibrated mobile phase and 1 mL fractions were collected, identifying barnase via the UV trace.

2.4.5.2 Large Scale S75 16/60

~3 mL of concentrate was applied to a Superdex™ 75 16/60 GL size exclusion column (GE Healthcare Life Sciences, UK) via injection into a 5 mL loop. Buffer B was the pre-equilibrated mobile phase and 2 mL fractions were collected, identifying barnase via the UV trace.

2.4.5.3 Final Dialysis

Eluant showing as barnase on SDS-PAGE gels (Section 2.4.1) was pooled and dialysed twice against 1 L of MQ water (both periods overnight) in 6-8 kDa cut-off dialysis membrane tubing. The final volume of 10-15 mL was stored at 4 °C in 15 mL tubes.

2.5 Characterisation of WT and Mutant Barnase

2.5.1 Protein Concentration Determination

Immediately after dialysis 1x, 5x, 10x, and 20x dilutions were made of each sample (WT and mutant). As in Section 2.2.2, the spectrometer was blanked against each final dialysis volume (diluted as above) and the A_{280} recorded. The linearity of the concentration, determined using the extinction coefficient 26930 L mol^{-1} cm^{-1}, was checked and 20x dilution points often discarded (due to low absorbances). An average value was obtained. Protein extinction coefficients were calculated using the known amino acid compositions and the online tool ProtParam (Gasteiger et al., 2003).

2.5.2 Mass Spectrometry

General methodology for gel extraction and matrix-assisted laser desorption ionisation time of flight mass spectrometry (MALDI-TOF MS) was provided by Jonathan Puddick (University of Waikato) and Joanna McKenzie (McKenzie, 2006).

2.5.2.1 Gel Extraction

Fragments of SDS-PAGE gel bands (from Section 2.4.5.3) were cut out with a sterile scalpel blade and transferred to a 1.5 mL tube. Gel fragments were repeatedly destained with aliquots of 0.5 mL 1:1 acetonitrile:25 mM NH_4HCO_3 whilst shaken at 37 °C at 200 rpm for 1 hour until free of stain. Removing destain solution, 100 μL of the above destain was added and the tube spun down at 13000 rpm in a MiniSpin™ Plus centrifuge (Eppendorf, Germany) then the supernatant removed. 50 μL acetonitrile (ACN) was used to dehydrate the fragment for 15 minutes, then the tube was spun down again.

With the supernatant removed, the tube was air-dried for 2 hours in a vacuum desiccator. For tryptic digests only, 1 μL Promega Trypsin Gold solution (aliquots stored at -80 °C) was resuspended in 199 μL of 25 mM NH_4HCO_3 to a final concentration of 0.02 μg/mL, then added and incubated at 4 °C for 1 hour. The excess trypsin solution was removed and

the fragment incubated at 37 °C for 5 hours, then at 4 °C until analysis (maximum of 24 hours). 15 μL of 20% ACN/0.1% trifluoro acetic acid (TFA) solution was added just prior to analysis for both whole protein and digested samples.

2.5.2.2 Matrices, Calibrant(s) and Sample Preparation

For tryptic-digested gel fragments, α-cyano-4-hydroxycinamic acid (HCCA) was used as matrix. For whole protein samples (from Section 2.4.5.3) a 9:1 mixture of 2,5-dihydroxybenzoic acid and 2-hydroxy-5-methoxybenzoic acid (Super-DHB) was used as matrix. Both were from Sigma-Aldrich (USA). A spot of peptide/whole-protein calibration standard II (Bruker Daltonics, USA, catalogue #206195) was used per 4 sample spots, as relevant to the samples being analysed.

Approximately 10 mg of the solid matrix of choice was added to a 1.5 mL tube with 30 μL of 2:1 ACN:0.1% TFA well-mixed in. Along with the sample tubes (containing gel fragments and 15 μL of 20% ACN/0.1% TFA solution), the matrix tube was sonicated on high for 10 minutes in a D-78224 water-bath sonicator (Elma, Germany). Tubes were spun down at 13000 rpm. On an AnchorChip™ MALDI-TOF peptide-target (Bruker Daltonics, USA) spot, 0.5 μL of the sample supernatant or calibrant solution was mixed with 0.5 μL matrix supernatant and left to air-dry. The chip was then attached to a frame.

2.5.2.3 MALDI-TOF Setup

An Autoflex™ II MALDI-TOF mass spectrometer (Bruker Daltonics, USA) was used to analyse samples. The electronic settings files summarised below are contained in Appendix C.

For peptide digests, ~10 sets of 30 shots at 20-40% laser power were summated for each spot using pulsed ion extraction at 60 ns and suppressing <500 Da ions. In RP mode, the mass range selector was set to "low range", detector gain to 1400 V, acceleration voltage to 19 kV, reflector voltage to 20 kV, and a range of 600-3500 Da was collected. FlexControl™ software (Bruker Daltonics, USA) was used to manually control all other settings. Before samples were analysed, the relevant peptide calibrant spots were collected using the same settings and the

spectrometer calibrated with an automatic polynomial correction. For I88V and L89V mutant proteins the same fingerprint was observed (digest parent ion was of the same mass) and, hence, LIFT™ mode (MS/MS) was used to give more information on the parent peptide composition.

For whole-protein samples LP mode was used, incorporating the linear detector, with the mass range selector set to "high range", pulsed ion extraction of 450 ns, gain to 2500 V, acceleration voltage to 20 kV and a range of 5-20 kDa collected. Laser power was often 30-60%. Calibration was as above, using the whole protein standard.

2.5.2.4 Analysis of Mass Spectra

Peptide spectra were saved and exported to FlexAnalysis™ software (Bruker Daltonics, USA) and peaks identified and labelled. The processed spectra were opened in BioTools (Bruker Daltonics, USA) and compared against the bacterial proteins section of the MASCOT database (Matrix Science, USA). Monoisotopic masses were used with a 1 missed-cleavage tolerance. Otherwise, settings were the software default. Results with a significance score of 70 or above were retrieved and the peptide fingerprint confirmed. For I88V and L89V the LIFT™ spectra were also compared. Whole-protein spectra had peaks identified to confirm full sequence length.

2.5.3 Rotavirus RNA RNAse Assays

To check for basic RNAse activity – indicating correct expression and clean purification of barnase – an assay using Rotavirus RNA was used. This assay was developed by Joanna McKenzie (University of Waikato). See Appendix A.7 for RNA preparation.

2.5.3.1 General Method

2x Formamide loading dye (FLD) was prepared. An Eppendorf Mastercycler Gradient PCR machine (Eppendorf, Germany) was set to 37 °C with 100 °C lid. In 600 μL PCR tubes held at 0 °C, 1 μL Rotavirus RNA stock (at 4000 ng/μL), 1 μL enzyme (at 0.1 mg/mL) and 1 μL of any other reagents were added at 0 °C and made up to 10 μL with DEPC-treated MQ water. A 0 min control was taken and quenched with 10 μL FLD, with the

rest of the tubes added to the PCR machine, removing and quenching tubes at timed intervals or at the conclusion.

5% urea denaturing gels (Appendix A.4.2) were pre-run in 1x TBE buffer at 50 V for 30 minutes using apparatus as in Section 2.4.1. 20 μL of each sample was separated at 150 V in constant voltage mode until the darkest band nearly ran off the gel. Gels were stained with SYBR green (Invitrogen, USA) (5 μL stock in 50 mL 1x TBE) and shaken at 240 rpm for 40 minutes in a foil-wrapped box. Gels were visualised and photographed on an Apollo UV light box (Airpro Scientific, NZ) with a Cohu CCD camera (Cohu Inc., USA), averaging 32 frames with Scion Image 4.0.2 software (Scion Corp., USA).

2.5.3.2 Contaminant Screens

The following samples were assayed at 37 °C with 1000 ng RNA for 15 minutes (except for the 0 min control) and run on gels as in Section 2.5.3.1. 10ML200 and GA13 are 1 μL of 0.1 mg/mL non-RNAse proteins from John Steemson and Marisa Till respectively (both University of Waikato) and "Inhibitor" is Protector RNAse Inhibitor at 20U concentration (Roche Applied Science, USA) – enough to inhibit ~20 ng of contaminating RNAse A.

Gel Lane	Duration (minutes)	Barnase (μL 0.1 mg/mL)	EDTA (μL 10 mM)	Other	Label
1	0	–	–	–	0 min control
2	15	1	–	–	WT Barnase
3	15	1	1	–	WT Barnase + EDTA
4	15	–	1	–	EDTA
5	15	–	–	10ML200	10ML200
6	15	–	–	GA13	GA13
7	15	–	–	Inhibitor	Inhibit.
8	15	1	–	Inhibitor	WT Barnase + Inhibit.
9	15	1	1	Inhibitor	WT Barnase + Inhibit. + EDTA
10	15	–	–	–	15 min control

Table 2.4 – RNAse contaminant screen conditions

2.5.3.3 Time-course Assays

10 μL volumes with 1 μL of 1 mg/mL barnase and 4000 ng of RNA were assayed for 1, 3, 5, 10, 15, 30, 45 and 60 minutes at 37 °C, with final and initial controls as above. The samples were run on 5% Urea denaturing gels described previously.

2.5.4 SYPRO™ Real-time Melts

Real-time protein melts were performed using a RotorGene-6000 Real-time PCR machine and analysed using supplied RotorGene software (version 1.7) (both Corbett Research, Australia). Barnase WT and mutant samples were diluted in triplicate with MQ water to a concentration of 280 μg/mL in 200 μL RT-PCR tubes along with 7.5 μL of 300x SYPRO™ orange protein gel stain (Sigma-Aldrich, USA) stock solution, giving a final volume of 25 μL. MQ blanks with dye were also recorded, as shown in the literature method (Ericsson et al., 2006).

Sample tubes were arranged in a 36-well rotor. After a 90 second equilibration at 25 °C, the machine was ramped to 99 °C in 0.2 °C increments with 5 second delays per increment. Samples were excited at 470 nm and emission measured at 555 nm with a gain of 9.67. Data points were output from the RotorGene software to an Excel spreadsheet. An average of the 3 blank runs was subtracted from each trace, and then all traces for each protein overlaid. Congruent traces were then averaged and overlaid for comparison between WT and the mutants.

The first derivative of each data set was then taken arithmetically, and plotted with a moving average line fitted (period 6). The T_m value was measured visually from the middle of the peak representing the inflection in the original melt slope. Fitting of data to a two-state equation (Ericsson et al., 2006) (e.g. Equation 2.1) was inappropriate, as the fluorescence did not level off linearly and fits would have been subjective.

2.5.5 Circular Dichroism

Circular Dichroism (CD) work was performed at The University of Canterbury (Christchurch, New Zealand) in the Biomolecular Interaction Centre. The instrument was a Jasco J-815 CD Spectrometer (ROM 1.01.13)

attached to a Jasco PTC-4235/15 peltier, with Spectra Manager™ (1.54.03 build 1) software used to analyse results (all Jasco Inc., USA).

2.5.5.1 Sample Preparation and Instrument Setup

50 μL of 3 mg/mL barnase stocks, in MQ water, were made up to a final volume of 3050 μL with assay buffer and added to a clean 5 mL quartz cuvette (1 cm pathlength). For I51V, 125 μL of 1.2 mg/mL stock was used.

Final (70 °C) and initial (20 °C) wavelength scans of the samples were performed in triplicate and averaged in software. A 200-260 nm range was collected with 0.5 nm data pitch, scanning continuously at 50 nm/minute, 1-second response, 1 nm bandwidth and 100 mdeg sensitivity.

For the sample time scans, spectra were measured at 230 nm (the point of largest difference between 20 and 70 °C), with 0.5 °C data pitch, 1 °C/minute temperature gradient, 1-second response, 1 nm bandwidth, 100 mdeg sensitivity and a 30 second delay time.

For WT barnase only, a refolding scan was performed. The time scan, as above but starting at 40 °C, was delayed at 70 °C for 1 minute, then reversed back to 40 °C. Background scans for both wavelength and time measurements were made of the assay buffer for later subtraction.

2.5.5.2 Data Fitting and Analysis

CD mdeg time-scan data was exported to Microsoft Excel™ 2004 (Microsoft Inc., USA) and the background scans subtracted. The temperature values were converted to degrees Kelivn (K) and the data sets exported to MATLAB R2009b (The MathWorks Inc., USA) as independent arrays of data. The 2D CurveFit module of MATLAB was invoked to fit a custom equation to the data; the equation used (Equation 2.1) corrects for both final and initial non-zero slopes and fits a ΔH and T_m value:

$$y = f(a + bT) - f(c + gT) + c + gT$$

Equation 2.1 – CD equation fitting mdeg data to temperature data

a, b, c and g are variables, y is CD mdeg data and T is temperature in K. f is the fractional contribution to the signal from the unfolded form; f is defined by the thermal equilibrium constant, K:

$$f = \frac{K}{K+1} \quad \text{and} \quad K = \exp\left(\frac{\Delta H}{R}\left(\frac{1}{T_m} - \frac{1}{T}\right)\right)$$

Equation 2.2 and Equation 2.3 – Fractional proportion of folded and unfolded forms with changes in thermal equilibrium constant

ΔH is the enthalpy of the unfolding process, T_m is the midpoint of the transition between the folded and unfolded forms and R is the gas constant.

In MATLAB, the fitting was a non-linear least squares approach. Robustness was set to LAR using a Trust-Region algorithm, with the minimum and maximum changes between iterations set to $1x10^{-8}$ and 0.1 respectively and the tolerances in both directions set to $1x10^{-6}$. Maximum number of function evaluations was 1000, with a maximum of 400 iterations. Values were defined as below:

Unknown	Initial Value	Lower Limit	Upper Limit	Units
ΔH	$5x10^5$	0	$1x10^7$	kJ mol^{-1}
T_m	323	273	373	K
a	0	$-\infty$	∞	–
b	0	$-\infty$	∞	–
c	0	$-\infty$	∞	–
g	0	$-\infty$	∞	–

Table 2.5 – Fitting parameters for CD data

The output unknowns for each sample were then used to fit a line to the raw data in Excel, with plotting of the data and fits in Prism 5.02 (GraphPad Software, USA). Statistics on the quality of fit and associated error were taken from MATLAB and files of the fits are available in Appendix C.

2.5.6 Differential Scanning Calorimetry

Differential Scanning Calorimetry (DSC) work was also performed at The University of Canterbury (Christchurch, New Zealand). The instrument was a NanoDSC with platinum 333 μL sample and reference cells running DSCRun software (version 3.3.0) and analysis was performed using NanoAnalyze (version 1.1.0) (all TA Instruments, USA).

2.5.6.1 Sample Preparation and Instrument Setup

125 μL of 3 mg/mL barnase stocks, in MQ water, were made up to a final concentration of 0.5 mg/mL with 75 μL 10x assay buffer (1 M Na-phosphate, pH 8.0) and 550 μL DEPC-water. For I51V, 312.5 μL of 1.2 mg/mL stock was used. All samples were degassed in a desiccator under vacuum for 5 minutes before being transferred to the cell(s), which were washed thoroughly in buffer between samples.

Each day before any runs were performed the instrument was conditioned from 40 °C to 90 °C with degassed assay buffer at 2 °C/minute, then back down to 40 °C. A reference run for background subtraction was performed using only buffer. Runs were at 1 °C/minute from 20-95 °C and at 3 atmospheres of pressure. Samples were left to equilibrate at 20 °C for 10 minutes before the gradient was started and runs were rejected and repeated if any obtrusive artefacts were observed in the trace.

2.5.6.2 Data Fitting and Analysis

Raw data had the reference run subtracted in NanoAnalyze software. The data was cropped to between 30 and 80°C to remove systematic artefacts and a baseline correction was applied using the built-in "scaled two-state model" which also fitted the data and gave values for ΔH and T_m, along with a scale factor (*aw*). This gave no statistics on the goodness of fit, so the fit was re-created in MATLAB using the same two-state equation (Prabhu & Sharp, 2005):

$$y = \left(\frac{(\Delta H)^2}{RT^2} \right) \cdot \frac{\exp\left(\Delta H \left(\frac{T - T_m}{RT \cdot T_m} \right) \right)}{\left(1 + \exp\left(\frac{-\Delta H}{R} \left(\frac{1}{T} - \frac{1}{T_m} \right) \right) \right)^2} \cdot \frac{aw}{1000}$$

Equation 2.4 – DSC equation fitting Cp data to temperature data

y is Cp data and T is temperature in K. ΔH is the enthalpy of the unfolding process, T_m is the midpoint of the transition between the folded and unfolded forms, *aw* is a scale factor and R is the gas constant.

In MATLAB, the fitting used a non-linear least squares approach with robustness set to LAR using a Trust-Region algorithm, the minimum and

maximum changes between iterations set to $1x10^{-8}$ and 0.1 respectively and the tolerances in both dimensions set to $1x10^{-6}$. Maximum number of function evaluations was 1000, with a maximum of 400 iterations. Values were defined as below:

Unknown	Initial Value	Lower Limit	Upper Limit	Units
ΔH	$5x10^5$	$-\infty$	∞	kJ mol^{-1}
T_m	323	273	373	K
aw	0.2	0	10	–

Table 2.6 – Fitting parameters for DSC data

The output unknowns for each sample were then used to fit a line to the raw data in Excel, with plotting of the data and fits in Prism 5.02 (GraphPad Software, USA). Statistics on the quality of fit and associated error were taken from MATLAB and files of the fits are available in Appendix C.

2.6 Equilibrium Model Data Collection

2.6.1 Initial Dinucleotide Trials

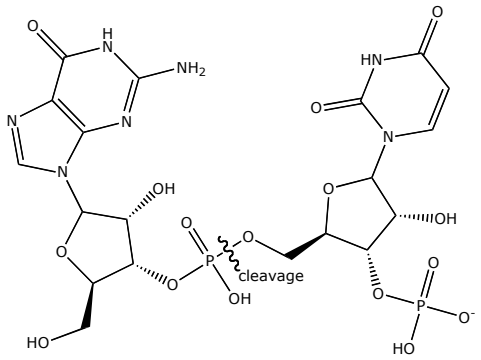

Figure 2.1 – GpUp dinucleotide substrate with cleavage site shown

GpUp (5′-guanosinephosphate-uridinephosphate-3′) was ordered from Invitrogen (USA) as a custom desalted RNA oligo with 3′ phosphate labelling. Two batches of 10 μmole synthesis scale were ordered.

2.6.1.1 Substrate and Enzyme Preparation

Substrate was shipped as a solution and concentration measured (Section 2.2.2) using the 260 nm 20.6 mM^{-1} cm^{-1} extinction coefficient found previously (Day et al., 1992). GpUp was approximately 50 mM and was

diluted to an intermediate stock of 8 mM in acetate buffer. WT barnase was diluted to 0.02 mg/mL in 0.1 M acetate buffer as above.

2.6.1.2 Sample Preparation and Instrument Setup

10 μL of 8 mM GpUp stock was added to 385 μL 0.1 M acetate buffer in a 4 mm pathlength quartz cuvette and equilibrated in a Helios γ UV/vis spectrometer with a SPU-1x0 single-cell peltier. 200 μM GpUp was approximately 10 x the K_M of GpUp at 25 °C (19.9 ± 2.0 μM) (Day et al., 1992). A H1 93530 thermocouple probe (Hanna Instruments, USA) was in the cuvette solution. Once the temperature was steady (± 0.1 degree over 30 seconds) and background data acquisition finished, the temperature probe was removed, 5 μL of 0.02 mg/mL barnase stock was added as a drop on a curved stirring rod. The solution was then mixed rapidly, the spectrometer lid shut and data collection started using Vision software (version 1.25) (Thermo Spectronic, UK). A data pitch of 0.25 seconds, bandwidth 2 nm, measuring absorbance at 257 nm (Day et al., 1992) for 5 minutes was used. All the conditions for valid EM measurements were met (Peterson et al., 2007).

Assays were performed in triplicate or until 3 runs were in consensus at 15, 20, 25, 30, 34, 38, 42, 46, 50 and 54 °C as set on the peltier. The temperature, as measured by the thermocouple, was ascribed to each run and corrected to the reference thermometer scale (Appendix A.8).

2.6.1.3 K_M Determinations

Assays were performed as above at 46 °C (where appreciable denaturation of barnase is not seen (Section 3.2.6)) in duplicate at 7 concentrations from 3.175-200 μM made via serial dilution of the 8 mM GpUp stock in acetate buffer. The data from each run was plotted (ΔA_{257} vs time) and the slope of the plots at time = 0 found by hand. The slopes for each concentration (in duplicate) were plotted against substrate concentration in Prism 5.02 (GraphPad Software, USA) and fitted with a non-linear least-squares analysis to the Michaelis-Menten equation (Section 1.1.3) to determine a value for K_M. Further data points at 150, 300 and 400 μM GpUp concentration were needed for a good fit. A linear relation to temperature was assumed between K_M data points (see Section 2.7.1.2).

2.6.2 Fluorogenic Substrate (FrG)

FrG was ordered as a custom non-catalogue request from IDT (USA) at a 10 μmole synthesis scale. 6-FAM™ is a fluorescein fluorophore attached via a C_6N linker 5′ to the first dAMP, BHQ-1® is a fluorescence quencher attached 3′ to the final dGMP, and rG indicates the ribo-guanotide residue (see Figure 2.2). All other bases were deoxyriboses, limiting the cleavage to one site.

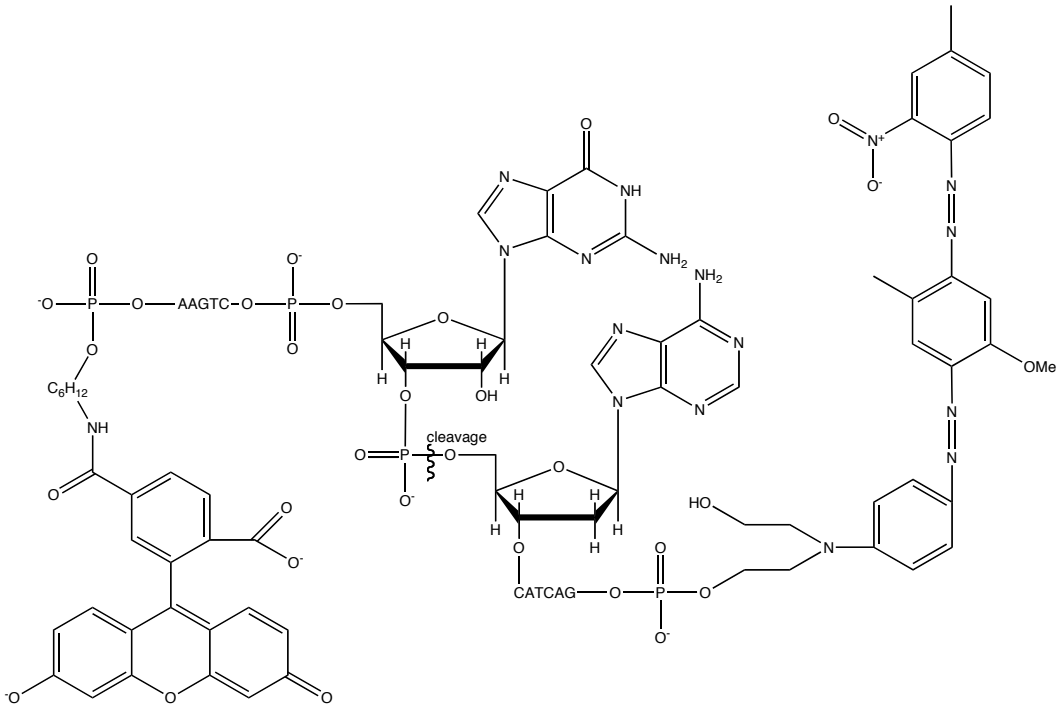

Figure 2.2 – FrG fluorogenic substrate with cleavage site shown

The products of cleavage were also ordered from IDT; they were designated "fluorophore" and "quench" at 1 μmole synthesis scales, see Table 2.7 below for supplied properties (from IDT) and sequences of compounds. The methods below were based from those in a paper on MazF, an *E. coli* RNase (Wang & Hergenrother, 2007).

Compound	Sequence	Extinction Coeff. (260 nm)	Yield (nmoles)
FrG	5′-6-FAM-AAGTCrGACATCAG-BHQ-1-3′	164060 $Lmol^{-1}cm^{-1}$	779.3
Fluorophore	5′-6-FAM-AAGTCG-3'	84560 $Lmol^{-1}cm^{-1}$	286.6
Quench	5'-ACATCAG-BHQ-1-3′	81300 $Lmol^{-1}cm^{-1}$	232.3

Table 2.7 – Properties of fluorogenic substrate and products

2.6.2.1 Substrate Stock and Preparation

FrG substrate was shipped as a lyophilised pellet and made up in DEPC water to ~1 mM using the provided synthesis yield as a guide. Dilutions for assays etc. were made up to 80% of required volume in 0.1 M assay buffer, concentrations determined spectroscopically (Section 2.2.2), then dilutions made to obtain the correct concentration. This was due to the viscous nature of the 1 mM stock causing pipetting issues.

2.6.2.2 Product Stocks and Preparation

Product halves were shipped as lyophilised powders and made up to ~2 mM in DEPC water using the provided synthesis yields as guides. 2 mM was so that equal mixed volumes would give a 1:1 ratio of product to substrate using similar dilutions to FrG. Dilutions were made as above to avoid concentration errors.

2.6.2.3 Substrate Stability (Real-time Melts)

Modifying the procedure from Section 2.5.4 by setting excitation to 470 nm and emission to 510 nm, the fluorescence of 25 μL 10 μM FrG in assay buffer was measured from 25 °C to 99°C and back to 25 °C. No dye was used and a blank of 25 μL buffer was recorded and subtracted.

2.6.2.4 Fluorometer Setup

A Hitachi F-7000 fluorescence spectrophotometer (Hitach High Technologies Corp., Japan) was fitted with a Hitachi thermostatted cell holder accessory; water being fed from a Julabo 13 water bath and MP pump (Julabo, Germany) at 5.8 L/min. 5 mm path-length thick-walled quartz cuvettes from Hitachi were used for all assays and tests. All work used a sample volume of 300 μL and experiments were controlled using FL Solutions software (Hitach High Technologies Corp., Japan). All time-scans used a 0.5 second data pitch and were recorded for 3 minutes with PMT set to 450 V, excitation (ex.) 485 nm, emission (em.) 518 nm, 5 nm slits, and 2 millisecond response time.

2.6.2.5 Substrate/Product Optimisation

Three-dimensional (3D) scans of the substrate with ex. 445-495 nm and em. 505-555 nm were performed to determine the optimum ex. and em. wavelengths for 10 μM FrG. PMT was at 450 V, data pitch of 1 nm in each dimension, a speed of 240 nm/s and response of 2 milliseconds.

A series of standards from 100% substrate to 100% product were made (substrate:product in μM): 10:0, 8.75:1.25, 7.5:2.5, 6.25:3.75, 5:5, 3.75:6.25, 2.5:7.5, 1.25:8.75, 0:10. Product concentration was 10 μM equivalents of each half, simulating time points of a barnase digest. The solutions were wave-scanned from 510-560 nm (em.) to determine if the emission peak moved with concentration or temperature; 25 and 50 °C were used. PMT was at 450 V, ex. 485 nm, 5 nm slit, 240 nm/s and 2 millisecond response time. Results were analysed for linearity at each wavelength.

2.6.2.6 Assay Method

Assays were based on the MazF method (Wang & Hergenrother, 2007) but, due to the relative speed of barnase and requirements of the EM (accurate temperature, mixing etc.), a plate reader was untenable. Substrate was prepared at 10 μM (Section 2.6.2.1) in assay buffer with enough 300 μL aliquots (4 aliquots per 1.5 mL storage tube) to do 36 runs for each assay. Barnase was prepared at ~0.002 mg/mL (162 nM, varies between mutants, see results Section 3.3.3) in assay buffer and stored in a 1.5 mL tube.

300 μL of FrG substrate was equilibrated in the fluorometer with a H1 93530 thermocouple probe (Hanna Instruments, USA) in the cuvette solution. 10 μM FrG was only approximately 2 x the K_M of any barnase variant at 25 °C and, hence, was corrected for in data processing (Section 2.7.1.1). Once the temperature was steady (± 0.1 degree over 30 seconds), 2 μL of ~0.002 mg/mL barnase stock was added as a drop on a 1 μL soft plastic sterile loop (TSC Ltd., UK), the solution rapidly mixed, the fluorometer lid shut and time-scan data collection started (Section 2.6.2.4) for 2 minutes. All the conditions for valid EM measurements were met (Peterson et al., 2007).

Assays were performed in duplicate or until 2 runs were in consensus at 26, 31, 35.5, 40.5, 45, 50, 55 and 60 °C as set on the water bath. The temperature measured by the thermocouple was ascribed to each run, and was corrected to the reference thermometer scale (Section A.8). Additional temperature points were added for some assays (Section 3.3).

2.6.2.7 K_M Determinations

Generally, assays were performed as above at 26 °C and 50 °C in duplicate or triplicate at 9 concentrations from 1-30 μM prepared via dilution of the 1 mM FrG stock in assay buffer. The data from each run was plotted (Fluorescence ($Fl._{518}$) vs time) and the slope of the plots at time = 0 found by hand. Otherwise, assays were performed as in Section 2.6.1.3.

2.7 Equilibrium Model Data Processing

2.7.1.1 General Data Workup

Data from absorbance (Section 2.6.1.2) or fluorescence (Section 2.6.2.6) assays were imported into Microsoft Excel 2004 and compiled into matrices with time down the left-hand side (seconds), temperature across the top (°C) and the absorbance or fluorescence values for each run filling the matrix points. From here, similar matrices of blanks could be made and backgrounds subtracted, K_M values corrected for and absorbance /fluorescence readings converted to product concentration, as explained below.

2.7.1.2 Absorbance Data Workup

Data was exported from Vision software as ΔA_{257}, the change in absorbance over the assay duration. Data was converted to product concentration (molar) using the extinction coefficient for GpUp (Day et al., 1992) and corrected for K_M effects using the results from Section 2.6.1.3 and the equation below (itself derived from Equation 1.5) (Fersht, 1999):

$$[\mathrm{P}]_x^{corr.} = [P]_x \cdot \frac{K_M + [S]_0 - [P]_x}{[S]_0 - [P]_x}$$

Equation 2.5 – Correction for working away from V_{max} via K_M values

where $[P]_x^{corr.}$ is the corrected substrate concentration at time x, $[P]_x$ is the substrate concentration at time x and $[S]_0$ is the initial substrate concentration. This equation effectively corrects the observed assay velocity, V, to V_{max}.

Corrected temperatures (Appendix A.8) for each run were converted to degrees K and 0.01 K added cumulatively to temperatures that had otherwise equivalent values. This stops fitting.exe (Section 2.7.2) from averaging runs and decreasing the number of data points fitted to the model.

2.7.1.3 Fluorescence Data Workup

Data was exported from FL Solutions software as raw fluorescence. Backgrounds for each individual run were subtracted (Section 2.7.1.1) in Excel and data converted to product concentration (M) using the upper (100% product, 10 μM) bound for each temperature (Sections 2.6.2.3 & 2.6.2.5) and the lowest value (generally at time = 0) as 0% product. K_M was corrected for using the results from Section 2.6.2.7 and Equation 2.5. Data was then "Δ'd" to bring absolute product concentration at time = 0 to zero by subtracting the lowest concentration point in each assay. Temperatures were corrected and adjusted as above.

2.7.2 Using MATBLAB fitting.exe

Fitting.exe is a stand-alone MATLAB run-time program written by previous contributors to the EM project (Daniel et al., 2007). It takes clean Excel .xls files containing matrices of [time (seconds) x temperature (K) x product concentration (M)] as described above (Section 2.7.1.1) and fits the data to the original EM (Section 1.2.2.1) using a least-squares approach initially, and a bootstrapping approach (Davison & Hinkley, 2006) if a "high-resolution" run is enabled in the graphical interface (GUI). As part of the input .xls file, starting values for ΔG_{cat}, ΔG_{inact}, ΔH_{eq} and T_{eq} were provided along with $[E_0]$, the concentration of enzyme in the assay.

Fitting was performed using various computers running Microsoft Windows XP SP3 (Microsoft, USA). High-resolution fitting with fitting.exe took on average 3-4 hours for a 3 minute, 10 temperature data set when

run on a Pentium 4 3.0 GHz with 2 GB RAM and was not multi-threaded. Multiple fitting runs were performed using the output values from the previous fit, until the output parameters were steady and did not vary outside of their 95% confidence intervals.

The following starting parameters were used for each initial fit, with the $[E_0]$ being slightly different for each mutant enzyme (see Table 3.10):

Output Parameter	Initial Value		Units
	GpUp fits	FrG fits	
$[E_0]$	20×10^{-9}	varies	M
$\Delta G^{\ddagger}_{cat}$	90000	80000	kJ mol^{-1}
$\Delta G^{\ddagger}_{inact}$	100000	95000	kJ mol^{-1}
ΔH_{eq}	120000	100000	kJ mol^{-1}
T_{eq}	320	320	K

Table 2.8 – Starting parameters for fitting.exe fitting runs

2.7.3 Using Alternative MATLAB Equations

For alternative EM equations (Section 4.1) it was deemed prohibitive to modify and check the fitting.exe MATLAB run-time program for each permutation in the equation. Hence, the SurfaceFitting tool in MATLAB R2009b (The MathWorks Inc., USA) was employed to fit data processed as above (Section 2.7.1). The original model was also fitted in this manner to compare with results from fitting.exe (see Section 2.7.2).

The tool required 1-by-x arrays of data for time (seconds), temperature (K) and product concentration (M). Matrix data (Section 2.7.1.1) was compiled into 3-value cells using the CONCATENATE function in Excel, in the format "time,temperature,product concentration". The data points were sorted using VisualBasic macros in Excel into a single column. The "text to columns" function was used to separate the concatenated data into three columns, one for each variable. These columns were then imported into a MATLAB workbook.

2.7.3.1 Fitting Settings and Methodology

The relevant custom equation was fitted using a least-squares approach. Equations in electronic format are in Appendix C. Robustness was set to LAR using a Trust-Region algorithm, with the minimum and maximum changes between iterations set to $1x10^{-8}$ and 0.1 respectively and the tolerances in both directions set to $1x10^{-6}$. Maximum number of function evaluations was 1000, with a maximum of $1x10^{7}$ iterations. Values were defined as below, with E_0 being input directly into the custom equation.

Fitting was performed using various computers running Microsoft Windows XP SP3 (Microsoft, USA) and Apple Mac OS X 10.6.2 (Apple Inc., USA). High-resolution fitting took on average ten seconds for a 3 minute, 10 temperature data set when run on a 2.66 GHz Core2 Duo processor with 4 GB RAM and was not multi-threaded. Multiple fitting runs were performed using the output values from the previous fit, until the output parameters were steady and did not vary outside of their 95% confidence intervals.

Output Parameter	Initial Value (Models N, R & Q)	Initial Value (All other models)	Lower Limit	Upper Limit	Units
$\Delta G^{\ddagger}_{cat}$	67000	80000	0	200000	kJ mol^{-1}
$\Delta G^{\ddagger}_{inact}$ $\left(\Delta G^{\ddagger}_{i}\right)$	93000	95000	0	200000	kJ mol^{-1}
$\Delta G^{\ddagger}_{deact}$ $\left(\Delta G^{\ddagger}_{a}\right)$	88000	95000	0	200000	kJ mol^{-1}
$\Delta G^{\ddagger}_{react}$ $\left(\Delta G^{\ddagger}_{-i}\right)$	93000	95000	0	200000	kJ mol^{-1}
$\left(\Delta G^{\ddagger}_{-a}\right)$	88000	95000	0	200000	kJ mol^{-1}
ΔH_{eq}	150000	100000	0	500000	kJ mol^{-1}
T_{eq}	315	320	273	373	K

Table 2.9 – Fitting parameters for custom equilibrium model equations

Note that the parameters in brackets apply to model Q only (Section 4.1.1.3).

3 Experimental Results and Discussion

In order to collect enzyme data for equilibrium model (EM) assays, sufficient protein had to be expressed and purified (Section 3.1) from wild-type (WT) and mutant barnase genes (see Section 2.3). Protein mass (indicating correct expression) was established using mass spectrometric (MS) means and activity confirmed through RNAse assays, then the variants were characterised for T_m and other thermostability parameters using DSC and CD techniques (Section 3.2). The collection of EM data against two substrates is then detailed, along with the fits and analyses of that data to the original EM (Section 3.3).

3.1 Protein Purification

WT and mutant barnase were purified as in Section 2.4. After the crude isolation steps (Section 2.4.3), the centrifuged dialysate was applied to a cation exchange column (CEC) and eluted with a gradient of buffer A to buffer B (Section 2.4.4). An example trace is shown below:

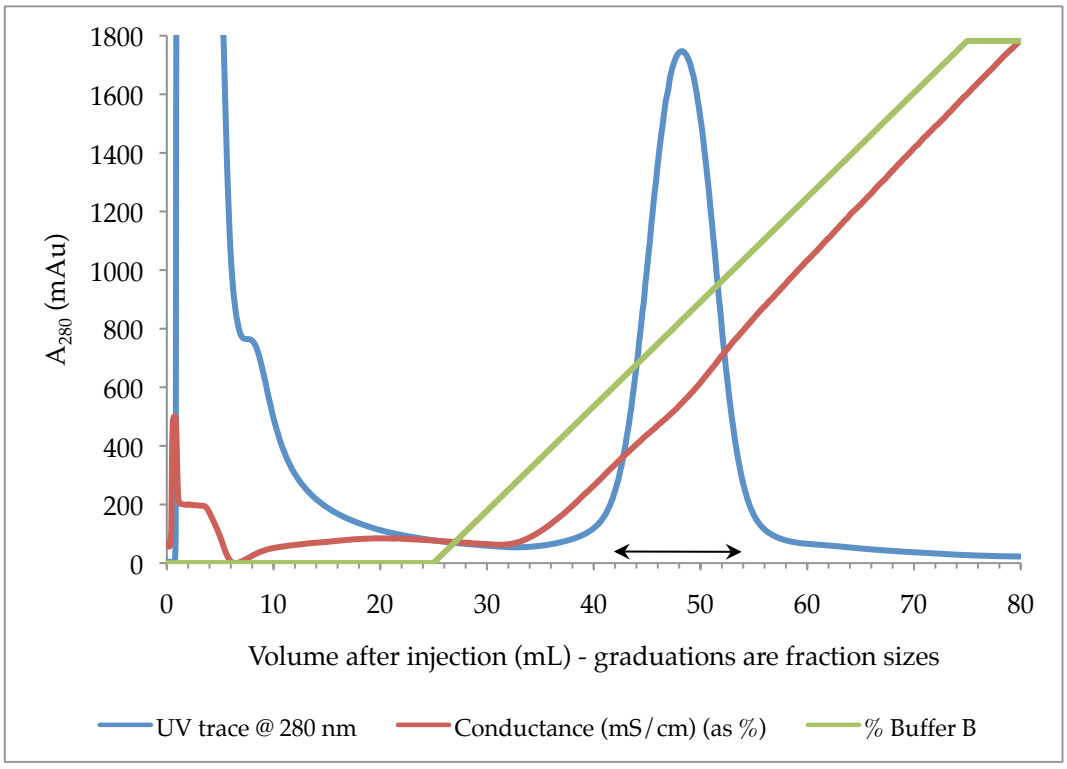

Figure 3.1 – Traces from L89V CEC protein purification

The column load was exhaustively dialysed against buffer A, as otherwise the low pH and high salt concentration of the resuspended pellet lessened the affinity of the column for barnase, weakening binding. This was exhibited through SDS-PAGE analyses (not shown) of column flow-through. SDS-PAGE analysis was performed at every step of purification. Figure 3.2 shows an example I51V CEC run, with A4 being the shoulder at 10 mL, A14 the start of the gradient, B5-B10 as indicated in Figure 3.1 (the peak) and the crude purification as loaded on to the column in the last lane. The collected fractions (usually 42-54 mL fractions, as indicated with black arrow on trace above) were then concentrated and applied to a size exclusion column (SEC) (Section 2.4.5).

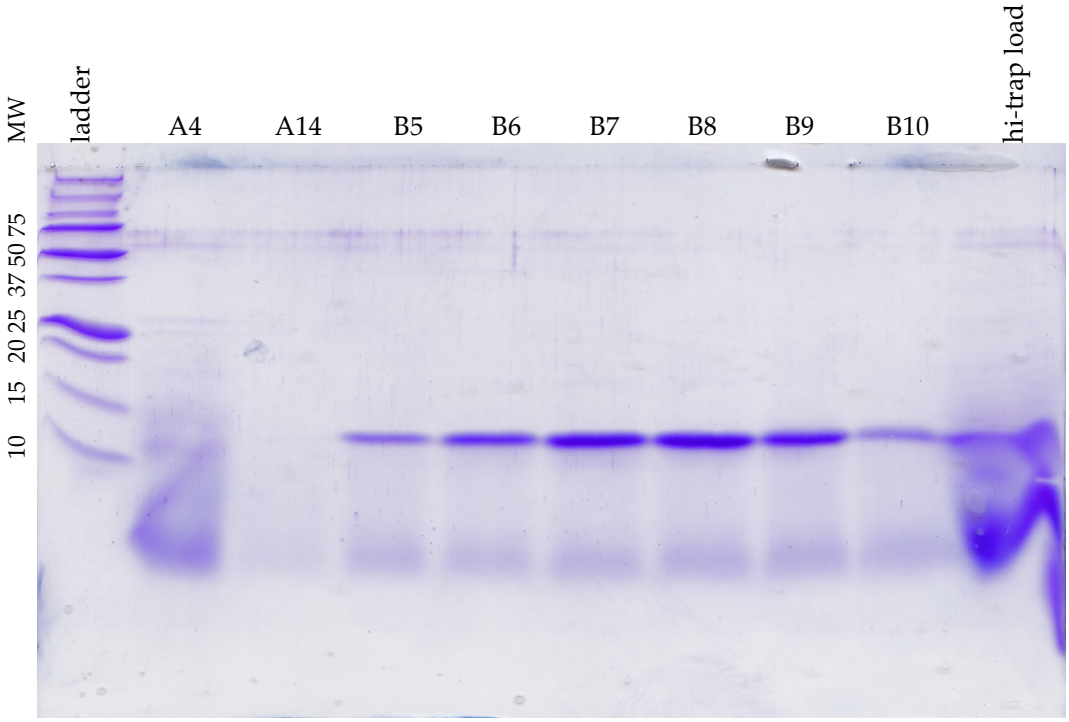

Figure 3.2 – SDS-PAGE gel of I51V CEC protein purification

The above gel shows small proteinaceous fragments in the CEC eluant. Hence, to ensure correct concentration measurements and ensure purity, a SEC step was included to further purify barnase.

Figure 3.3 shows the trace for a large-scale S75 16/60 purification. The resulting fractions (usually 80-88 mL fractions, as indicated with black arrow below peak in Figure 3.3) were then dialysed and/or concentrated as needed and concentrations measured (Section 2.5.1).

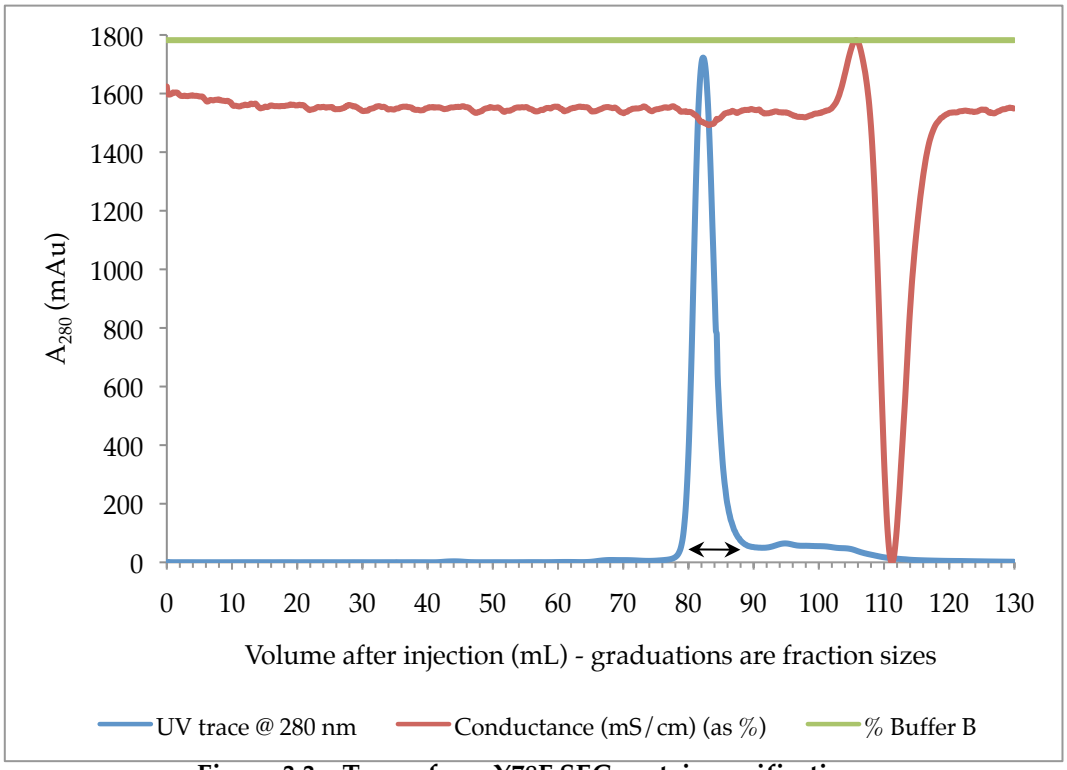

Figure 3.3 – Traces from Y78F SEC protein purification

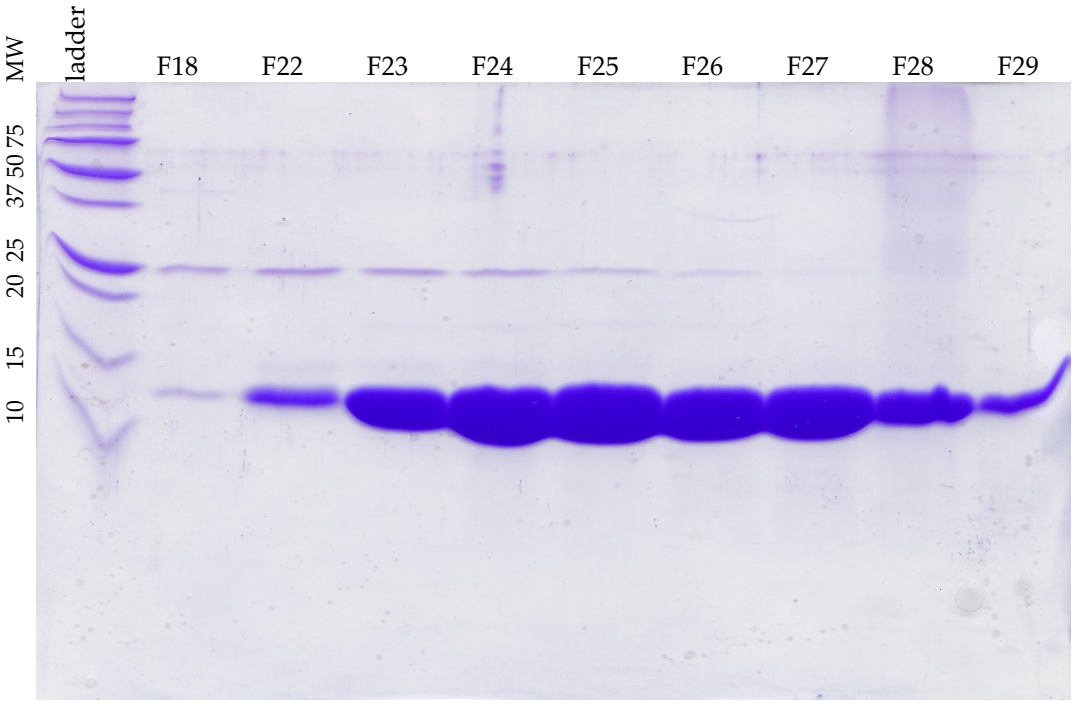

Figure 3.4 – SDS-PAGE gel of I88V SEC protein purification

Above, F18 is the slight bump at 68 mL, and F22-29 cover 76-92 mL from the large-scale S75 16/60 purification. This is indicative of the pattern seen on all size-exclusion eluant gels; mature barnase predominates at ~12.5

kDa and there is a small band at ~25 kDa that decreases in intensity through the main peak (see Section 3.2.1.4).

Final yields (in mg/L of culture) are tabulated below. The variation in yield was mainly due to the length of incubation of the expression culture, the cell density of the overnight culture used for inoculation and the experience of the operator increasing with time.

Preparation	WT	S80C/A43C	Y78F	I51V	I88V	L89V
Yield (mg/L)	12	75	12	0.9	124	103

Table 3.1 – Final yields of WT and mutant barnase

3.2 Characterisation of WT and Mutants

3.2.1 Mass Spectrometry (MS)

3.2.1.1 Full Protein Results

Whole WT and whole S80C/A43C (DM) barnase solutions were analysed as in Section 2.5.2. The following ions (M^+ and M^{2+} for singly and doubly-charged ions) were observed, compared with the theoretical mass (M):

Sample	**M (Da)**	**MH^+ (Da)**	**M^+-M (Da)**	**MH_2^{2+} (Da)**	**$2MH_2^{2+}$ (Da)**
WT	12382.7	12375.9	-6.8	6183.2	12366.4
S80C/A43C	12430.8	12419.0	-11.8	6205.6	12411.2

Table 3.2 – Whole-protein MALDI-TOF MS results for WT and DM barnase

These results, coupled with those to follow, show complete sequence expression and purification of WT barnase, as the MH^+ ion is within 0.05% of the theoretical mass for both samples. Additionally, the doubly-charged MH_2^{2+} ions still show a protein mass within 0.2% of that expected.

3.2.1.2 Peptide Digest Results

Identity of barnase variants was confirmed via gel extraction, tryptic digestion and MS (Section 2.5.2). Results are tabulated below, giving the degree of fragment coverage for each mutant and the reference for the top hit. It should be noted that fragments unambiguously showing I88V and

L89V mutations were not matched and hence LIFT™ analysis was performed (see below). Full results are in Appendix C.

Sample	Intensity Coverage (%)	Sequence Coverage (%)	MASCOT Score	Sequence Reference
WT	74.8	89.1	119.0	(Buckle et al., 1993)
S80C/A43C	62.7	92.7	152.0	(Clarke & Fersht, 1993)
Y78F	93.4	86.4	150.0	(Chen et al., 1993)
I51V	83.4	89.1	140.0	(Buckle et al., 1993)
I88V	78.0	95.5	207.0	(Buckle et al., 1993)
L89V	90.6	77.3	143.0	(Buckle et al., 1993)

Table 3.3 – WT and mutant tryptic digest mass spectrometry results

3.2.1.3 LIFT™ Results for I88V and L89V

LIFT™ MS/MS analysis was performed on the 1387.6 Da MH^+ parent ions for residues 88-98 of both I88V and L89V. The L89V MS/MS fragmentation pattern was unambiguously matched to the full barnase mutant (Buckle et al., 1993) with a MASCOT score of 38.0, but I88V also falsely matched to the L89V fragmentation pattern. When an *in silico* fragmentation of the I88V parent ion (BioTools, Bruker Daltonics, USA) was compared with the experimental fragmentation pattern, it was found to be an unambiguous match incorporating the fragmentation of a valine residue at the N-terminus.

3.2.1.4 Unknown ~25 kDa SDS-PAGE Band Analysis

A ~25 kDa band was excised from an SDS-PAGE gel of I88V (lane F23 from Figure 3.4) and analysed as in Section 2.5.2. The tryptic digest fragmentation showed an intensity and sequence coverage of 30.9% and 56.4% respectively and a MASCOT score of 66.7 for I88V barnase (Buckle et al., 1993). The band seen might be a dimer of barnase, as the SDS-PAGE weight is approximately 2 x 12382.7 Da. It also purifies before the main monomeric barnase peak in size exclusion (see Figure 3.4), although the band is not seen on the cation exchange trace or gel (Figure 3.1 & Figure 3.2). Barnase is not known to form dimers in solution and, as the SDS gel

band intensity and UV absorption in traces is low, the effect of this species on concentration measurements and assays is thought to be negligible.

3.2.2 Rotavirus RNA RNAse Assays

The RNAse activity of barnase was checked using rotavirus RNA as per Section 2.5.3.2. Figure 3.5 is a 5% urea denaturing gel comparing WT barnase with two non-RNase protiens (10ML200 and GA13), as well as with RNAse inhibitor.

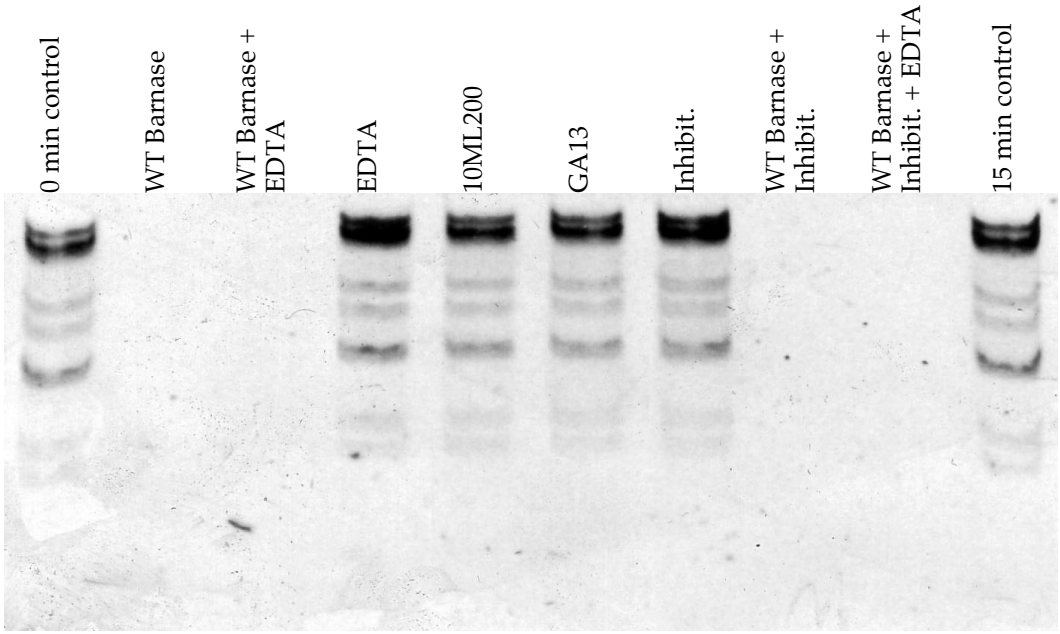

Figure 3.5 – RNAse assay screen of WT barnase

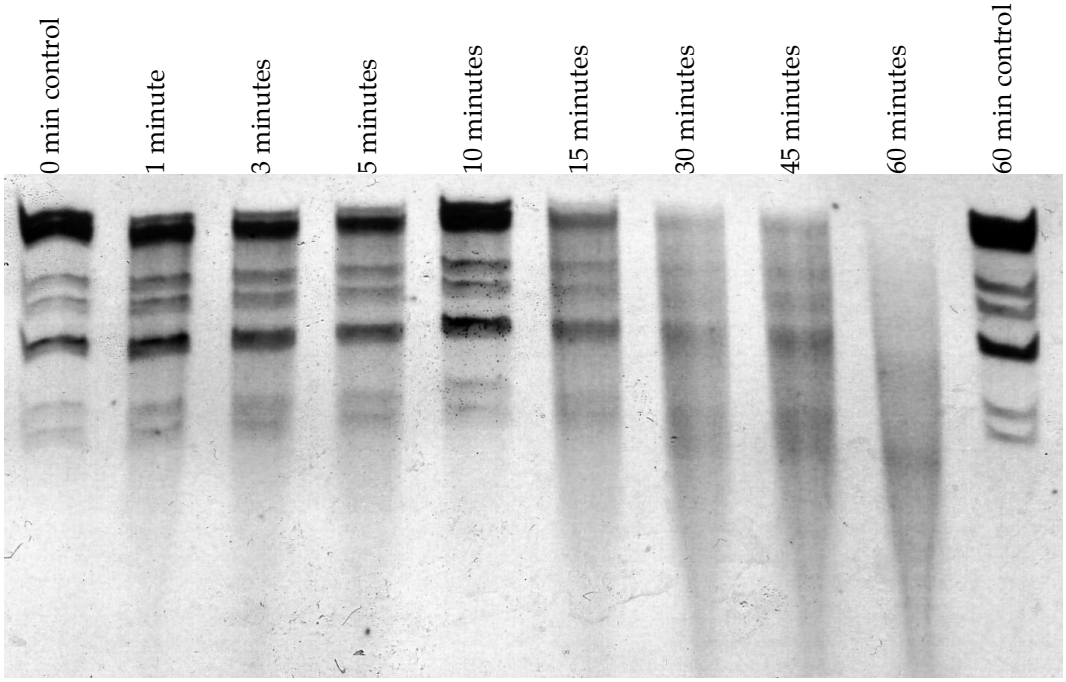

Figure 3.6 – RNAse assay time-course of WT barnase activity

Figure 3.6 shows a time-course of WT barnase acting upon rotavirus RNA as per section 2.5.3.3. The two assays show that barnase cleaves rotavirus RNA at 37 °C, yet is not affected by RNAse inhibitor or EDTA (therefore is not metal-ion dependent). Hence, RNAse inhibitor was used in preparations in this thesis to exclude alternative RNAse contamination (RNase A, T1 etc.). It is also shown that barnase is not highly sequence specific, as all rotavirus RNA bands are digested in the time-course assay and in the +ve lanes for Figure 3.5. The preference for GpN sequences still holds, however (see Section 1.3.2).

3.2.3 SYPRO™ Real-time Melts

Protein melts of WT and mutant barnase were performed as in Section 2.5.4. However, I51V was at 78.4 μg/mL (c.f. 280 μg/mL) due to low expression yield. From average traces with backgrounds subtracted, T_m values are determined from the steepest part of the face of the curve (Figure 3.7). ΔT_m is the difference from the WT (Table 3.4). Uncertainties are estimates based on experimental error and visual inspection accuracy.

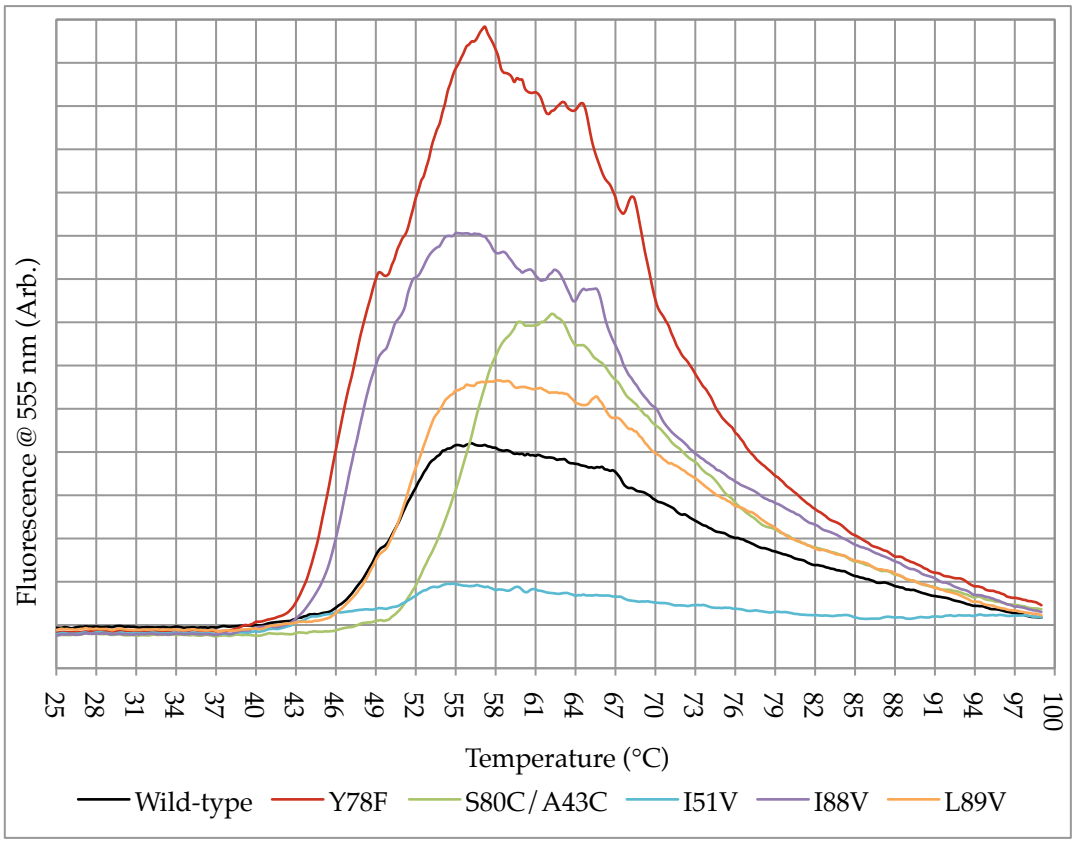

Figure 3.7 – Average SYPRO™ real-time melts for WT and mutant barnase

The bumps on each trace in Figure 3.7 at ~49.5 °C are present across all mutants. It is unlikely that they reflect an actual property of barnsae, as the pathway of folding is well-known and the mutations made (e.g. I88V) (Buckle et al., 1993) should change the temperature of any related peaks. It is likely just an artefact of the dye or method (RT-PCR machine etc.). I51V results are unreliable, due to the low fluorescence observed.

Variant	WT	S80C/A43C	Y78F	I51V	I88V	L89V
T_m (°C)	52.5 ± 0.5	57.0 ± 0.5	47.0 ± 0.5	53.0 ± 0.5	48.0 ± 0.5	52.5 ± 0.5
ΔT_m (°C)	–	4.5 ± 1.0	-5.5 ± 1.0	0.5 ± 1.0	-4.5 ± 1.0	0.0 ± 1.0

Table 3.4 – T_m values for WT and mutant barnase from differential SYPRO™ melts

3.2.4 Circular Dichroism

Circular dichroism work was performed as in Section 2.5.5. The CD signal of WT and mutant barnase was followed from 20-70 °C at 230 nm (Figure 3.8), with full wavelength (200-260 nm) scans performed at the extremes (Figure 3.9). In Table 3.5, uncertainties are the largest (+ve or –ve) 95% confidence interval from fitting, and for T_m are greater than the experimental error in temperature (0.1 °C). ΔH_{VH} is the enthalpy of unfolding. Values should be more precise than stated, as fitting errors are mainly due to data noise (Prabhu & Sharp, 2005; Vuilleumier et al., 1993). General data noise (see Figure 3.8) is due to the high concentration (0.1 M) of assay buffer causing CD voltage to increase, compensating for signal loss. The high buffer concentration was to ensure thermostability measurements were made under the same conditions as the EM assays.

Variant	WT	S80C/A43C	Y78F	I51V	I88V	L89V
T_m (°C)	54.5 ± 0.4	59.4 ± 0.9	50.7 ± 0.7	50.0 ± 0.3	50.9 ± 0.4	53.8 ± 0.4
ΔT_m (°C)	–	4.9 ± 1.3	-3.8 ± 1.5	-4.5 ± 1.0	-3.6 ± 0.7	-0.7 ± 0.8
ΔH_{VH} (kJ mol^{-1})	572.0 ± 95.3	503.7 ± 131.8	427.7 ±106.0	561.2 ±85.4	573.4 ±98.1	507.1 ±72.5
R^2 of fit	0.9895	0.9797	0.9728	0.9912	0.9876	0.9921

Table 3.5 – T_m values for WT and mutant barnase from circular dichroism unfolding

Data in Figure 3.8 were corrected for background signal and fitted to a two-state model for unfolding (Section 2.5.5.2). Figure 3.9 was also background corrected and illustrates the peak followed at 230 nm, due to

residue W94 (Sancho & Fersht, 1992). The data is very noisy below 210 nm as the voltage had to increase, amplifying noise, to compensate for the high buffer background signal. All data for CD is in Appendix C.

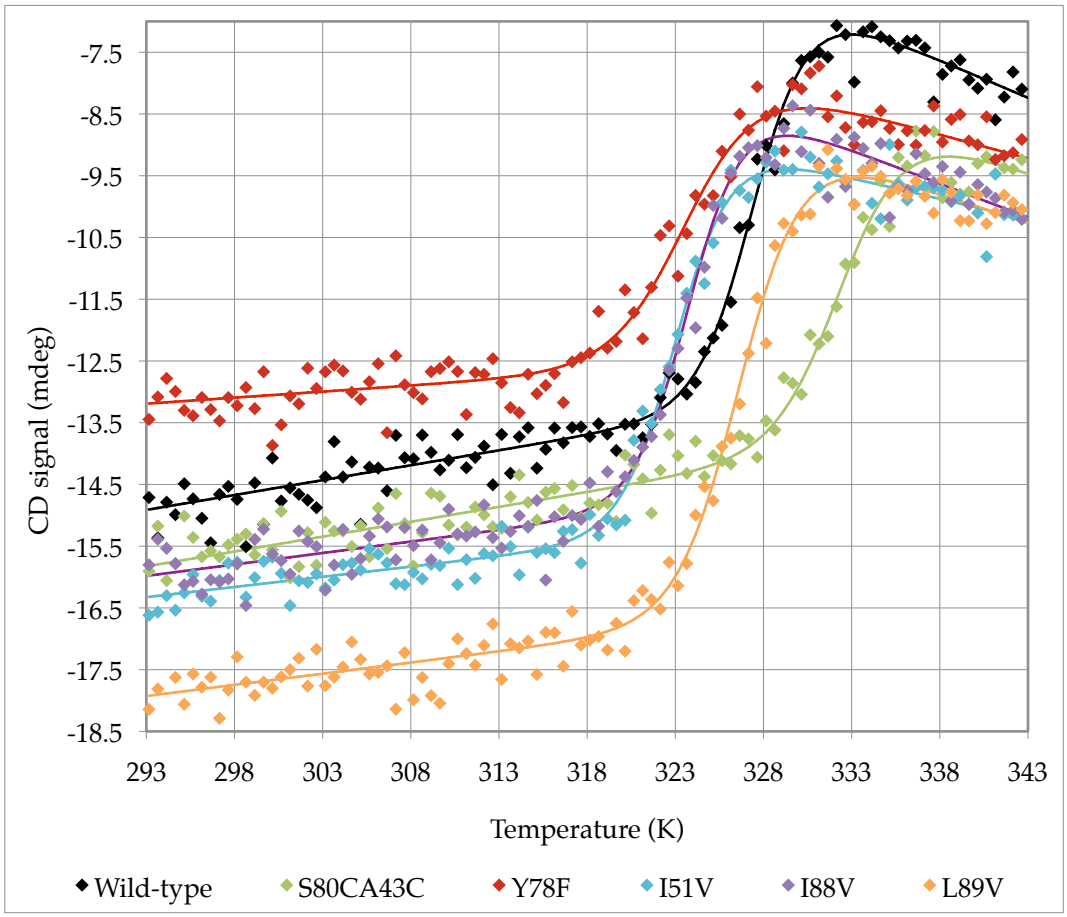

Figure 3.8 – Fitted circular dichroism signal data for WT and mutant barnase unfolding

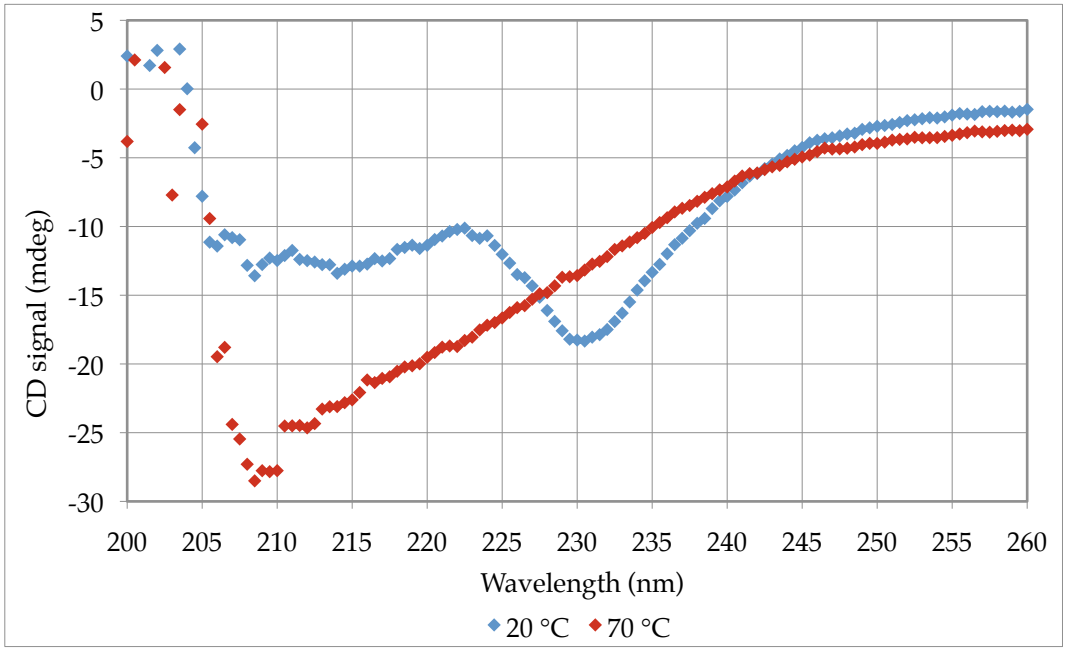

Figure 3.9 – 20 (folded) and 70 °C (unfolded) circular dichroism wave scans of WT

3.2.4.1 Refolding Scans of WT Barnase

Similar to scans as in Figure 3.8, WT barnase was refolded via scanning from 40-70 °C and back to 40 °C again, after a 1 minute delay at 70 °C (Figure 3.10).

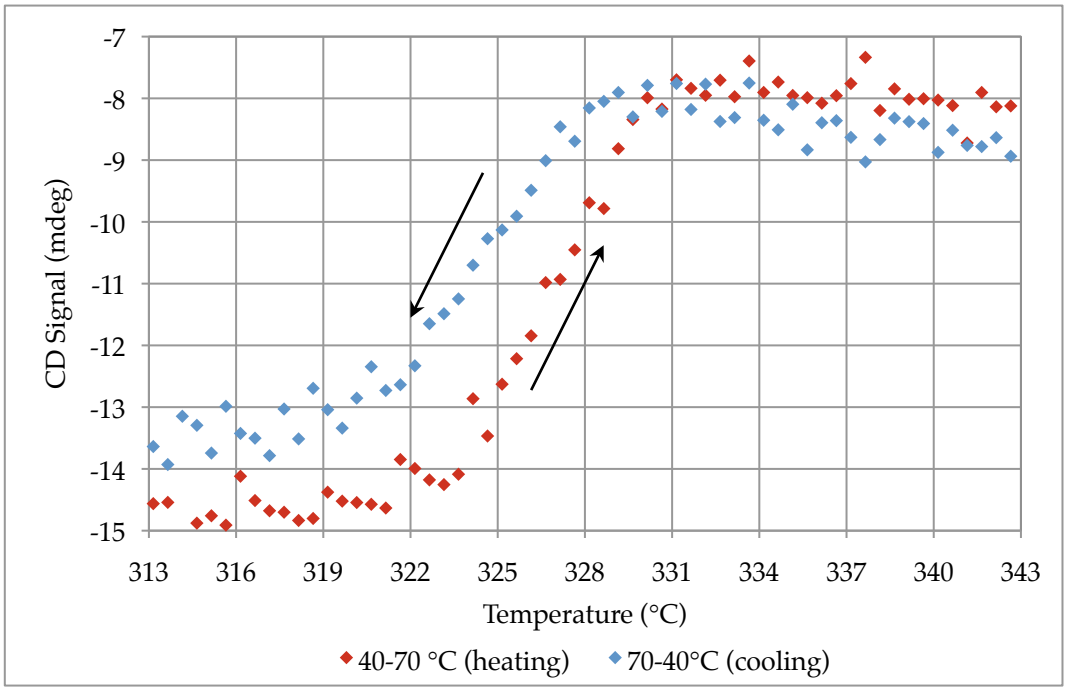

Figure 3.10 – Circular dichroism refolding scan of WT barnase between 40-70 °C

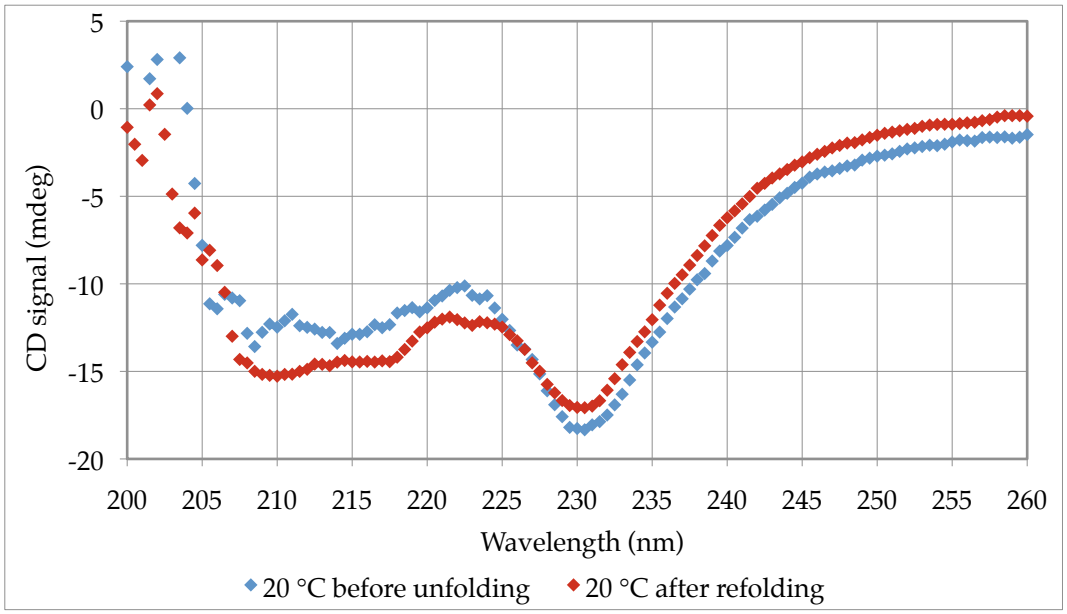

Figure 3.11 – 20 °C circular dichroism wave scans of WT barnase before and after refolding

Figure 3.10 shows the refolding of barnase. As the temperate gradient was quick at 1 °C/minute, there is a suspected delay in the signal. This leads to

an ~2 °C delay in the signal, meaning both traces may overlap in reality. In addition, although barnase is stable in assay buffer, it may not have the optimal conditions for refolding. Figure 3.11 shows the same sample before and after the 40-70-40 °C refolding measurements at 20 °C (the first 20-40 °C was quickly scanned for Figure 3.10 due to time constraints). It should be noted that the CD voltage does not linearly change with wavelength or between runs, and hence the two runs are only qualitatively comparable. This work shows how barnase can renature in solution without chaperones, making it a possible exception to the original EM, which only allows for irreversible denaturation (see Section 1.3.3.3).

3.2.5 Differential Scanning Calorimetry

Differential scanning calorimetry (DSC) was performed as in Section 2.5.6. The heat capacity (C_p) of WT and mutant barnase was recorded over the range 20-95 °C and data was fitted to a two-state model for unfolding (Section 2.5.6.2) for the 30-80 °C range due to artefacts occurring at low and high temperatures. Data files are in Appendix C; baselined and normalised raw data (for comparison of mutants) is shown in Figure 3.12.

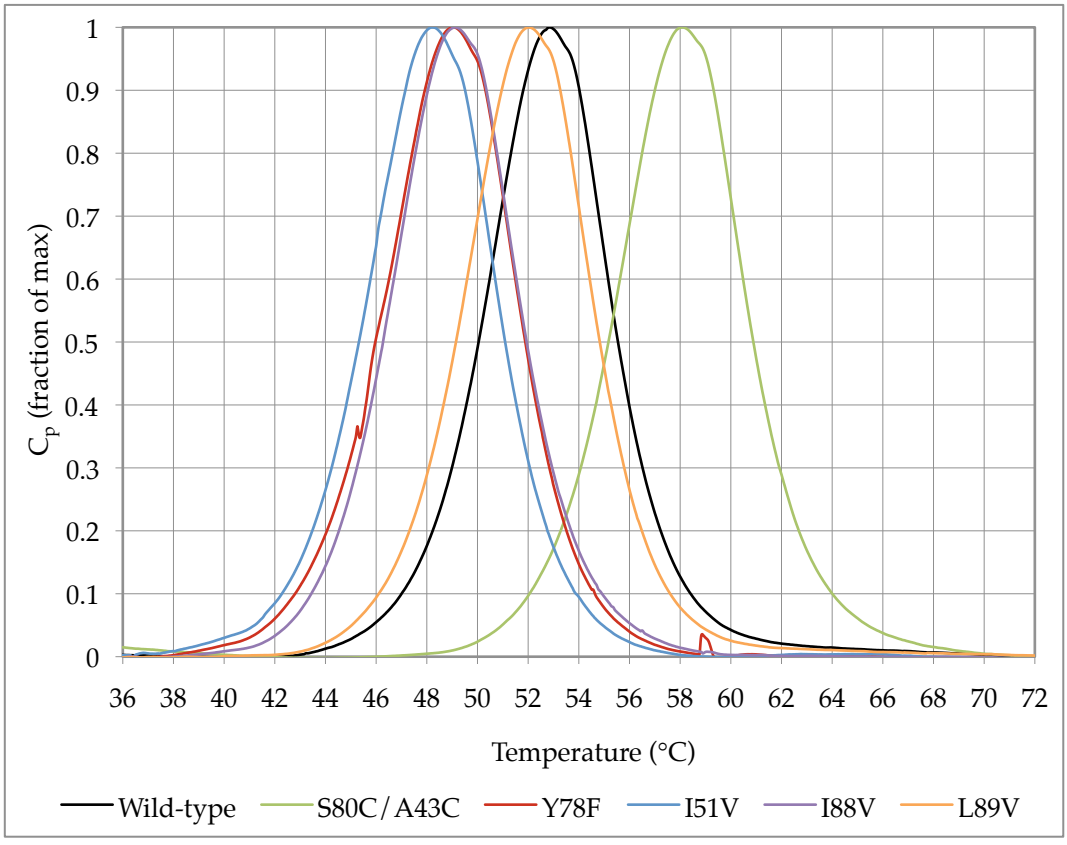

Figure 3.12 – Differential scanning calorimetry scans of WT and mutant barnase

Variant	WT	S80C / A43C	Y78F	I51V	I88V	L89V
T_m (°C)	52.9 ± 0.1	58.1 ± 0.1	49.0 ± 0.1	48.3 ± 0.1	49.2 ± 0.1	52.1 ± 0.1
ΔT_m (°C)	–	5.2 ± 0.1	-3.9 ± 0.1	-4.6 ± 0.1	-3.7 ± 0.1	-0.8 ± 0.1
ΔH_{VH} (kJ mol^{-1})	562.2 ± 0.3	557.8 ± 0.2	523.6 ± 0.3	525.8 ± 0.3	546.7 ± 0.2	546.7 ± 0.2
R^2 of fit	0.9999	0.9999	0.9999	0.9999	0.9999	0.9999

Table 3.6 – T_m values for WT and mutant barnase from DSC

In Table 3.6, uncertainties are the largest (+ve or –ve) 95% confidence interval from fitting. For DSC this is over-estimated to be ± 0.1 °C for T_m to allow for experimental errors, as the fitting error was ± 0.01 °C on average. ΔH_{VH} is the Van 't Hoff enthalpy change. Raw data, not fitted data, was plotted in Figure 3.12 due to the high degree of accuracy in the fitting, as shown by the R^2 values of 0.9999 for all the variants.

3.2.6 Summary of Thermostability Results

Due to the suspected lag in CD signal behind temperature (Section 3.2.4.1), it should be noted that the relative T_m compared with the WT (ΔT_m) is most important, not the absolute T_m. For the absolute value, the accuracy of DSC (Table 3.6) is considered most applicable (Martinez et al., 1994).

	ΔT_m from WT (°C)				
Variant	S80C / A43C	Y78F	I51V	I88V	L89V
SYPRO™	4.5 ± 1.0	-5.5 ± 1.0	0.5 ± 1.0	-4.5 ± 1.0	0.0 ± 1.0
CD	4.9 ± 1.3	-3.8 ± 1.5	-4.5 ± 1.0	-3.6 ± 0.7	-0.7 ± 0.8
DSC	5.2 ± 0.1	-3.9 ± 0.1	-4.6 ± 0.1	-3.7 ± 0.1	-0.8 ± 0.1

Table 3.7 – Summary of ΔT_m from WT for barnase mutants between three methods

Figure 3.13 shows the concordance of CD and DSC measurements compared with the values obtained via the differential SYPRO™ method. It should be noted that Figure 3.7 shows how low the I51V fluorescence was, which is likely the cause of the non-concordant SYPRO™ value in Figure 3.13. The relatively large error in CD measurements has been considered elsewhere (Section 3.2.4), and is probably erroneous. The agreement between determined T_m values and the urea denaturation free energy differences (the same trends are seen) (see Section 1.3.3.2) lends

support to the validity of T_m results. As expected, the T_m of the DM is raised significantly, which may aid in decoupling activity from stability if the T_{eq} of barnase variants is not affected by the mutations (see Section 3.3.4 and Section 4.3). Also, if the L89V mutation lowers T_{eq}, a similar decoupling may be seen as the T_m of L89V is very similar to the WT.

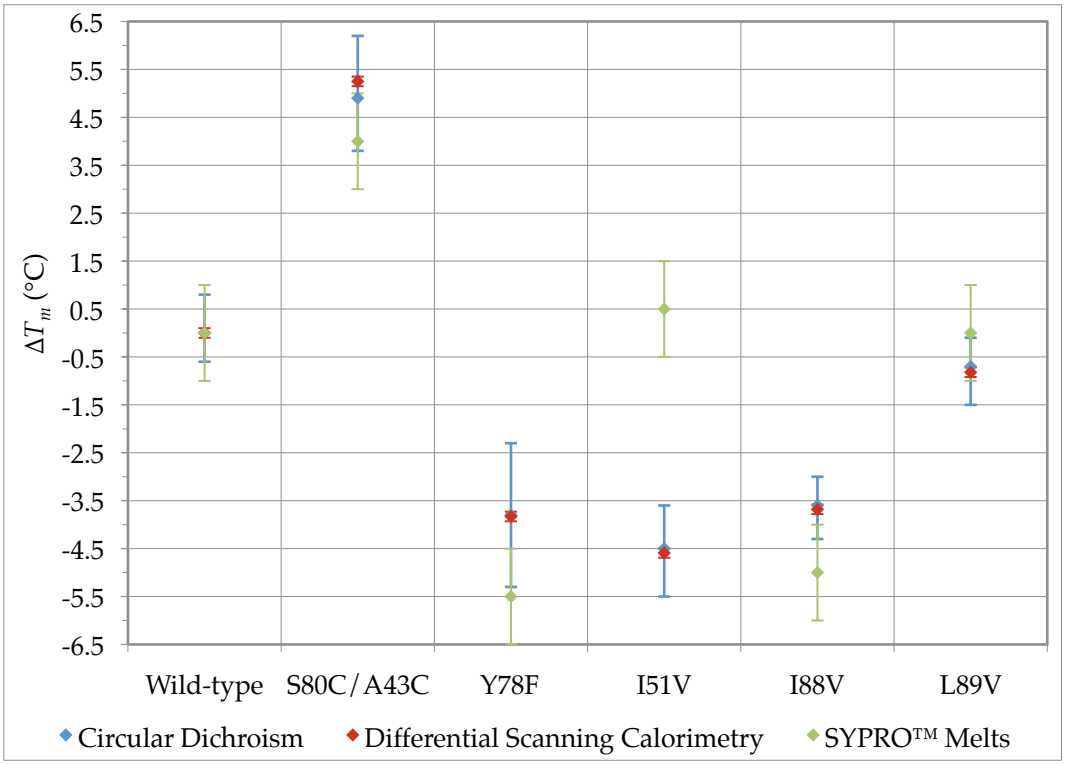

Figure 3.13 – Comparison of ΔT_m from WT for barnase mutants between three methods

Although the Van 't Hoff enthalpy of unfolding is not directly considered in the original EM (Section 1.2.2.1), it could be important for alternative models (Section 4.1) if reversible refolding equilibria are present. Table Table 3.8 summarises the ΔH_{VH} values for the variants of barnase as determined using DSC. CD measurements of ΔH_{VH} had large errors associated with fitting the pre- & post-transitional slopes and are not included.

	ΔH_{VH} (kJ mol^{-1})					
Variant	WT	S80C / A43C	Y78F	I51V	I88V	L89V
DSC	562.2 ± 0.3	557.8 ± 0.2	523.6 ± 0.3	525.8 ± 0.3	546.7 ± 0.2	546.7 ± 0.2

Table 3.8 – Summary of ΔH_{VH} from WT for barnase mutants from DSC measurements

3.3 Original Equilibrium Model Assays

3.3.1 Initial Dinucleotide Trials

3.3.1.1 Experimental

To gather WT barnase data for fitting to the original equilibrium model, the enzymatic hydrolysis of GpUp was measured according to Section 2.6.1. The change in absorbance (ΔA_{257}) for the GpUp substrate was minimal – a change of +0.04 absorbance units was seen for full hydrolysis of 200 μM GpUp. Hence, assay runs had to be highly accurate and baseline corrections were important. The option of following cleavage at higher wavelengths (as in Day et al., 1992) was excluded as protein (barnase) could possibly interfere and the ΔA would still be approximately the same. In any case, linearity of absorbance with concentration was suspect at high concentrations (> ~400 μM) as A_{257} became greater than 1.

The literature K_M for GpUp in 0.1 M acetate buffer (pH 5.8) was previously measured at 25 °C and found to be 19.9 ± 2.0 μM (Day et al., 1992). A K_M determination at 46 °C (approximately the temperature optimum of barnase with GpUp) was performed, as in Section 2.6.1.3.

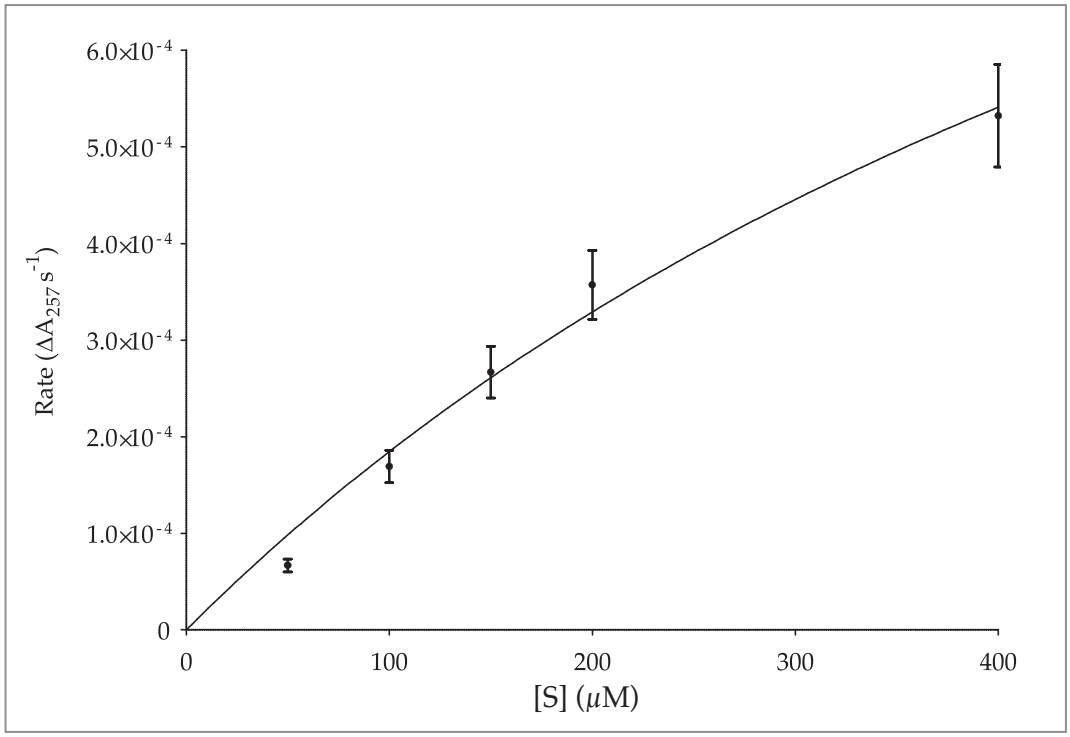

Figure 3.14 – K_M determination at 46 °C for GpUp and WT barnase

Concentrations of substrate > 400 μM were insoluble, but the fit (although not conclusive as V_{max} was not approached) gave a K_M of 725.6 ± 337.1 μM. The uncertainty in K_M is the standard error, as 95% confidence intervals were not determined. Hence, assays for GpUp were at < 10 x K_M (200 μM) for a significant portion of the temperature range (see Section 2.7.1.1).

3.3.1.2 MATLAB fitting.exe Results

Data points were acquired (Section 2.6.1.2), processed (Section 2.7.1.2) and used for fitting to the original EM as in Section 2.7.2. The best-fit output parameters are given below for WT barnase. The full data set was acquired over 5 minutes, with truncated data sets being fitted using the same methodology for 60 s, 30 s and t_0 lengths (Section 1.2.3.1).

Length of Data	Full	60 s	30 s	t_0
$\Delta G^{\ddagger}_{cat}$ **(kJ mol^{-1})**	62.62 ± 0.15	63.67 ± 0.10	63.84 ± 0.16	64.10
$\Delta G^{\ddagger}_{inact}$ **(kJ mol^{-1})**	93.33 ± 0.27	90.03 ± 0.43	88.96 ± 0.86	–
ΔH_{eq} **(kJ mol^{-1})**	71.76 ± 0.04	106.3 ± 3.3	121.9 ± 6.5	155.6
T_{eq} **(K)**	295.8 ± 1.0	313.2 ± 0.8	314.9 ± 1.0	315.6
SSE	1.35x10^{-4}	4.09x10^{-6}	5.75x10^{-7}	1.47x10^{-11}
R^2 of fit	0.9457	0.9724	0.9699	0.9664

Table 3.9 – Output parameters for WT barnase and GpUp substrate for the original EM

Uncertainties are the largest (+ve or –ve) 95% confidence interval from fitting; there are no statistics available from t_0 runs. SSE is the total sum of squares for the fitting. The full data set did not fit well to the model. At long times (> ~120 seconds) the data showed lower rates than expected, most likely due to substrate depletion or product inhibition. The shorter times did not account for ΔH_{eq} or $\Delta G^{\ddagger}_{inact}$ as precisely because there were less data points available. The 60-second data outputs from the fitting.exe program are in Figure 3.15, and full statistical analyses for each parameter (histograms) output from fitting.exe are in Appendix C.

As an example of fitting.exe output, Figure 3.15 shows the data (blue lines) against the fitted EM product profile curve on the left; the residuals (difference between the fitted curve and the data) in the middle; and the simulated rate curve (the derivative of the product curve) on the right. 0-60 axis is time (s), 280-340 axis is temperature (K) and vertical axes are [P] (left-hand and middle plots) and rate (V_{max}) (right-hand plot).

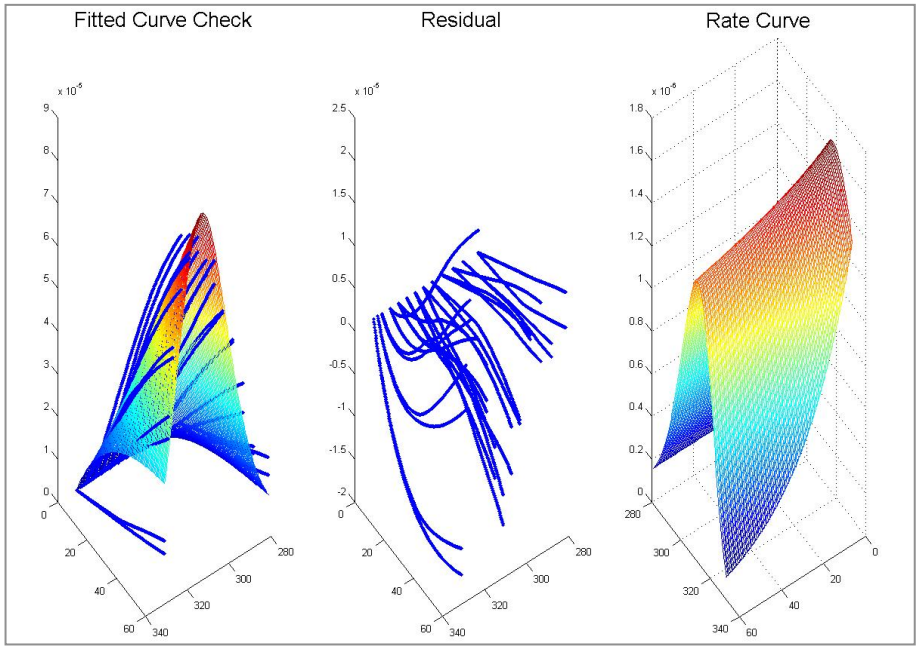

Figure 3.15 – Fitting.exe output figures for WT barnase with GpUp (60 s data set)

It was decided that, with the K_M at 46 °C for the WT being more than 30 x that at 25 °C, testing mutants against the substrate would likely lead to similarly high K_M values or worse. Corrections with Equation 2.5 for K_M are still not ideal as they introduce another processing step and associated errors, and in some instances the measured V would be several orders of magnitude below V_{max}, magnifying errors. Issues with substrate solubility and maximum absorbances compounded the problems, and led to the investigation of an alternative substrate.

3.3.2 Fluorogenic Substrate Characterisation

An alternative substrate has previously been used for the analysis of MazF (Wang & Hergenrother, 2007), with the CrGAC motif at the cleavage site (see Section 1.3.2). The authors found that fluorescence increases proportionately to [P]. The ex./em. maxima for FrG were found to be 485/518 nm respectively via 3D scans of excitation and emission (Section 2.6.2.5). This also holds for the product halves (Fluorophore & Quench).

3.3.2.1 Real-time Melts

Melts of the FrG product halves were performed as in Section 2.6.2.3. Figure 3.16 shows the heating and cooling of the fluorophore and the quench halves at 10 μM (maximum product concentrations/initial substrate concentrations in the EM assays) in assay buffer. Temperatures were scanned from 25-99 °C and back to 25 °C with a 1 minute pause at 99 °C.

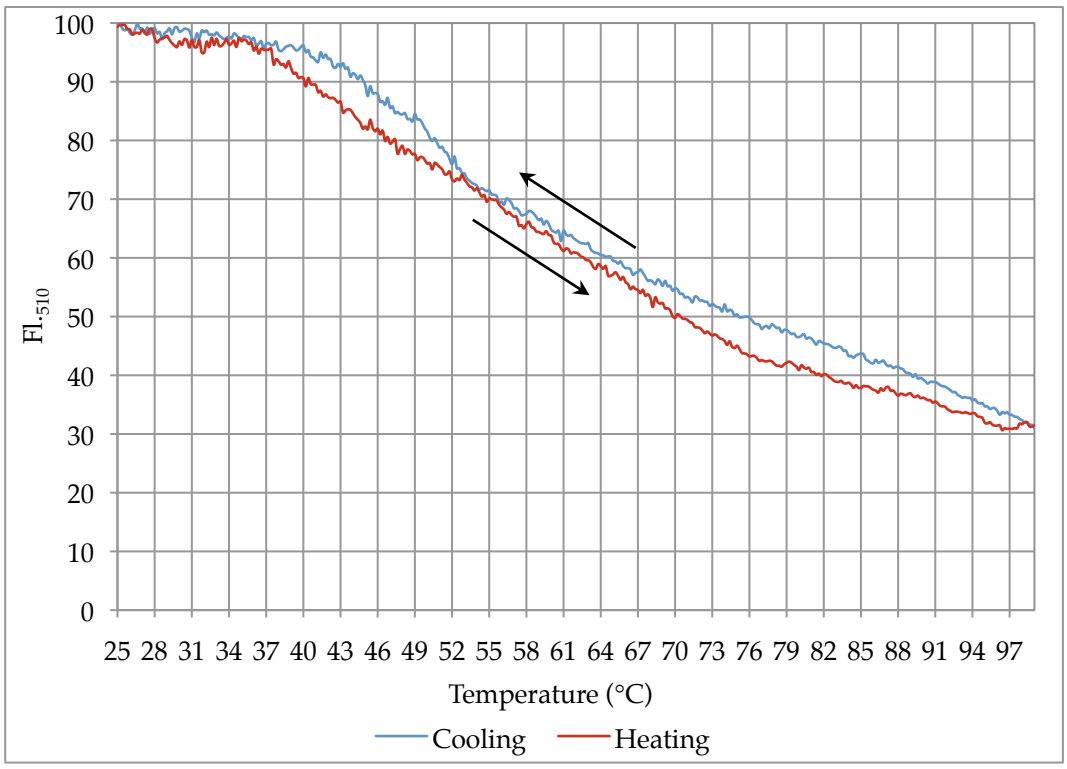

Figure 3.16 – Real-time melts of FrG substrate 25-90-25 °C in assay buffer

Fluorescence is plotted on an arbitrary scale. This plot demonstrates that the FrG substrate is not susceptible to a significant degree of temperature-induced cleavage or photobleaching, as the cooling plot is only slightly higher in fluorescence than that for heating. However, the amount of fluorescence is not linear with temperature and must be corrected for when converting fluorescence to product concentration, [P], for MATLAB fitting procedures (see Section 2.7.1.3).

3.3.2.2 Linearity of Fluorescence with Concentration

Standards ranging from 10 μM FrG substrate to 10 μM products were wave-scanned as in Section 2.6.2.5 at 25 °C and 50 °C (Figure 3.17 & Figure

3.18). Legend is ratio substrate:product in μM. The maximal values at 518 nm were plotted against concentration of the product (not shown) and found to be linear with increasing [P] ($R^2 = 0.9985$ for 25 °C and 0.9973 for 50 °C. Hence, fluorescence at 518 nm ($Fl._{518}$) can be used as a proxy measure of [P] over a wide temperature range.

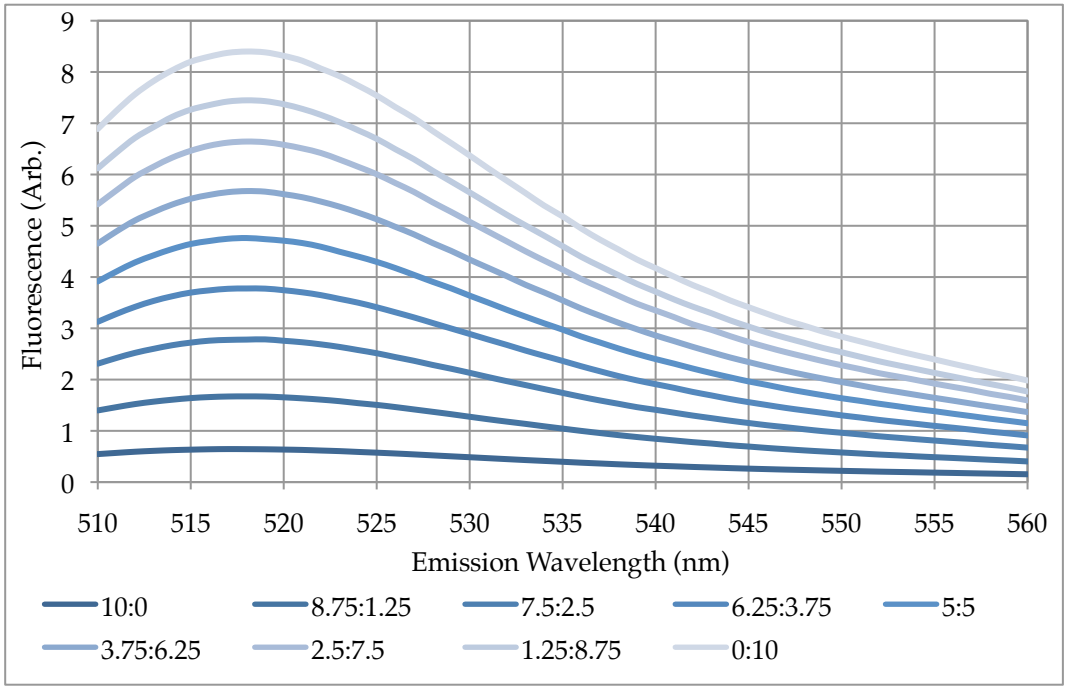

Figure 3.17 – Wave scan of increasing FrG product concentration at 26 °C

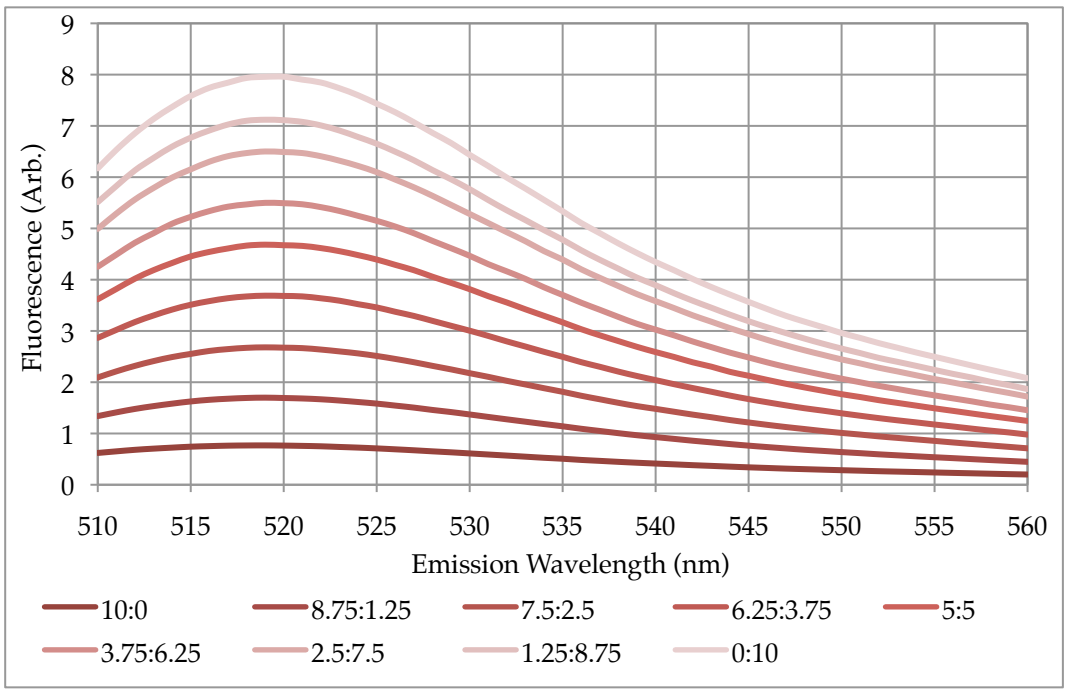

Figure 3.18 – Wave scan of increasing FrG product concentration at 50 °C

It should be noted that there was FrG substrate present in diminishing amounts to simulate "real" time points along the course of an enzyme assay. This is a deviation from the literature method (Wang & Hergenrother, 2007), where only the product halves were used.

3.3.3 Fluorogenic Substrate Assays (WT, DM and L89V)

3.3.3.1 Data Gathering and K_M Determinations

Assays were performed as in Section 2.6.2.6 for EM data collection, with approximately 1 nM of each barnase variant acting upon 10 μM of FrG over 2 minutes and a temperature range of 26-60 °C (see Table 3.10). K_M values were obtained using the methods in Section 2.6.2.7 and temperature-dependent changes were accounted for as part of data processing (Section 2.7.1.3) before data fitting. K_M plots for WT, DM and L89V barnase are on the following pages and the results are tabulated below. Due to time constraints, other barnase mutants were not assayed.

WT K_M determinations are given in Figure 3.19 and Figure 3.20. Data was very hard to acquire (hence the large ranges in values, see error bars) as the methodology for mixing enzyme was not yet perfected. For the DM K_M determinations, 10 x the concentration of enzyme was used, leading to much higher rates and substrate depletion. Hence, at higher [S], product inhibition was seen (Figure 3.21 and Figure 3.22) and those points were not fitted. For L89V K_M determinations a slight drop in K_M with temperature was seen just outside of error bounds. This is not usually observed (Thomas & Scopes, 1998) and potentially shows that the error in fitting the K_M curves does not represent the real, experimental inaccuracies. Changes in K_M were nonetheless accounted for in the data processing (Section 2.7.1.3) before data fitting. For both the DM and L89V variants, [S] is in M.

Variant	$[E_0]$ (nM)	K_M (25-26 °C) (μM)	K_M (50 °C) (μM)
WT	1.07	2.9 ± 1.2	5.3 ± 1.7
DM	1.04	5.1 ± 1.3	7.8 ± 0.8
L89V	1.07	3.5 ± 0.5	2.4 ± 0.4

Table 3.10 – K_M (at 25-26 & 50 °C) and $[E_0]$ values for WT, Dm and L89V EM assays

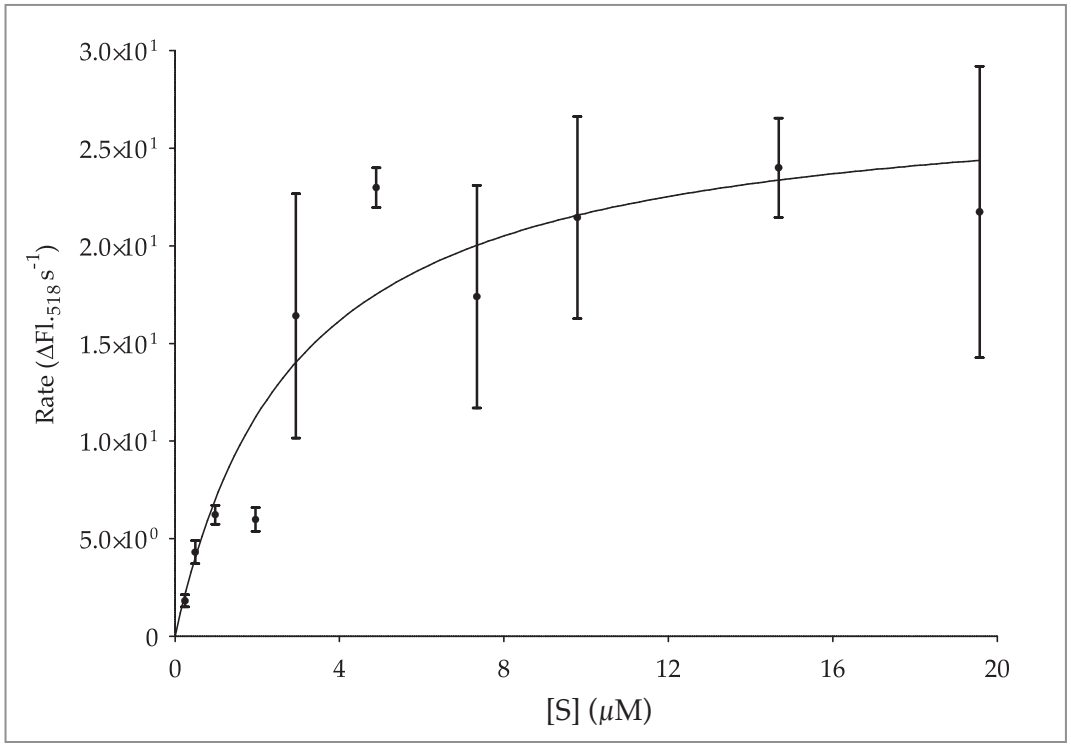

Figure 3.19 – K_M determination at 26 °C for FrG and WT barnase

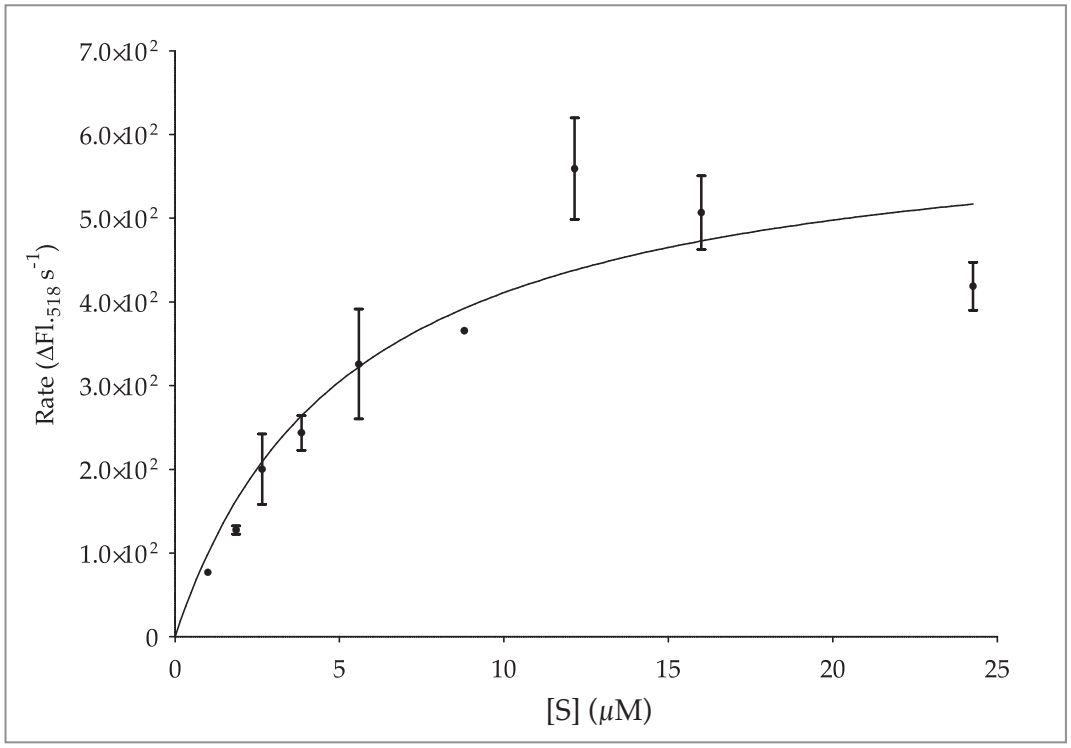

Figure 3.20 – K_M determination at 50 °C for FrG and WT barnase

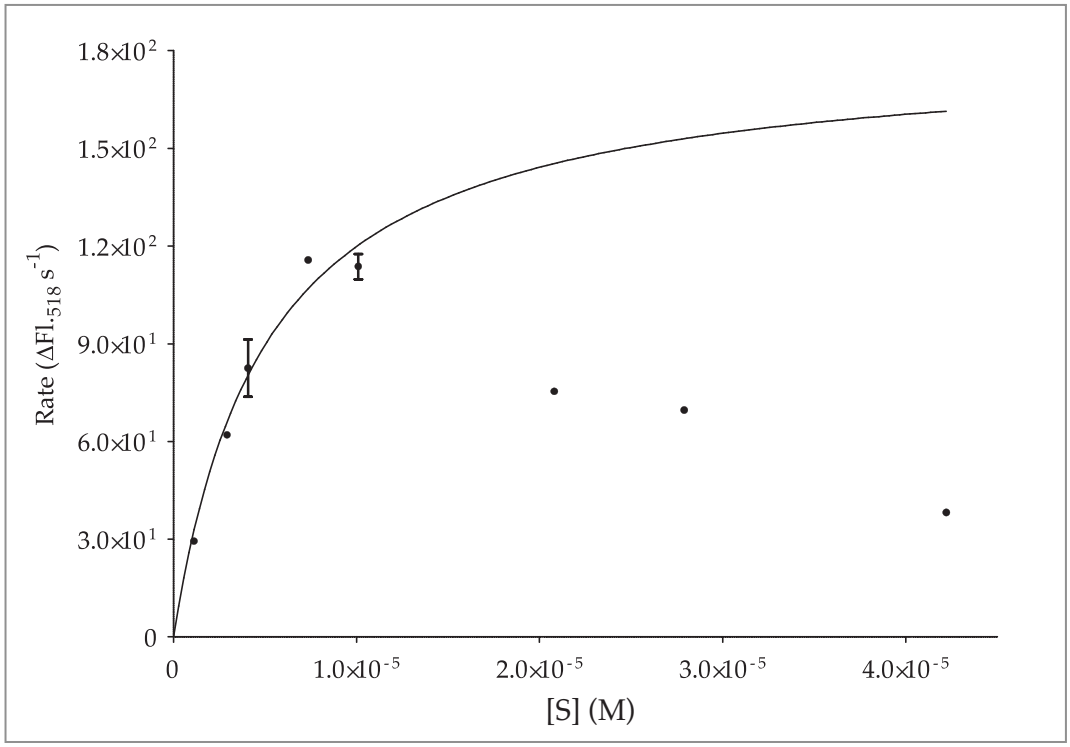

Figure 3.21 – K_M determination at 26.5 °C for FrG and DM barnase

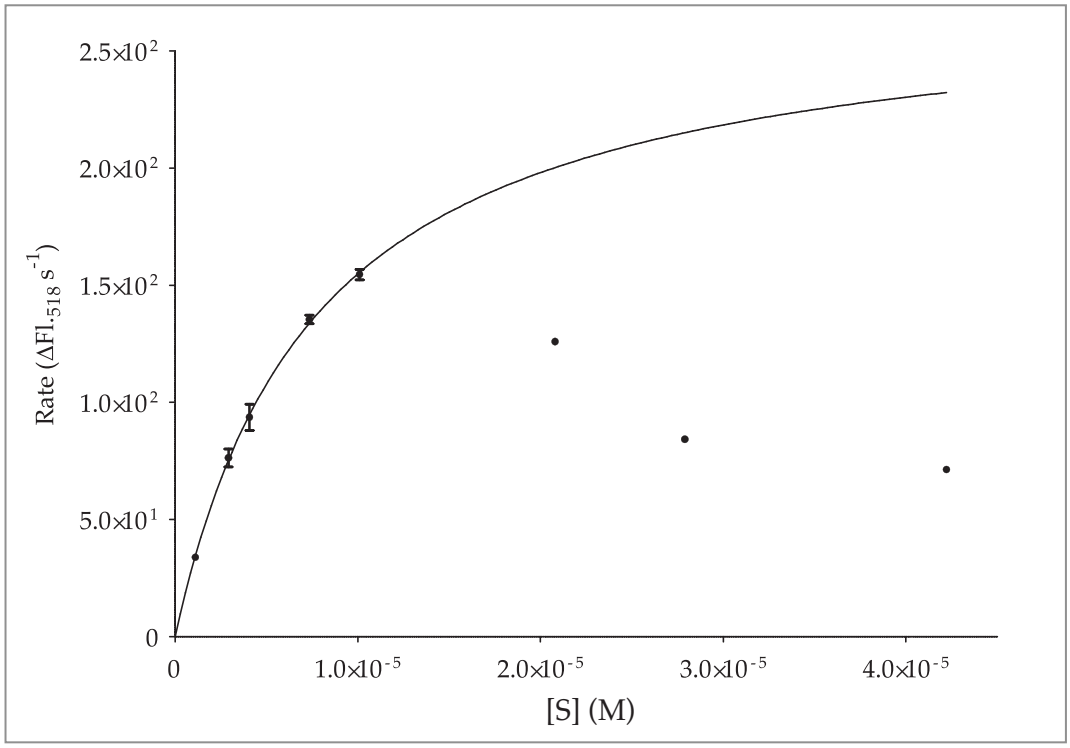

Figure 3.22 – K_M determination at 50 °C for FrG and DM barnase

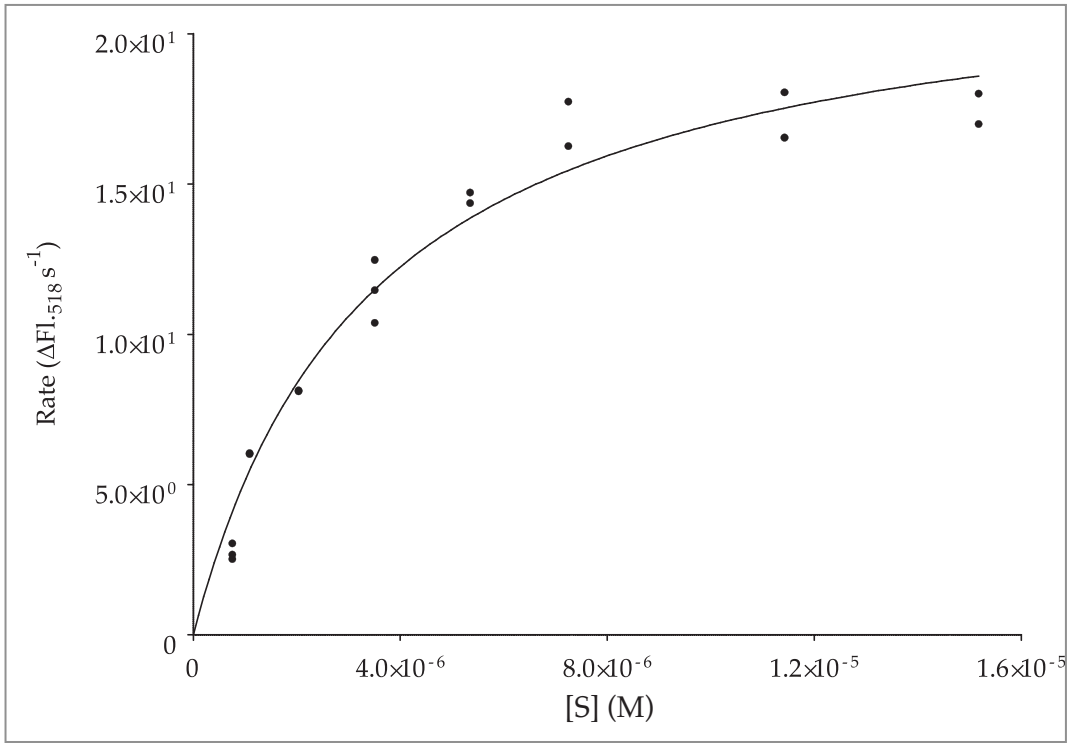

Figure 3.23 – K_M determination at 25 °C for FrG and L89V barnase

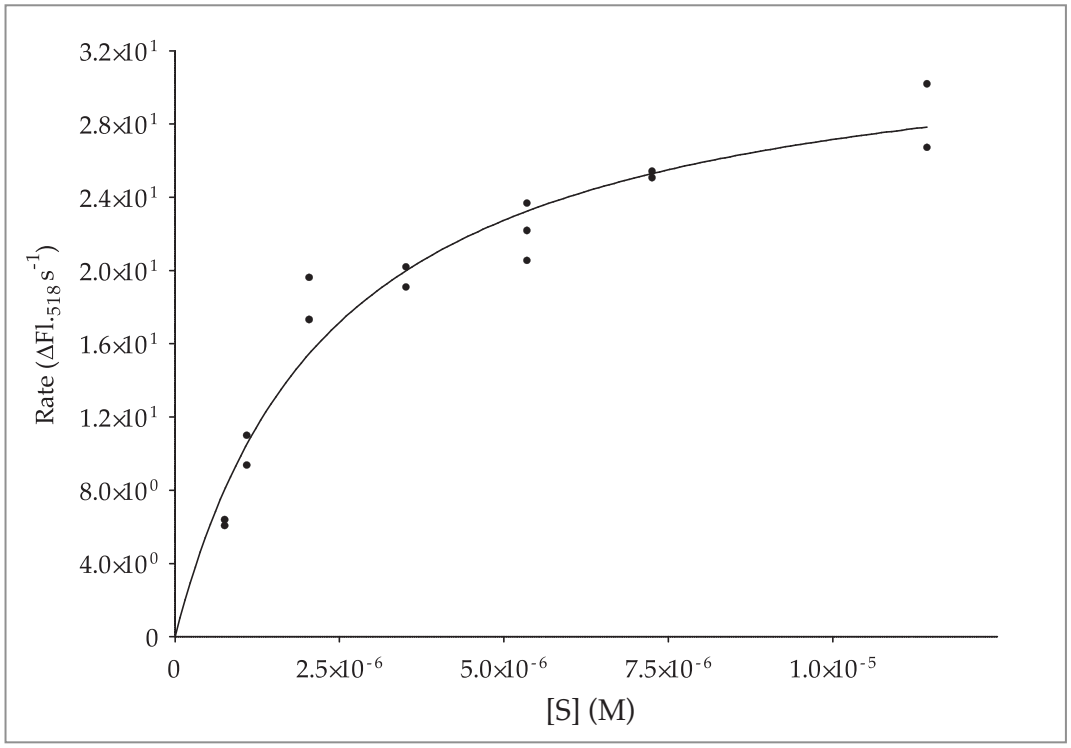

Figure 3.24 – K_M determination at 50 °C for FrG and L89V barnase

3.3.3.2 Fitting Results to the Original EM

Data were acquired for WT, DM and L89V barnase variants (see Section 3.3.3.1), processed as in Section 2.7.1.3 and then fitted to the original equilibrium model using fitting.exe. Using the MATLAB SurfaceFitting tool, the same data was fitted to the original EM (Section 2.7.3) for comparison and validation of the technique.

For the WT enzyme, four rounds of each fitting procedure was required to maintain parameters within their 95% confidence values. For all parameters below, uncertainties are the largest (+ve or –ve) 95% confidence interval from fitting and column headings have been described previously (Section 3.3.1.2).

Fitting Procedure	$\Delta G^{\ddagger}_{cat}$ (kJ mol^{-1})	$\Delta G^{\ddagger}_{inact}$ (kJ mol^{-1})	ΔH_{eq} (kJ mol^{-1})	T_{eq} (K)	SSE	R^2 of fit
fitting.exe	67.00 ± 0.05	92.06 ± 0.43	170.1 ± 4.7	315.7 ± 0.3	3.69x10^{-9}	0.9791
Surface Tool	67.09 ± < 0.01	92.51 ± 0.04	190.6 ± 0.3	315.8 ± < 0.1	4.76x10^{-10}	0.9995

Table 3.11 – Output parameters for WT barnase and FrG substrate for the original EM

For the DM enzyme, four rounds were required to maintain parameters within their 95% confidence values for fitting.exe and for the SurfaceFitting tool three rounds were necessary.

Fitting Procedure	$\Delta G^{\ddagger}_{cat}$ (kJ mol^{-1})	$\Delta G^{\ddagger}_{inact}$ (kJ mol^{-1})	ΔH_{eq} (kJ mol^{-1})	T_{eq} (K)	SSE	R^2 of fit
fitting.exe	65.84 ± 0.05	93.14 ± 0.59	142.7 ± 3.5	314.9 ± 0.3	7.74x10^{-9}	0.9910
Surface Tool	65.78 ± < 0.01	94.88 ± 0.03	146.7 ± 0.2	314.6 ± < 0.1	2.63x10^{-10}	0.9998

Table 3.12 – Output parameters for DM barnase and FrG substrate for the original EM

With L89V, five rounds of fitting.exe were required to maintain parameters within their 95% confidence values and for SurfaceFitting tool eight rounds were necessary. This shows how the number of fitting rounds is not a reflection on how well the data finally fits the model (see R^2 values) but is more an indication of how the different parameters

compensate for one another and can "mask" the effects of each other, making fitting troublesome. There is an element of user input into the fitting process, mainly in the choice of starting parameters and the quality-assurance in deciding wether data is accurate with regards to K_M, product inhibition and other experimental sources of error (see Section 2.7).

Fitting Procedure	$\Delta G^{\ddagger}_{cat}$ (kJ mol^{-1})	$\Delta G^{\ddagger}_{inact}$ (kJ mol^{-1})	ΔH_{eq} (kJ mol^{-1})	T_{eq} (K)	SSE	R^2 of fit
fitting.exe	66.09 ± 0.07	91.44 ± 0.43	174.2 ± 5.5	317.2 ± 0.4	9.89x10^{-9}	0.9787
Surface Tool	65.96 ± 0.01	90.18 ± 0.03	160.0 ± 0.4	316.7 ± 0.1	1.04x10^{-9}	0.9996

Table 3.13 – Output parameters for L89V barnase and FrG substrate for original EM

The tables above show how both fitting procedures give good statistical fits to the data, with R^2 values between 0.9787 and 0.9998. There is more certainty in the parameters output using the SurfaceFitting tool procedure (as reflected in the smaller errors, sum of squared errors (SSE) and larger R^2 values), but, once experimental errors are considered, this becomes negligible (see Section 3.3.4). Except for ΔH_{eq}, there is good agreement in all the other parameters between fitting processes; this exception is also considered later.

Figure 3.25, Figure 3.26 & Figure 3.27 (next page) show the output plots for the fitting.exe method for WT, DM & L89V barnase and the FrG substrate respectively, as in Figure 3.15. Data points (blue lines) are shown against the fitted EM product profile curve on the left; the residuals (difference between the fitted curve and the data) are in the middle; and the simulated rate curve (the derivative of the product curve) is on the right. 0-150 axes are time (s), 290-340 axes are temperature (K) and vertical axes are [P] (left-hand and middle plots) and rate (V_{max}) (right-hand plot). All statistical analyses of output parameters are given in Appendix C.

The key figure of these is the residual plot. An ideal fit would give random traces of minimal amplitude either side of the zero-rate plane. In the case of the variants (next page), there is clearly a systematic tendency to have positively curving residuals from data points at 320-330 K and negatively curving ones above 330 K. This is considered in Section 4.1.

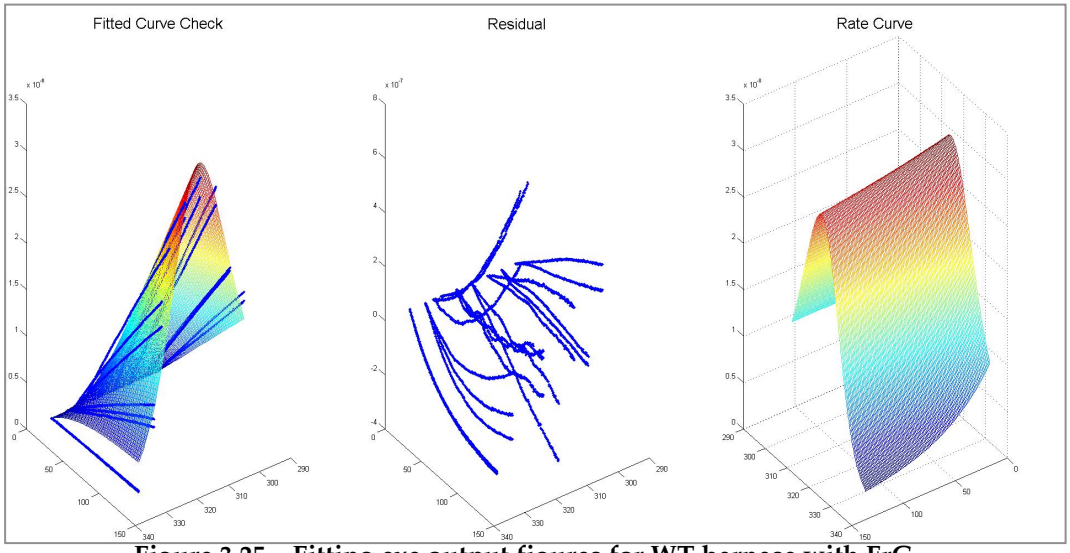

Figure 3.25 – Fitting.exe output figures for WT barnase with FrG

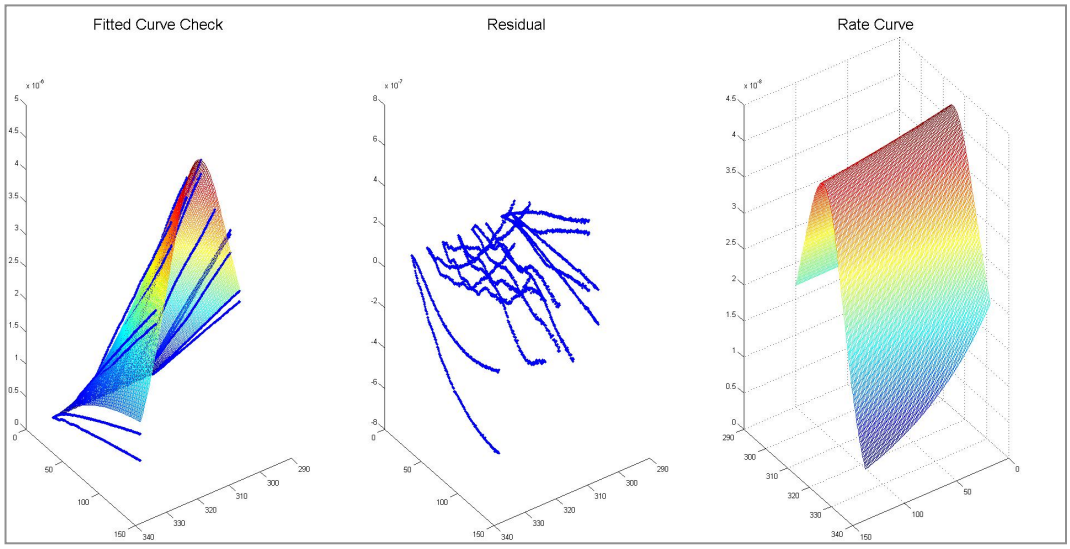

Figure 3.26 – Fitting.exe output figures for DM barnase with FrG

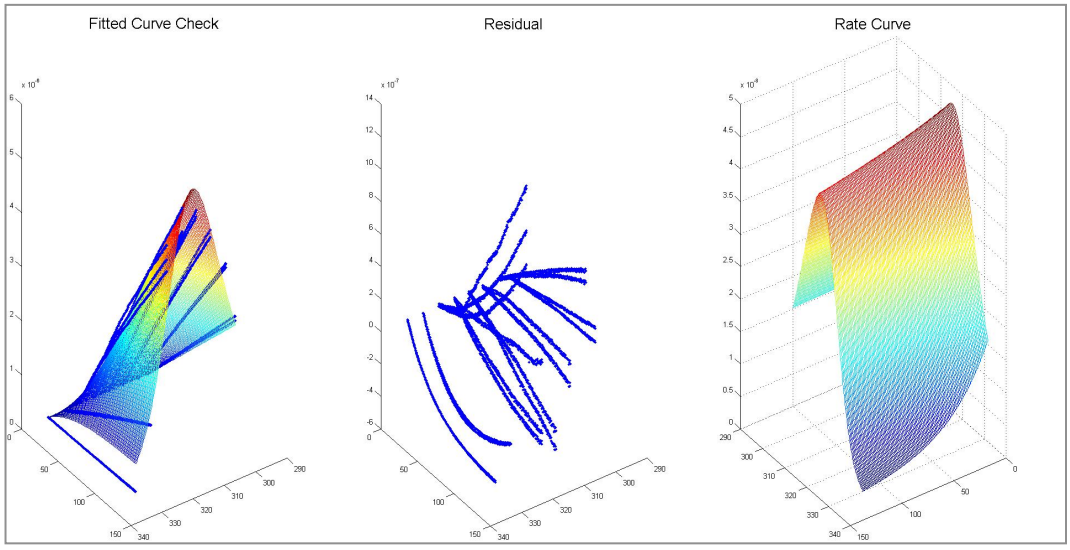

Figure 3.27 – Fitting.exe output figures for L89V barnase with FrG

Data points at temperatures below 320 K show more straight deviations from the fitted product curve – these indicate random error as the amplitude is small (especially compared with data points above 320 K) and they deviate in a linear fashion. This could be caused by inaccuracies in the amount of enzyme added in individual runs, as opposed to an actual deviation from the EM kinetics. Aside from showing that the original EM does not fit well at high temperatures, this could point to the reversible denaturation properties of barnase conflicting with the irreversibility implied in the EM kinetics (see Section 4.1).

3.3.4 Discussion of Output Parameters for WT, DM and L89V Barnase

The results from Section 3.3.3 are amalgamated below for comparison, this time with experimental errors in addition to fitting errors (the last section only included errors derived from the fitting procedures). Experimental error has been dealt with in detail previously (Peterson et al., 2007), finding a maximum of 0.5% deviation in $\Delta G^{\ddagger}_{cat}$, $\Delta G^{\ddagger}_{inact}$ & T_{eq} and 6% in ΔH_{eq} experimentally. This thesis follows those guidelines. Values that are significantly different between the WT and a mutant (do not overlap within stated error) are in italics.

Variant	Fitting Procedure	$\Delta G^{\ddagger}_{cat}$ (kJ mol^{-1})	$\Delta G^{\ddagger}_{inact}$ (kJ mol^{-1})	ΔH_{eq} (kJ mol^{-1})	T_{eq} (K)
Wild-type	fitting.exe	67.00 ± 0.39	92.06 ± 0.89	170 ± 15	315.7 ± 1.9
	Surface Tool	67.09 ± 0.35	92.51 ± 0.50	191 ± 12	315.8 ± 1.7
S80C / A43C (DM)	fitting.exe	*65.84 ± 0.38*	93.1 ± 1.1	143 ± 12	314.9 ± 1.9
	Surface Tool	*65.78 ± 0.34*	*94.88 ± 0.50*	*146.7 ± 9.0*	314.6 ± 1.7
L89V	fitting.exe	*66.09 ± 0.40*	91.44 ± 0.89	174 ± 16	317.2 ± 2.0
	Surface Tool	*65.96 ± 0.34*	*90.18 ± 0.48*	*160 ± 10*	316.7 ± 1.7

Table 3.14 – Summary of output parameters for WT and mutant barnase

Compared with the WT, both mutants have marginally significant drops in $\Delta G^{\ddagger}_{cat}$. At 42 °C (~315 K, approximately the T_{eq} of all variants) however,

where no variant is more than 1% denatured (see Section 3.2.6), the change in $\Delta G^{\ddagger}_{cat}$ amounts to a 41-65% increase in k_{cat} (due to the exponential terms in Equation 1.1). Increases in catalytic rate due to non-active site mutations are common (for example, Schanstra et al., 1997). This finding is apparent when the simulated EM rate plots are overlaid (using output parameters from fitting.exe) as the mutants have "taller" rate profiles at their maximal values (Figure 3.28).

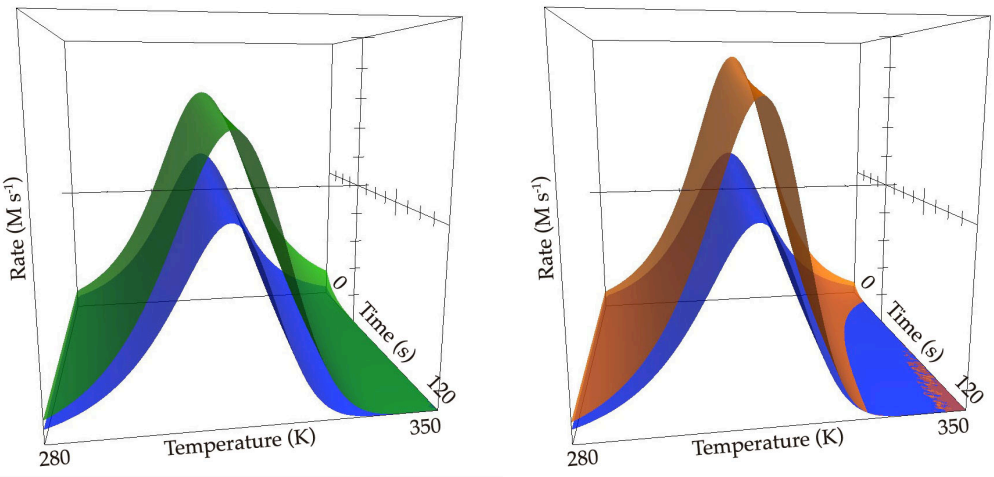

Figure 3.28 – (Left) Simulated rate profiles of WT (blue) and DM (green) barnase & (Right) Simulated rate profiles of WT (blue) and L89V (orange) barnase

Table 3.14 also highlights the variability in ΔH_{eq} values. Although T_{eq} never differs by more than 0.5 K between the fitting procedures, ΔH_{eq} can vary between procedures relatively more so (although the values all match within stated errors). This reflects the difficulty in fitting ΔH_{eq} in that a large change in ΔH_{eq} can be partially compensated for by very small changes in the $\Delta G^{\ddagger}_{cat}$ and $\Delta G^{\ddagger}_{inact}$ parameters.

It should be noted (and particularly with the SurfaceFitting tool derivations) that, compared with the WT enzyme, the value of $\Delta G^{\ddagger}_{inact}$ decreases for L89V and increases for the DM. These relative changes are expected, but the magnitude of each change does not match the literature or experimental values (see Table 1.2 and Section 3.2.6 respectively). As discussed in Section 4.3, this implies that the model has not taken the true denaturation properties of each enzyme into account. Hence, the other parameters (which are all connected in Equation 1.15) might have compensated for this incorrect value and, therefore, are possibly incorrect.

4 Theory and Modelling of the Equilibrium Model

To help understand how the kinetic description of the EM fits to the assay data sets (Section 3.3), several different models were derived to cover the most likely kinetic situations for denaturation from the E_{act}/E_{inact} equilibrium species (Section 4.1). These models were fitted to an ideal data set and the WT barnase data set (from Section 3.3.3) to compare an irreversibly and reversibly denaturing enzyme, respectively (Section 4.2). To benchmark dynamics measurements of assayed enzymes and validate the mathematics behind the model derivations, equations to simulate the concentrations of species with time and temperature were derived and analysed using model output parameters (Section 4.3).

4.1 Derivation of Alternative Models

The equilibrium model (EM) fits well with experimental data analysed to date (Section 1.2.3.2). Barnase, despite hypotheses to the contrary (Section 1.3.3), also fits the model kinetics satisfactorily, although not so well at high temperatures above T_{eq} (Section 3.3.3.2). However, the physical basis for the E_{act}/E_{inact} equilibrium is not known and, although the EM more accurately describes experimental data compared with the classical kinetics approach (Section 1.1.3), there is no evidence for what is implied by the mathematics. As stated before (Section 1.4.2), if a model is given enough degrees of freedom to fit a data set, then that model will fit the data even if the mathematics behind the kinetics do not accurately describe what is physically happening.

As covered in Section 1.2.2.1, the original EM assumes denaturation from the E_{inact} species only (Daniel et al., 2001) (see Table 4.1). This implies that the E_{inact} species is on-path to denaturation, and could be thought of as an intermediate state that is populated in a temperature-dependent manner. Hence, if other models were developed with alternate species schemes, it was hoped that the experimental data would fit best to those that most accurately represent the changes that are physically happening.

4.1.1 Species Schemes and Rate Equations for Alternate Models

Model names are arbitrary, as the letters M-R were available as variables in the program Grapher (see Appendix B) that was used for comparison and simulation of the product and rate curves for each model.

Model	Species Scheme	Rate Equation
EM	$E_{act} \overset{K_{eq}}{\rightleftharpoons} E_{inact} \xrightarrow{k_{inact}} X$	$V_{max} = \frac{k_{cat} \cdot [E_0]}{1 + K_{eq}} \cdot \exp\left(\frac{-k_{inact} \cdot K_{eq} \cdot t}{1 + K_{eq}} \right)$
O	$X \xleftarrow{k_{deact}} E_{act} \overset{K_{eq}}{\rightleftharpoons} E_{inact}$	$V_{max} = \frac{k_{cat} \cdot [E_0]}{1 + K_{eq}} \cdot \exp\left(\frac{-k_{deact} \cdot t}{1 + K_{eq}} \right)$
P	$X \xleftarrow{k_{deact}} E_{act} \overset{K_{eq}}{\rightleftharpoons} E_{inact} \xrightarrow{k_{inact}} X$	$V_{max} = \frac{k_{cat} \cdot [E_0]}{1 + K_{eq}} \cdot \exp\left(\frac{-\left(k_{inact} \cdot K_{eq} + k_{deact}\right) \cdot t}{1 + K_{eq}} \right)$
M	$\left[E_{act} \overset{K_{eq}}{\rightleftharpoons} E_{inact} \right] \xrightarrow{k_{inact}} X$	$V_{max} = \frac{k_{cat} \cdot [E_0]}{1 + K_{eq}} \cdot \exp\left(-k_{inact} \cdot t\right)$
N	$\left[E_{act} \overset{K_{eq}}{\rightleftharpoons} E_{inact} \right] \underset{k_{react}}{\overset{k_{inact}}{\rightleftharpoons}} X$	$V_{max} = \frac{k_{cat} \cdot [E_0]}{1 + K_{eq}} \cdot \left(1 - \frac{k_{inact}}{A} \cdot \left(1 - \exp\left(-A \cdot t\right)\right) \right)$ where: $A = k_{inact} + k_{react}$
R	$E_{act} \overset{K_{eq}}{\rightleftharpoons} E_{inact} \underset{k_{react}}{\overset{k_{inact}}{\rightleftharpoons}} X$	$V_{max} = \frac{k_{cat} \cdot [E_0]}{1 + K_{eq}} \cdot \left(1 - \frac{D}{A} \cdot \left(1 - \exp\left(-A \cdot t\right)\right) \right)$ where: $D = \frac{k_{inact} \cdot K_{eq}}{1 + K_{eq}}$ & $A = \frac{k_{inact} \cdot K_{eq}}{1 + K_{eq}} + k_{react}$
Q	$X \underset{k_a}{\overset{k_{-a}}{\rightleftharpoons}} E_{act} \overset{K_{eq}}{\rightleftharpoons} E_{inact} \underset{k_{-i}}{\overset{k_i}{\rightleftharpoons}} X$	$V_{max} = \frac{k_{cat} \cdot [E_0]}{1 + K_{eq}} \cdot \left(1 - \frac{D}{A} \cdot \left(1 - \exp\left(-A \cdot t\right)\right) \right)$ where: $D = \frac{k_a + k_i \cdot K_{eq}}{1 + K_{eq}}$ & $A = \frac{k_a + k_i \cdot K_{eq}}{1 + K_{eq}} + k_{-a} + k_{-i}$

Table 4.1 – Comparison of original EM to newly derived alternative models

For full derivations of all the models, including the original EM, see Appendix B. New rate constants are introduced in some variants, and are defined in the appendix also. The equations given in Table 4.1 can be extensively expanded, as explained in Appendix B, to include all the $\Delta G^{\ddagger}$, ΔH_{eq} and T_{eq} terms as required for fitting.

4.1.1.1 Models "O" and "P"

Models O and P were derived to probe whether the assumption that E_{inact} is on-path to denaturation is valid. By reversing the situation compared to the original EM, model O implies denaturation through the E_{act} species (through a new rate constant k_{deact}). If it fits data better than the original EM, then the assumption of denaturation from E_{inact} made to date must be questioned. As E_{act} is more prominent at low temperatures due to the K_{eq} equilibrium (where the denaturation rate is known to be lower), the likelihood of denaturation purely occurring via this species is low. Model P allows for both routes to the denatured species (X), and hence fits for both k_{inact} and k_{deact} rates. It should fit well, as it allows for the equilibrium model as it stands, but ideally one of the two denaturation rates will be favoured. This may shed light on which species, if either, is on-path to denaturation. If neither rate is favoured over the other ($k_{inact} \approx k_{deact}$), then the model simplifies to the next case, model M.

4.1.1.2 Model "M"

Model M differs from those mentioned so far in that it treats the E_{act}/E_{inact} equilibrium pair as an ensemble, allowing denaturation from either species. The treatment implies that neither species is more on-path to denaturation than the other and, by corollary, implies that both the E_{act} & E_{inact} species are overall natively folded. In comparison, the original EM scheme (see Table 4.1) only absolutely implies this for the E_{act} species. As the E_{act}/E_{inact} equilibrium is no longer important for denaturation, compared with the original EM, the mathematics is simplified in the rate equation (compare with Equation 1.15). This removes two K_{eq} terms from the exponential, and hence makes fitting ΔH_{eq} and T_{eq} parameters much more direct. If model M fits data better than the original EM, it suggests either of two scenarios: a) that the speed of the E_{act}/E_{inact} equilibrium is so fast that assay data is insufficient to show if either species is on-path to

denaturation or b) that both species denature with equal rate constants and, hence, the original EM is unnecessarily complex.

4.1.1.3 Models "N, "R" and "Q"

No enzymes assayed prior to this thesis have exhibited reversible thermal denaturation. That is to say, the assumption of the original EM that *X* is a kinetic "trap" for denatured enzyme (as precipitate/aggregate or non-functional unfolded enzyme) holds true for the vast majority of enzymes (Stempfer et al., 1996). Barnase does renature (see Section 1.3.3.3), which could hypothetically repopulate the E_{act}/E_{inact} equilibrium and cause deviation from the original EM, O, P & M model kinetics. Model N allows for the re-population of an E_{act}/E_{inact} ensemble, yet is otherwise as in model M. It is theorised that the renaturation rate (k_{react}) will be substantially greater for reversibly denaturing enzymes such as barnase, yet essentially zero (have a large $\Delta G^{\ddagger}$ value) for irreversibly denaturing enzymes. Hence, model N is expected to be applicable to all enzymes, as the model should fit itself to data depending on the tendency to renature of the enzyme/substrate system being measured.

Model R is a compromise; on one hand the mathematics is more complicated, as the E_{act}/E_{inact} equilibrium has to be accounted for with regard to denaturation (compared with model N); but on the other hand, it means only one species is denaturing (E_{inact}), therefore maintaining the assumption that E_{inact} is on-path to denaturation. By definition, this should mean that the denaturation process is modelled to occur at a higher temperature. Hence, if the original EM holds true over model M for general enzymes, model R is the alternative model for renaturing enzymes such as barnase.

Model Q expands on models N and R by allowing for all possible routes to and from the denatured state. For clarity, k_{inact}, k_{react} and k_{deact} are replaced by k_i, k_{-i} and k_a respectively, with the renaturation rate constant of the k_a process being k_{-a}. Sub-script characters *a* and *i* are short for "active" and "inactive" respectively, the species they relate to. This model, whilst theoretically capable of fitting insignificant rates (very high $\Delta G^{\ddagger}$ values) to irrelevant processes, also has the potential to fit a data set incorrectly, due to the large number of degrees of freedom it contains (see Section 1.4.2).

The fitting of data sets to the model illustrates this possibility. In any case, it is expected that all the other models would be suitably limited cases that can encompass any enzyme/substrate data set when chosen correctly.

4.2 Comparison of Alternative Models

For both data sets fitted below, plots of the fits (curve+data and residuals) are available on the included CD-ROM, as listed in Appendix C.

4.2.1 Ideal Data Set

Model data for a ß-glucosidase from *Caldicellulosiruptor thermosaccharolyticus* (substrate *para*-nitrophenol-ß-D-glucopyranoside) was provided by Colin Monk (University of Waikato). This data set had no corrections for K_M or substrate stability and represents as close to raw data as possible. The data set was used as a fair test for comparing EM, O, P and M models, as well as to see if the reversible denaturation models would fit denaturing data sets, perhaps through fitting near-zero rate constants for irrelevant processes. Note that errors in the output parameters tabulated below are purely 95% confidence interval fitting uncertainties, as the data fits are most important when comparing the different models.

4.2.1.1 Original Model Fitting

This fitting was performed as in Section 2.7.2 & Section 2.7.3 for fitting.exe and SurfaceFitting tool processes respectively. E_0 was 5.86×10^{-7} M.

Fitting Procedure	$\Delta G^{\ddagger}_{cat}$ (kJ mol^{-1})	$\Delta G^{\ddagger}_{inact}$ (kJ mol^{-1})	ΔH_{eq} (kJ mol^{-1})	T_{eq} (K)	SSE	R^2 of fit
fitting.exe	78.50 ± 0.05	104.3 ± 0.2	131.1 ± 1.8	349.2 ± 0.4	8.42×10^{-4}	0.9918
Surface Tool	78.19 ± < 0.01	104.6 ± < 0.1	116.9 ± 0.1	346.9 ± < 0.1	1.16×10^{-7}	0.9998

Table 4.2 – Output parameters for the ideal data set for the original EM

The output parameters from the fitting procedures were very close to one another, with $\Delta G^{\ddagger}_{cat}$, $\Delta G^{\ddagger}_{inact}$ & ΔH_{eq} being close enough to make no difference in a visual fit. T_{eq}, whilst matching within experimental errors, is different enough to cause a slight shift in the fitted product concentration

peak. The parameters showed more concordance than those for the barnase variants in Section 3.3.3.2.

4.2.1.2 Custom MATLAB Fitting of Alternative Models

As in Section 2.7.3, the ideal data set was fitted to the alternative models using the SurfaceFitting tool method. Data from Section 4.2.1.1 is included. For an explanation of the relevant $\Delta G^{\ddagger}$ terms, see Table 4.1 and Appendix B. Note that some parameters are only required for certain models and the bracketed terms are only relevant for model Q (see Section 4.1.1.3).

Output Parameter	Orig. EM	O	P	M	N	R	Q
$\Delta G^{\ddagger}_{cat}$ **(kJ mol^{-1})**	78.19 ± < 0.01	78.40 ± 0.01	78.20 ± 0.01	78.28 ± < 0.01	78.31 ± 0.45	78.46 ± 0.01	78.44 ± 0.41
$\Delta G^{\ddagger}_{inact}$ $\left(\Delta G^{\ddagger}_{i}\right)$ **(kJ mol^{-1})**	104.6 ± < 0.1	–	104.6 ± < 0.1	105.4 ± < 0.1	94.69 ± 5.35	110.2 ± 2.3	93.67 ± 52.34
$\Delta G^{\ddagger}_{deact}$ $\left(\Delta G^{\ddagger}_{a}\right)$ **(kJ mol^{-1})**	–	101.9 ± < 0.1	159.2 ± large	–	–	–	96.56 ± 8.86
$\Delta G^{\ddagger}_{react}$ $\left(\Delta G^{\ddagger}_{-i}\right)$ **(kJ mol^{-1})**	–	–	–	–	89.39 ± 2.12	100.2 ± 10.5	91.49 ± large
$\left(\Delta G^{\ddagger}_{-a}\right)$ **(kJ mol^{-1})**	–	–	–	–	–	–	91.49 ± large
ΔH_{eq} **(kJ mol^{-1})**	116.9 ± 0.1	173.3 ± 0.2	117.3 ± 0.1	127.7 ± 0.1	165.1 ± 0.9	153.7 ± 0.3	167.8 ± 4.3
T_{eq} **(K)**	346.9 ± < 0.1	350.1 ± < 0.1	346.9 ± < 0.1	348.0 ± 0.1	348.9 ± 0.2	347.8 ± 0.1	349.6 ± 20.3
SSE	1.16 x10^{-7}	2.12 x10^{-7}	9.92 x10^{-8}	8.27 x10^{-8}	2.41 x10^{-5}	1.26 x10^{-6}	2.36 x10^{-5}
$\mathbf{R^2}$	0.9998	0.9997	0.9999	0.9999	0.9665	0.9983	0.9672

Table 4.3 – Output parameters for the ideal data set for original and alternative models

All of the models show excellent agreement in $\Delta G^{\ddagger}_{cat}$. This is the main parameter that influences the shape of the product curve at low temperatures, as the denaturation rate constants have larger $\Delta G^{\ddagger}$ terms and, hence, require higher temperatures to be of significance. T_{eq} is also well correlated between all models – the observed range of 3.2 K is considered within experimental error (see Section 3.3.4). Other parameters are discussed in following sections as appropriate to each group of models. Uncertainties labelled "large" mean that the 95% confidence bounds were greater than the magnitude of the value fitted (e.g., lower confidence bounds were giving negative values for the parameter).

The overall fits of the irreversibly denaturing models were markedly better than the reversibly denaturing ones, as measured by R^2 & SSE values, and this is discussed in Section 4.2.1.4 as well. Generally, this discrepancy is attributable to the N, R and Q fitting procedures having too many degrees of freedom. It should be noted that all of the models show a good surface fit to the data sets and even residuals are remarkably similar (see Appendix C). It is only in the individual output parameters for each model that a lack of confidence is observed, if at all, this being the purpose of the fitting experiments.

4.2.1.3 Analysis of Irreversibly Denaturing Models (EM, O, P and M)

Within these models, the $\Delta G^{\ddagger}_{inact}$ and $\Delta G^{\ddagger}_{deact}$ values are all very similar, with the exception of $\Delta G^{\ddagger}_{deact}$ for model P. Because model P allows for denaturation via both E_{act} and E_{inact}, it was expected that one rate might be favoured – as $\Delta G^{\ddagger}_{deact}$ is ~55 kJ mol^{-1} greater than $\Delta G^{\ddagger}_{inact}$, this leads to a ~$10^8$-fold difference in denaturation rate constant (at 350 K, ≈ T_{eq}) in favour of the k_{inact} process. This is expected as, at lower temperatures, the rate of denaturation is inevitably slower and, hence, the higher-temperature E_{inact} species is a more likely source for denaturable enzyme. Model P has parameters so close to EM, and excludes the k_{deact} process so well, that it gives exactly the same fit as the original EM, within error.

Model O does not allow for the k_{inact} process, instead defining the E_{act} species as the sole source of denaturable enzyme. The $\Delta G^{\ddagger}_{deact}$ parameter

fits well to the model (95% CI < 0.01 kJ mol^{-1}), however, and the overall quality of fit is comparable to both models EM and P. Seeing as model P so clearly disfavours this route for denaturation, other processes had to be compensating to allow for the good mathematical fitting of the data to model O. ΔH_{eq} for the EM and P models is a very closely matched parameter, almost within fitting error. With model O the ΔH_{eq} value is ~55 kJ mol^{-1} greater, meaning that the E_{act}/E_{inact} transition is more pronounced (K_{eq} changes from small to large over a shorter temperature range). It is postulated that this allows more E_{act} to be present at temperatures approaching T_{eq} and, hence, more susceptible to denaturation (e.g. in model O the E_{inact} is an off-path refuge from denaturation). T_{eq} itself is also marginally higher and $\Delta G^{\ddagger}_{deact}$ marginally lower than $\Delta G^{\ddagger}_{inact}$ from models EM and P, both factors aiding in lower-temperature denaturation of E_{act}. It must be remembered that the E_{act}/E_{inact} equilibrium still accounts for the majority of the inactivation observed at low temperature, and that this process is still resolved in the model.

Thus far, the case can be made that the mathematics favours denaturation almost exclusively through the E_{inact} species. Although the k_{deact} pathway can be fitted to data sets, other parameters are varied to compensate, and the evidence from model P refutes k_{deact} as a favoured process. One objective of this thesis was to attempt to simplify the kinetics used in the fitting of parameters to the equilibrium model, and whilst models O and P help to clarify which species are involved in which processes, they have equally or more complicated derivations than the original EM. Model M, in comparison, simplifies the kinetics by assuming both E_{act} and E_{inact} are so closely related (and quickly inter-converting) that the denaturation pathway is mathematically independent of the exact E_{act}/E_{inact} species. The $\Delta G^{\ddagger}_{inact}$ value for model M is almost exactly the same as for models EM and P, which use or favour denaturation via E_{inact}. A slight increase of ~10 kJ mol^{-1} is seen in ΔH_{eq}, making the E_{act}/E_{inact} transition more prominent (see previous model O discussion), but it still matches models EM and P within standard experimental error, along with T_{eq}.

Model M fits the ideal data set the best of all models, as evidenced by R^2 and SSE values, closely followed by model P. Within experimental error

(see Peterson et al., 2007), the output parameters for this data set are the same as those fitted to the original EM, for the time and temperature range of the data fitted. This, coupled with the lack of evidence to date about the nature of the E_{act}/E_{inact} transition (see Section 1.2.3.2), means that there is no reason to favour the more mathematically complicated original EM over the simplified model M for modelling this data set.

4.2.1.4 Analysis of Reversibly Denaturing Models (N, R and Q)

Models N, R and Q all fitted data with less certainty than the irreversibly denaturing models. With model Q this was expected as it allowed for two pathways to and from X from the E_{act}/E_{inact} ensemble and hence had a large degree of freedom to vary parameters during the fitting process. There can be no conclusions drawn from the non-catalytic $\Delta G^{\ddagger}$ output parameters, as they have such large confidence intervals and, although $\Delta G^{\ddagger}_{cat}$ and T_{eq} are in agreement with all the other models, the fit as a whole is not sound. This model is too mathematically complicated, with too many variables for the data it has to fit and, therefore, it does not give useful information about any processes occurring within the ideal data set.

Model N was derived to be the reversibly denaturing version of model M. As model M fitted the ideal data set well, it was thought that model N would show a near-zero rate constant for the k_{react} process and then fit similarly in all other parameters, as it then degrades to the Model M mathematics. However, the fitting process uses the new degree of freedom to compensate for the higher ΔH_{eq} parameter – a higher ΔH_{eq} means that the transition from E_{act} to E_{inact} populations is more pronounced and, hence, inactivation due to K_{eq} is more dramatic with temperature. The flexibility of models with increasingly complex or altered mathematics is discussed in Section 5.2.2 as well. If denaturation is modelled as a partially reversible process, then a loss of activity via K_{eq} can be compensated for by an overall slower loss of E_{act} and/or E_{inact} to X, increasing the relative concentration of E_{act} and restoring activity. The confidence in $\Delta G^{\ddagger}_{inact}$ and $\Delta G^{\ddagger}_{react}$ is lower than in the irreversible models discussed so far, but model N still gives a reliable fit for T_{eq} and $\Delta G^{\ddagger}_{cat}$.

Model R has an improved fit over model N for all output parameters except $\Delta G^{\ddagger}_{react}$. As model R is the reversible counterpart to the original EM model, the fit provides evidence that the original EM implication that E_{inact} is on-path to denaturation is correct. For model R, $\Delta G^{\ddagger}_{react}$ is very similar to $\Delta G^{\ddagger}_{inact}$ (they match within error) and as such the k_{inact}/k_{react} processes might represent a reversible equilibrium, suggesting that the ideal data set is from a reversibly denaturing enzyme (this is not known). The forward and reverse rates vary with temperature and time (compare with K_{eq}), as they are themselves dependent on species that are time-dependent. It is interesting that both models N and R do not purely reject the k_{react} process (by fitting near-zero rate constants); instead, they compensate for the availability of the new parameter by increasing ΔH_{eq} (as explained previously). T_{eq} and $\Delta G^{\ddagger}_{cat}$ for model R both match the values output for all other models. As illustrated in the R^2 and SSE statistics, model R fits the ideal data set better than the other reversibly denaturing models. This may be due to simplified kinetics over model Q, but could also imply that the pathway to the denatured species goes via E_{inact}.

4.2.2 WT Barnase Data Set

The fitting of the original EM to the FrG substrate has been analysed previously using SurfaceFitting tool (see Section 3.3.3.2). The results tabulated below are from those fitting runs in addition to the new results for alternate models (as performed in Section 2.7.3). Errors in the output parameters tabulated below are purely fitting errors, as above. Only WT barnase is included in this thesis for several reasons: brevity; to compare two wild-type enzymes, excluding the effects of mutations on fits; and due to the similarity of the conclusions that can be drawn from the fits of all barnase variants (data not shown).

All of the models show excellent agreement in $\Delta G^{\ddagger}_{cat}$ and T_{eq}, as they did for the ideal data set. The overall fits of the irreversibly denaturing models were only slightly better than the reversibly denaturing ones, as measured by R^2 & SSE values (compare with Section 4.2.1.2 onwards). Again, all the models show a good visual surface fit to the data sets and residuals are remarkably similar between models.

Output Parameter	Orig. EM	O	P	M	N	R	Q
$\Delta G^{\ddagger}_{cat}$ (kJ mol^{-1})	67.09 ± < 0.01	66.99 ± < 0.01	67.01 ± 0.01	67.03 ± < 0.01	65.52 ± 7.01	67.14 ± 0.01	66.16 ± 8.33
$\Delta G^{\ddagger}_{inact}$ $\left(\Delta G^{\ddagger}_{i}\right)$ (kJ mol^{-1})	92.51 ± 0.04	–	93.06 ± 0.06	93.15 ± 0.03	76.49 ± 18.34	87.21 ± large	84.17 ± large
$\Delta G^{\ddagger}_{deact}$ $\left(\Delta G^{\ddagger}_{a}\right)$ (kJ mol^{-1})	–	90.97 ± 0.03	92.19 ± 0.08	–	–	–	77.37 ± 35.23
$\Delta G^{\ddagger}_{react}$ $\left(\Delta G^{\ddagger}_{-i}\right)$ (kJ mol^{-1})	–	–	–	–	76.22 ± 5.23	78.80 ± large	77.62 ± 23.38
$\left(\Delta G^{\ddagger}_{-a}\right)$ (kJ mol^{-1})	–	–	–	–	–	–	76.89 ± 11.98
ΔH_{eq} (kJ mol^{-1})	190.6 ± 0.3	219.8 ± 0.3	198.3 ± 0.6	199.7 ± 0.2	212.0 ± 0.8	211.8 ± 19.5	212.2 ± 27.9
T_{eq} (K)	315.8 ± < 0.1	315.9 ± < 0.1	316.1 ± < 0.1	315.9 ± < 0.1	315.6 ± 0.1	315.6 ± 13.6	314.2 ± 31.8
SSE	4.76 x10^{-10}	4.35 x10^{-10}	4.98 x10^{-10}	2.92 x10^{-10}	6.81 x10^{-9}	3.91 x10^{-9}	3.09 x10^{-9}
R^2	0.9995	0.9996	0.9995	0.9997	0.9935	0.9963	0.9970

Table 4.4 – Output parameters for WT barnase and FrG for original and alternative models

4.2.2.1 Analysis of Irreversibly Denaturing Models (EM, O, P and M)

Compared with the ideal data set, most of the conclusions with respect to the original EM and model M fits are the same (see Section 4.2.1.3). The output parameters for Model P, however, do not distinguish between denaturation from either E_{act} or E_{inact}. In this case, the model simplifies to model M as $k_{inact} \approx k_{deact}$ (note the similarity of other output parameters). This provides further evidence that model M is a good representation of simplified equilibrium model kinetics, with the best statistical fit to data

for the time and temperature ranges assayed. The other parameters output from the original EM fitting are identical to those from models M and P, within experimental error.

4.2.2.2 Analysis of Reversibly Denaturing Models (N, R and Q)

The fit of barnase to irreversibly denaturing models, in particular the original EM (Section 3.3.3.2), has been discussed before. It was hoped that the reversible versions of each model would account for barnase data more thoroughly and give a better fit at higher temperatures, reflecting renaturation. Models N, R or Q fit better to the WT barnase data than to the ideal data set but still have large fitting errors, in particular for model R. Model Q has the best fit of the reversible models, but also large uncertainties for $\Delta G^{\ddagger}$ parameters, meaning no conclusions could be drawn from their values. Rises in ΔH_{eq} for models N, R and Q are statistically significant in comparison to the irreversible models but, when experimental error is considered, they become insignificant.

Model N is the only reversible model fitted to WT barnase data with output parameters of numerical uncertainties (the uncertainties are not labelled "large"). The similarity of $\Delta G^{\ddagger}_{inact}$ and $\Delta G^{\ddagger}_{react}$ rates resembles the situation with models N and R for the ideal data set, in that a reversible equilibrium might exist (although this observation is not explainable for the ideal data set). The observed drop in $\Delta G^{\ddagger}_{inact}$ (and its resulting faster denaturation) is compensated for by, activity-wise, a marginal decrease in $\Delta G^{\ddagger}_{cat}$ (increasing the activity of E_{act}). Despite these conclusions, the confidence in parameters from model N (as measured by the given uncertainties) is far below those derived using models EM, M & P, meaning that it has limited use in comparing enzymes (and mutants of the same enzyme) to each model.

4.3 Species Concentration Simulations

For the purposes of NMR dynamics experiments (see Section 1.3.3.4 and Section 1.4.1) an enzyme (native or mutant) needed to be identified with two main properties. Firstly, due to the long nature of NMR dynamics experiments (on the scale of days), there must not be a "sink" of denatured

and aggregated protein over temperature ranges where the E_{act}/E_{inact} equilibrium would be observable; hence, reversibly denaturing enzymes such as barnase or other RNAses are ideal. Secondly, for the transition between E_{act} and E_{inact} to be observable, ideally the T_{eq} will be at least ~5 °C lower than the T_m, so that the major species present at higher temperatures (past T_{eq}) is E_{inact}, and not denatured enzyme (X). As any dynamics experiments would be benchmarked against the EM, species simulations based on fits to the EM needed to be derived. For example, the relative amounts of species present at specific times and temperatures (E_{act}, E_{inact} and X) need to be quantified to explain any changes observed in dynamics experiments. Hence particular dynamic states could then be ascribed to different species and reflect the physical basis for the E_{act}/E_{inact} transition.

Equations for all models are derived in full in Appendix B.1.7. Only those for the original EM are given below as the exponential term is the only element that changes between models (see Table 4.1).

Species	Concentration Equation
E_{act}	$[E_{act}] = \frac{[E_0]}{1+K_{eq}} \cdot \exp\left(\frac{-k_{inact} \cdot K_{eq} \cdot t}{1+K_{eq}}\right)$
E_{inact}	$[E_{inact}] = \frac{[E_0]}{1+1/K_{eq}} \cdot \exp\left(\frac{-k_{inact} \cdot K_{eq} \cdot t}{1+K_{eq}}\right)$
X	$[X] = [E_0] \cdot \left(1 - \exp\left(\frac{-k_{inact} \cdot K_{eq} \cdot t}{1+K_{eq}}\right)\right)$

Table 4.5 – Species concentration equations for the original EM

4.3.1 Simulations of Different Data Sets and Models

The output parameters from the original EM (from fitting.exe) for the ideal data set (Section 4.2.1.1) and WT & DM barnase (Section 3.3.3.2) were used to simulate species concentrations for the original EM over suitable ranges of temperature for 120 minutes using the equations from Table 4.5 (long enough to demonstrate the full interplay between species, essentially to $t \approx \infty$). Three-dimensional interactive models (for the program Grapher, Apple Inc., USA) are available in Appendix C.

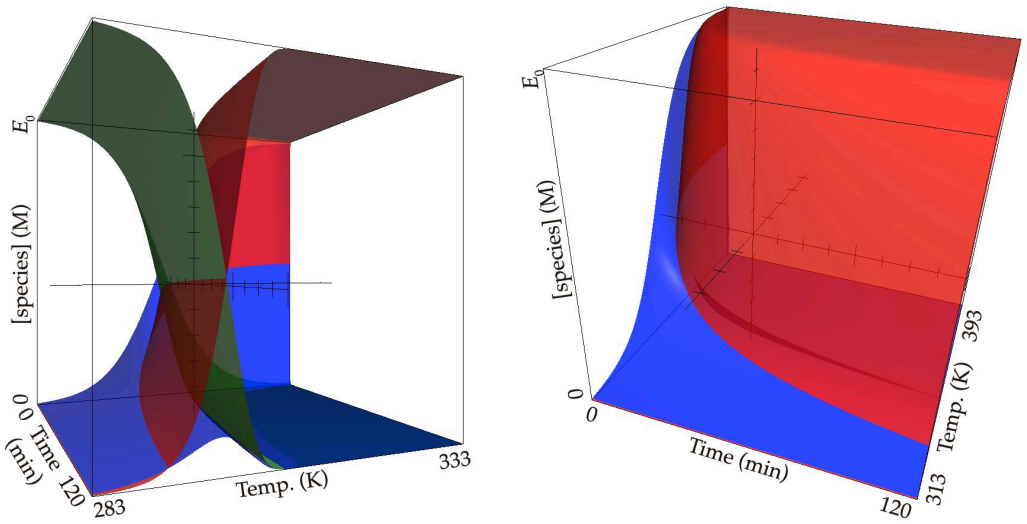

Figure 4.1 – Species simulations for the ideal data set in the original EM. (Left) View showing E_{act} (green), E_{inact} (blue) and X (red) and (Right) View with E_{act} removed.

Figure 4.1 (Left) shows clearly how the three species in the original EM relate. As temperature increases, the E_{act}/E_{inact} equilibrium is apparent with increasing amounts of E_{act} being converted to E_{inact}, most obviously at shorter assay times (in the first ~10 minutes) (Figure 4.1 (Right)). The denatured species (X) shows a curve that is prominent at short time-scales & high temperatures and at long time-scales & lower temperatures, reflecting the time dependency of the denaturation process. At long assay times (> ~10 minutes) and temperatures approximating the E_{inact} peak, the irreversible denaturation process in the original EM causes the majority of E_0 to be either in the E_{act} or X forms, essentially making X an immediate "sink" for any E_{inact} species formed. This illustrates why previous attempts to determine the structural changes involved in the E_{act}/E_{inact} transition have proven difficult (see Section 1.2.3.1); any enzyme present in the E_{inact} form only accounts for ~10% of the total enzyme concentration, with ~45% in both E_{act} and X forms.

With regard to measuring the dynamics of the E_{act}/E_{inact} transition via NMR or any other means (see the beginning of Section 4.3), it is important that E_{act} and E_{inact} are the primary species present at long time scales and over the temperature range of the equilibrium. Diagrammatically, the species simulations for the applicable model need to show the blue E_{inact} curve at $>80\%$ of E_0 concentration at long time scales. This is because NMR will measure resonances over the whole population of enzyme (E_0),

and therefore the E_{inact} species must be in excess over the X and E_{act} species so its dynamics can be determined. With the original EM derivation this only occurs at short (< ~1 minute) time scales (e.g. Figure 4.1 (Right) and Figure 4.4). Ideally, the red X curve would rise in concentration at temperatures higher than the E_{inact} peak, so that at long time scales, the E_{inact} form would dominate and be protected against denaturation.

Species simulations from WT and DM barnase fits to the original EM are shown in Figure 4.2 and Figure 4.3. It is known from DSC measurements (see Section 3.2.6) that WT barnase does not start to denature appreciably until ~315 K (with a T_m of ~326 K). Because the original EM does not take into account reversible denaturation, the loss of activity at temperatures well below the T_m is ascribed to X formation by the fitting process, not the E_{act}/E_{inact} equilibrium. Therefore, the red X curve should be ~10 K higher than that fitted by the EM mathematics. This deviation is seen even more drastically with the DM barnase data set (using output parameters from Section 3.3.3.2). From DSC measurements, the DM does not start to denature until ~321 K (with a T_m of ~331 K). This is not reflected in the position of the X curve in Figure 4.3, which should (at long time points) show a midpoint approximating T_m. At 2 minutes time in Figure 4.4 ~80% of DM barnase is in the denatured (X) species at 330 K. Yet we know that only ~50% of the enzyme population should be denatured at this temperature, as the T_m is ~331 K.

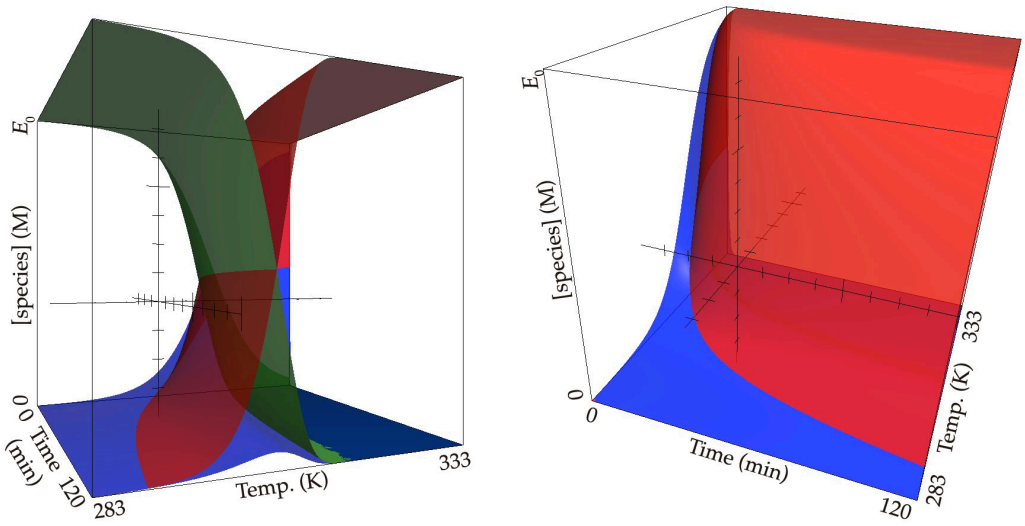

Figure 4.2 – Species simulations for WT barnase and FrG in the original EM. (Left) View showing E_{act} (green), E_{inact} (blue) and X (red) and (Right) View with E_{act} removed.

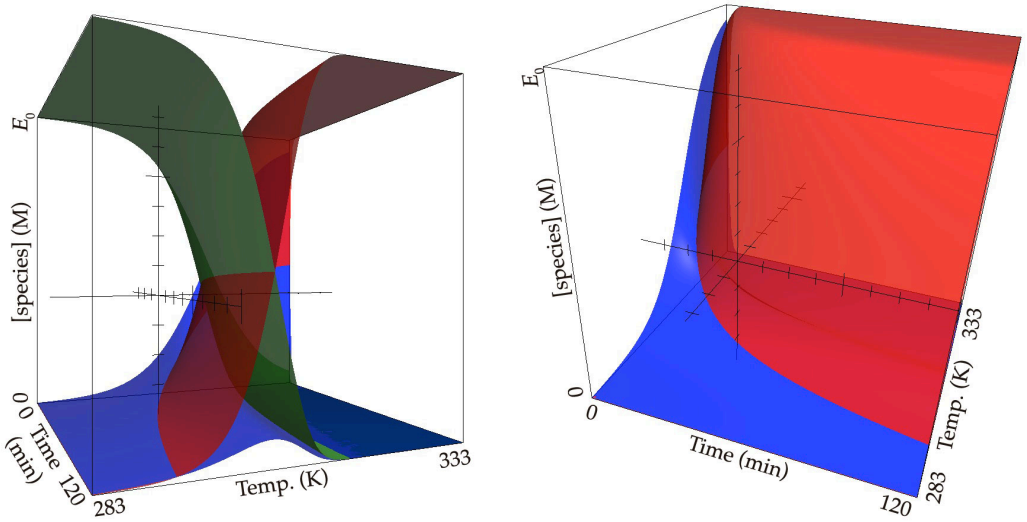

Figure 4.3 – Species simulations for DM barnase and FrG in the original EM. (Left) View showing E_{act} (green), E_{inact} (blue) and X (red) and (Right) View with E_{act} removed.

These findings are easier to see in two dimensions if temperature is plotted against time for the first 10 minutes of a DM barnase assay (Figure 4.4). Using the original EM output parameters and plotting the regions in which each species makes up 80% or more of the E_0 population, we can see that a sufficient population of E_{inact} (blue) for dynamics measurements is only fleetingly present. The populations of both E_{act} (green) and X (red) are, however, dominant over wide time and temperature ranges.

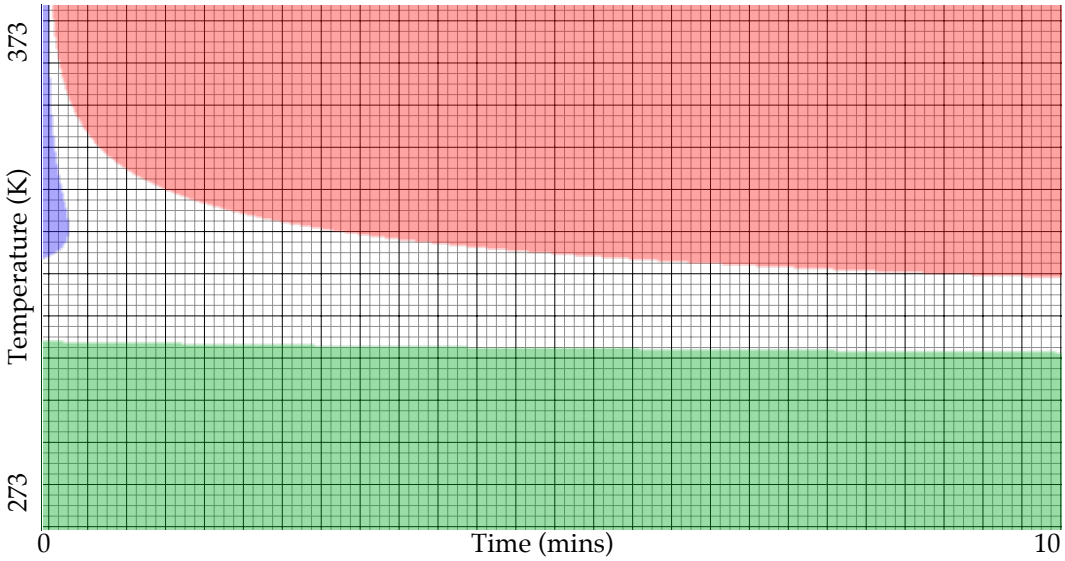

Figure 4.4 – 2D temperature/time plot of EM species at > 80% E_0 for DM barnase

The stabilising effect of substrate on enzyme T_m values is well known (Lejeune et al., 2001). Hence, the situation described, where the original EM model does not reflect the DSC thermostability results, could be worse

if the FrG substrate used for barnase assays stabilises barnase significantly. This would mean that, although the model fits parameters suggesting a small E_{inact} population, in reality that population is much more dominant.

4.3.2 Modelling an Ideal Enzyme

If the original EM parameters for DM barnase are adjusted to separate E_{act} and X populations, simulations show that it is possible to have a large proportion of the E_{inact} species present for long time periods, if denaturation occurs at sufficiently higher temperatures. By setting the values as in Table 4.6 (modified from the DM barnase EM output parameters), Figure 4.5 shows a peak for E_{inact} that is well separated from the denaturation peak, allowing long time-scale dynamics measurements to be made of E_{inact}. The value of $\Delta G^{\ddagger}_{inact}$ is realistic, but high, as the DM is ~9 kJ mol^{-1} stabilised relative to the WT (Table 1.2).

Simulated Parameter	Value
$[E_0]$	1.04x10^{-9} M
$\Delta G^{\ddagger}_{inact}$	107000 kJ mol^{-1}
ΔH_{eq}	200000 kJ mol^{-1}
T_{eq}	315 K

Table 4.6 – Simulation parameters of an ideal enzyme for the original EM

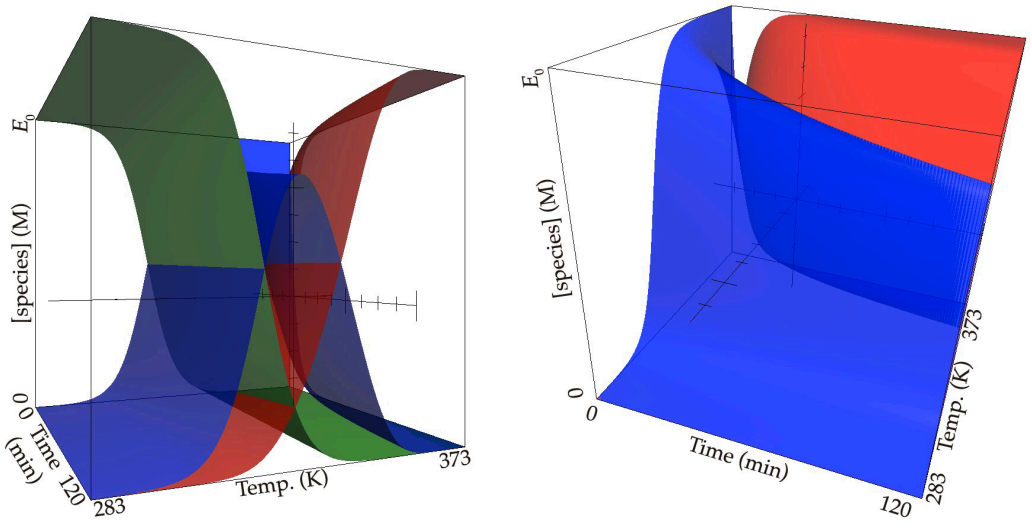

Figure 4.5 – Species simulations for an ideal enzyme in the original EM. (Left) View showing E_{act} (green), E_{inact} (blue) and X (red) and (Right) View with E_{act} removed.

This is a drastic example, used for effect, and lower $\Delta G^{\ddagger}_{inact}$ values can still have a marked effect of the size and position of the E_{inact} peak. The major change is due to a high enough $\Delta G^{\ddagger}_{inact}$ and a low enough T_{eq} that lead to separation of the X curve from the E_{inact} curve. The denaturation process needs higher temperatures to obtain a significant rate constant and hence the E_{inact} population is protected from the k_{inact} process. Figure 4.5 shows a mid-point for the denaturation curve (X) at about 335 K, ~5 K higher than the T_m of the DM (Section 3.2.6). A lower $\Delta G^{\ddagger}_{inact}$ value, closer to that suggested by the literature (see Table 1.2), would potentially remedy this. The T_{eq}, however, remains the same and ΔH_{eq} is also similar.

The parameters in Table 4.6 could describe a highly-stabilised barnase mutant that fits to the original EM kinetics. The idea of super-stabilising an enzyme, to reveal a prominent E_{inact} population, is discussed further in Section 5.3.1. The above findings are presented in Figure 4.6 for comparison to Figure 4.4; note the same profile for E_{act} and the clean transition to E_{inact}, which is now protected from denaturation for the time scale of hours, not seconds.

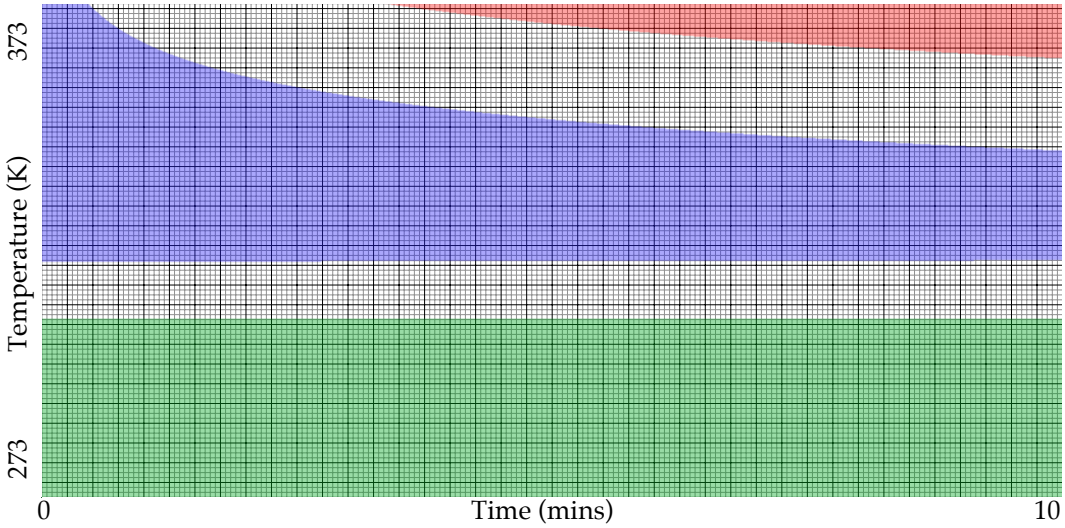

Figure 4.6 – 2D temperature/time plot of EM species at > 80% E_0 for an ideal enzyme

5 Discussion and Conclusions

The overall goal of this thesis was to identify a mutant of barnase that would allow direct observation of the structural changes which occur over the E_{act}/E_{inact} equilibrium. This could be achieved through decoupling the thermal stability of the enzyme from its activity through mutation(s) that either lower T_{eq} and/or raise T_m. If successful, this would allow the dynamics of the E_{act}/E_{inact} equilibrium to be measured via NMR. The experimental results, summarising the acquisition and fitting of EM data (Section 5.1.1) and thermostabilities of WT, DM & L89V barnase variants (Section 5.1.2), respectively, are discussed in this chapter.

In addition, to understand and potentially improve the mathematics behind the EM, new model derivations were fitted to an ideal data set and to the WT barnase data set. A review of findings from the fitting experiments is given in Section 5.2.1. To benchmark the potential dynamics measurements of any enzyme, equations to simulate the concentrations of species with time and temperature were derived and analysed (Section 5.2.2). Finally, future work that might result from the findings in this thesis is summarised in Section 5.3.1 and Section 5.3.2, dealing with potential new experimental and theoretical approaches, respectively.

5.1 Experimental

5.1.1 Assays and Fitting Results to the Original EM

The WT barnase assays performed using the GpUp dinucleotide substrate were not extended to the five barnase mutants. Declining rates with time that could not be attributed to either formation of the E_{inact} species or denaturation were observed, and these led to poor fits between the data set and the original EM. These declining profiles may be due to product inhibition or the secondary hydrolysis step of the substrate becoming prevalent in assays (see Section 1.3.2). The K_M values at high temperatures were also large which limited assays, due to substrate solubility and cost. The absorbance change upon hydrolysis of GpUp is very small and has large experimental errors so, although output parameters from fits to the

original EM were reasonable, the experimental difficulties made this substrate poor and unreliable for collection of EM data.

The FrG substrate also had several experimental difficulties. The temperature dependence of the substrate (and product) fluorescence (see Section 3.3.2.1) meant that corrections had to be made in data processing (Section 2.7.1.3) to ensure linearity between fluorescence and product concentration. Mixing of enzyme was often a problem and a refined protocol was developed. K_M values were much more stable with temperature for the FrG fluorescent substrate (see Section 3.3.3.1). This meant that corrections for K_M, even though applied to all the data sets used in this thesis, were much less important than for the GpUp substrate. The low background and large change in fluorescence upon cleavage of FrG led to higher sensitivity and reliability than in the GpUp-based assays; hence, data was collected for WT, S80C/A43C (DM) and L89V barnase (Section 3.3.3). Three remaining mutant barnase enzymes studied (Y78F, I51V and I88V barnase) are yet to be assayed with FrG.

The results from fitting the WT, DM and L89V assay data to the original EM (using fitting.exe) are detailed in Section 3.3.4. The important parameter with regard to dynamics measurements, T_{eq}, did not change outside of experimental error between the WT and the DM or L89V mutants. Relative to the WT enzyme, $\Delta G^{\ddagger}_{inact}$ has not changed outside of error for fitting.exe results, although it has for the SurfaceTool method. Both fitting procedures show the correct direction of change in $\Delta G^{\ddagger}_{inact}$ for each mutant, but do not reflect the absolute values or differences suggested in the literature values (Table 1.2) or thermostability experiments (see Section 5.1.2 and Section 3.3.4). Therefore, as described by the EM model fits, the E_{inact} species is not more significantly present than in the WT enzyme.

5.1.2 Thermostability and Decoupling T_m from T_{eq}

The T_m values for WT and mutant barnase were measured under assay conditions (but excluding substrate) using CD and DSC methods (see Section 3.2). As the two mutants assayed so far show no significant changes in T_{eq} from the WT, an increase in T_m could protect the E_{inact} species

from denaturation and make it available for dynamics experiments at temperatures where it is mainly denatured in the WT assays.

DM barnase has a T_m 5.2 ± 0.1 °C higher than the WT enzyme (Section 3.2.6). Because T_{eq} has not changed for the DM over the WT, this is an example of successfully decoupling thermal activity from denaturation. If the T_m values are correct, and fitted $\Delta G^{\ddagger}_{inact}$ values are incorrect (see Section 5.1.1), the E_{inact} species in the DM enzyme might be more accessible in a significant concentration at temperatures between T_{eq} and T_m than fits to the original EM suggest (see Section 5.3.1). The ΔT_m of L89V barnase is -0.8 ± 0.1 °C, which suggests a decoupling in the opposite direction; the enzyme is marginally destabilised, yet T_{eq} has not significantly changed.

5.2 Theory and Modelling

5.2.1 Fitting Results for all Models

WT, DM and L89V barnase all fit to the original EM with good R^2 and SEE statistics and individual output parameters are well defined (Section 3.3.3.2). However, all barnase data sets show systematic deviations from the fits at high temperatures in the residual plots. These deviations were thought to be due to poor fitting at high temperatures, as the denaturation of barnase is reversible but not allowed for in the original EM (see discussion below).

The results in Section 4.2.1.1 illustrate how the original EM fits ideal data accurately with much less systematic deviation in the residuals (see Appendix C for all fitting plots). Denaturation from the E_{inact} species can be fitted well using model O but, if the model includes a choice (as in model P), the preferred and best-fitting pathway is via E_{inact} using the original EM derivation (see Section 4.2.1.3). This corroborates the original assumption of the EM, that E_{inact} is on-path to denaturation (Daniel et al., 2001). A simplification of the derivation kinetics to model M results in concordant output parameters compared with the original EM without making the distinction between E_{act} or E_{inact} denaturation. Model M also fits statistically better than any other model to the two data sets compared to date, for the ranges of data acquired. However, data sets with longer time periods may not fit as well to model M, as denaturation will be more pronounced at

lower temperatures, due to the lack of a reservoir of E_{act} (which is present in the original EM). This is a failing in model M, as it inherently needs a larger $\Delta G^{\ddagger}_{inact}$ value to compensate for both E_{act} and E_{inact} denaturing. In conclusion, the EM as it stands is the best model for the current data.

Reversibly denaturing models (Section 4.2.1.4) have too many degrees of freedom to fit to data sets unaided. A potential solution to this is given in Section 5.3.2. Fits performed in this thesis do show reasonable, yet uncertain, values for parameters and, hence, could be improved by a better understanding of how the different rates interact with one another. More sensible starting values and less freedom to move (narrower search spaces for each parameter) might aid in this, but require extensive optimisation to define starting values that still allow for unbiased fitting to all data sets. Model N was the only reversibly denaturing model to fit reliably to the WT barnase data (see Section 4.2.2.2). However, it is not a fair comparison to the original EM model analysed in Section 4.2.2.1 because it allows for an E_{act}/E_{inact} ensemble to denature, not just E_{inact}. This means that, although it fits the data well at short time scales, model N overestimates the amount of denaturation present in an assay, leading to poor fits at long time scales (like its irreversible counterpart, model M).

Finally, it must be kept in mind that fitted output parameters are all inferred from rate data (and variables in exponentials of exponentials fitted to it). That is, the E_{inact} and X species are removed from the E_{act} species (the activity of which is measured directly via assays) by at least one process (K_{eq}, k_{inact} et al., or both). Hence, there is potential for a model to ascribe rate losses to a denaturation process when it would be more correctly defined via a K_{eq} equilibrium process, and vice versa (see Section 5.2.2). This hazard has potential for remediation (see Section 5.3.2). All of the models have the same rate profile at zero-time (see Table 4.1) and, hence, the longer the assay data is, whilst remaining valid, the more chance the fitting procedure has to fit the correct parameters to each model. This is a good reason to not shorten data sets unnecessarily (see Section 3.3.1.2). A better statistical fit may obscure true parameter values through poor fitting, especially with the inactivation parameters such as $\Delta G^{\ddagger}_{inact}$ that require time to reveal their effect on the data set.

5.2.2 Species Simulations

The species simulations provide useful insight into the movement of species within the assay data sets. It is interesting to note that the concentrations of species are vastly different from what was assumed until recently. For example, with the ideal data set, the concentration of E_{inact} is much lower at time points greater than a few minutes, making the nature of E_{inact} hard to observe. This could explain why researchers have not found physical evidence for the E_{inact} species to date (Daniel et al., 2009). Due to time constraints, the analyses of derived models other than the original EM have not been completed. The simulations show promise as a tool for understanding how the different models work and for validating their fits to experimental data for future dynamics experiments.

The simulations for WT and DM barnase for the original EM do not reflect their denaturation properties (see Section 4.3.1). The curves simulated for [X] have midpoints (50% of E_0) at approximately 10 and 15 K less than where DSC and CD measurements place the WT and DM T_m values (see Section 5.1.2). This means that the absolute value of $\Delta G^{\ddagger}_{inact}$ is incorrect and much lower than it should be. The flow-on effects from misrepresenting the concentration of X in this way are important because the concentration of E_{inact} could be, in reality, much higher at a given temperature, as denaturation is not really occurring at the temperatures indicated by the simulation. As the output parameters from the fits to the original EM are used to simulate the X curve, either the fitted $\Delta G^{\ddagger}_{inact}$ value is incorrect (see Section 5.1.1) or the EM itself does not represent what is really occurring in the barnase assays.

The simulation of an ideal enzyme for dynamics measurements shows that the separation of E_{inact} from X is possible using the original EM kinetics (Section 4.3.2). Hence, the kinetics of the model do allow for a situation where E_{inact} is the major species. Barnase dynamics measurements may be possible if the variants' $\Delta G^{\ddagger}_{inact}$ values were incorrectly fitted to the model (see Section 5.1.1). It is postulated that a highly-stable enzyme might be engineered that could approach the same kind of E_{inact}/X separation seen in the ideal enzyme simulations (see Section 5.3.1).

5.3 Future Research

Numerous interesting details remain hidden within the available data. Many of the theoretical conclusions are recent developments (early 2010), therefore, many opportunities for better understanding and development of the EM are available. The following are suggestions for promising areas of future research based on the aforementioned conclusions.

5.3.1 Experimental

There are three mutant barnase enzymes (Y78F, I51V and I88V barnase) that have not been assayed for equilibrium model data collection. As they all show lower thermostability (lower T_m values), compared with the WT and L89V, they will need to possess significantly lowered T_{eq} values to provide a good source for measuring E_{inact} dynamics. It would be interesting, however, to see if they possess altered output parameters due to their lower stabilities, but this is not expected based on WT, L89V and DM trends (where T_{eq} and $\Delta G^{\ddagger}_{inact}$ did not change markedly) (see Section 5.1.1).

The stabilising effect of substrate on enzymes has not been tested in any previous work on the EM, but it is well known that substrates may enhance protein stability with regard to thermal denaturation (Lejeune et al., 2001). It would be useful to see if DSC and CD stability values are altered by the presence of substrate, compared to those in this thesis, which were measured in the absence of substrate. Due to the length of time required for these measurements, a non-hydrolysable FrG analogue (exactly the same, but with no ribose-guanoside residue) could be employed to enable stabilisation of the enzyme to be studied without substrate degradation. A related experiment is explained in Section 5.3.2.

The DM barnase enzyme has shown a good fit to the original EM and a T_{eq} that is similar to WT barnase. Although the species simulations (see Section 5.2.2) do not show a large E_{inact} population present for dynamics measurements, it is thought that the raised T_m of the double mutant may allow NMR experiments to observe the E_{inact}/E_{act} transition. If fitted $\Delta G^{\ddagger}_{inact}$ parameters from the original EM are incorrect (see Section 5.2.2), then

there may be a much larger E_{inact} population present than what is shown in the simulations. ^{15}N-labelled DM barnase, prepared for this purpose, has been sent to The University of Sheffield, UK, for protein dynamics measurements.

It would also be useful to investigate if a highly-stable mutant of barnase could be prepared. The obvious choice for this is in combining multiple disulfide bonds to raise the T_m as high as possible. The mutations would have to be carefully selected, as the only other stabilising cross-link made to date incorporates an active-site residue which is no use for activity assays and would also perturb the active-site dynamics (Clarke et al., 1995a). If a similar stabilising mutation raised $\Delta G^{\ddagger}_{inact}$ to a level approaching that of the theoretical "ideal enzyme" (Section 4.3.2), then the E_{inact} species would be well protected from denaturation and, therefore, available for dynamics measurements.

5.3.2 Modelling and Mathematics

There is always the possibility that a better model could be derived for the EM. Based on the remarkably good statistical fit of model O to the data sets, a reversibly denaturing counterpart could be easily derived, for example. This would be of little utility, however, as models EM, P and M all point towards model O being an exception (see Section 4.2.1.3).

Although not attempted in this thesis, if the denaturation process under assay conditions could be measured directly, and then accounted for separately from activity, that would leave the fitting procedures free to fit the K_{eq} equilibrium parameters (ΔH_{eq} & T_{eq}) and $\Delta G^{\ddagger}_{cat}$ more accurately. Essentially, the concentration of X could be input alongside the time, temperature and rate data as another independent variable. This would simplify the mathematics greatly, as equation (8) in Appendix B could be directly fitted to activity. The largest benefit would be that the actual model (e.g., models EM & M-R) fitted to the data becomes irrelevant (because all the models presented in this thesis have the E_{act}/E_{inact} equilibrium at their core, yet differentiate from each other by describing different denaturation pathways). If [X] is input directly, then the renaturation properties of the enzyme are already accounted for in the fit.

Expanding the idea for the purposes of barnase assays, the denaturation could be followed using fluorescence spectroscopy at all the temperature points assayed. Stopped-flow apparatus may be required. It is well known that barnase folding and unfolding can be followed with intrinsic fluorescence at excitation of 293 nm and emission at 338 nm (Horovitz & Fersht, 1992). This data set could be collected using a modified procedure (including substrate) as described in Section 2.6.2.6, then added to existing data sets, as described above. Interactions between substrate and barnase fluorescence would have to be explored, as well as fluorometer settings and sensitivity. The experiment could also give information on the stabilising influence of substrate on enzyme stability, which is important if DSC and CD measurements are to be used analytically (see Section 5.1.2). An approach such as this would confirm if the original EM as it stands outputs reasonable $\Delta G^{\ddagger}_{inact}$ values or not (as discussed in Section 5.1.1). Although this idea is ambitious, the benefits in terms of understanding how the current parameters are fitted to and relate to each model could be very large indeed.

References

Arcus VL, Vuilleumier S, Freund SMV, Bycroft M, Fersht AR (1995) A comparison of the pH, urea, and temperature-denatured states of barnase by heteronuclear NMR - implications for the initiation of protein-folding. *J Mol Biol* **254**(2)**:** 305-321

Arnott MA, Michael RA, Thompson CR, Hough DW, Danson MJ (2000) Thermostability and thermoactivity of citrate synthases from the thermophilic and hyperthermophilic archaea, *Thermoplasma acidophilum* and *Pyrococcus furiosus*. *J Mol Biol* **304**(4)**:** 657-668

Benkovic SJ, Hammes-Schiffer S (2003) A perspective on enzyme catalysis. *Science* **301**(5637)**:** 1196-1202

Briggs GE, Haldane JB (1925) A Note on the Kinetics of Enzyme Action. *Biochem J* **19**(2)**:** 338-339

Buchanan CL, Connaris H, Danson MJ, Reeve CD, Hough DW (1999) An extremely thermostable aldolase from *Sulfolobus solfataricus* with specificity for non-phosphorylated substrates. *Biochem J* **343:** 563-570

Buckle AM, Fersht AR (1994) Subsite binding in an rnase - structure of a barnase tetranucleotide complex at 1.76-angstrom resolution. *Biochemistry* **33**(7)**:** 1644-1653

Buckle AM, Henrick K, Fersht AR (1993) Crystal structural analysis of mutations in the hydrophobic cores of barnase. *J Mol Biol* **234**(3)**:** 847-860

Bycroft M, Ludvigsen S, Fersht AR, Poulsen FM (1991) Determination of the 3-dimensional solution structure of barnase using nuclear-magnetic-resonance spectroscopy. *Biochemistry* **30**(35)**:** 8697-8701

Chen YW, Fersht AR, Henrick K (1993) Contribution of buried hydrogen bonds to protein stability: The crystal structures of two barnase mutants. *J Mol Biol* **234**(4)**:** 1158-1170

Clarke J, Fersht AR (1993) Engineered disulfide bonds as probes of the folding pathway of barnase: Increasing the stability of proteins against the rate of denaturation. *Biochemistry* **32**(16)**:** 4322-4329

Clarke J, Henrick K, Fersht AR (1995a) Disulfide mutants of barnase I: Changes in stability and structure assessed by biophysical methods and x-ray crystallography. *J Mol Biol* **253**(3)**:** 493-504

Clarke J, Hounslow AM, Fersht AR (1995b) Disulfide mutants of Barnase II: Changes in structure and local stability identified by hydrogen exchange. *J Mol Biol* **253**(3)**:** 505-513

Dalby PA, Oliveberg M, Fersht AR (1998) Movement of the intermediate and rate determining transition state of barnase on the energy landscape with changing temperature. *Biochemistry* **37**(13)**:** 4674-4679

Daniel RM, Danson MJ (2001) Assaying activity and assessing thermostability of hyperthermophilic enzymes. In *Hyperthermophilic Enzymes, Pt C* Vol. 334, pp 283-293. San Diego: Academic Press Inc

Daniel RM, Danson MJ, Eisenthal R (2001) The temperature optima of enzymes: a new perspective on an old phenomenon. *Trends BiochemSci* **26**(4)**:** 223-225

Daniel RM, Peterson ME, Danson MJ, Price NC, Kelly SM, Monk CR, Weinberg CS, Oudshoorn ML, Lee CK (2009) The molecular basis of the activity of temperature on enzyme activity. *Biochem J* **In publication**

Davison AC, Hinkley D (2006) *Bootstrap Methods and their Application*, 8th edn.: Cambridge University Press.

Day AG, Parsonage D, Ebel S, Brown T, Fersht AR (1992) Barnase has subsites that give rise to large rate enhancements. *Biochemistry* **31**(28)**:** 6390-6395

DeLano WL. (2002) The PyMOL Molecular Graphics System. DeLano Scientific, Palo Alto.

Eisenthal R, Peterson ME, Daniel RM, Danson MJ (2006) The thermal behaviour of enzyme activity: implications for biotechnology. *Trends Biotechnol* **24**(7)**:** 289-292

Ericsson UB, Hallberg BM, DeTitta GT, Dekker N, Nordlund P (2006) Thermofluor-based high-throughput stability optimization of proteins for structural studies. *Anal Biochem* **357**(2)**:** 289-298

Fersht AR (1999) *Structure and mechanism in protein science: A guide to enzyme catalysis and protein folding*, New York: W.H. Freeman and Company.

Fersht AR, Matouschek A, Serrano L (1992) The folding of an enzyme: I. Theory of protein engineering analysis of stability and pathway of protein folding. *J Mol Biol* **224**(3)**:** 771-782

Fiaux J, Bertelsen EB, Horwich AL, Wuthrich K (2002) NMR analysis of a 900K GroEL-GroES complex. *Nature* **418**(6894)**:** 207-211

Fulton KF, Devlin GL, Jodun RA, Silvestri L, Bottomley SP, Fersht AR, Buckle AM (2005) PFD: a database for the investigation of protein folding kinetics and stability. *Nucleic Acids Res* **33:** D279-D283

Gasteiger E, Gattiker A, Hoogland C, Ivanyi I, Appel RD, Bairoch A (2003) ExPASy: the proteomics server for in-depth protein knowledge and analysis. *Nucleic Acids Res* **31**(13)**:** 3784-3788

Hartley RW (1988) Barnase and barstar - expression of its cloned inhibitor permits expression of a cloned ribonuclease. *J Mol Biol* **202**(4)**:** 913-915

Hartley RW, Both V, Hebert EJ, Homerova D, Jucovic M, Nazarov V, Rybajlak I, Sevcik J (1996) Barstar inhibits extracellular ribonucleases of *Streptomyces* and allows their production from recombinant genes. *Protein Pept Lett* **3**(4)**:** 225-231

Horovitz A, Fersht AR (1992) Cooperative interactions during protein folding. *J Mol Biol* **224**(3)**:** 733-740

Johnson CM, Oliveberg M, Clarke J, Fersht AR (1997) Thermodynamics of denaturation of mutants of barnase with disulfide crosslinks. *J Mol Biol* **268**(1)**:** 198-208

Killick TR, Freund SMV, Fersht AR (1998) Real-time NMR studies on folding of mutants of barnase and chymotrypsin inhibitor 2. *FEBS Lett* **423**(1)**:** 110-112

Kippen AD, Sancho J, Fersht AR (1994) Folding of barnase in parts. *Biochemistry* **33**(12)**:** 3778-3786

Kubelka J, Hofrichter J, Eaton WA (2004) The protein folding "speed limit". *Current Opinion in Structural Biology* **14**(1)**:** 76-88

Laidler K, King C (1983) Development of transition-state theory. *Journal of Physical Chemistry* **87**(15)**:** 2657

Lejeune A, Vanhove M, Lamotte-Brasseur J, Pain RH, FrËre J-M, Matagne A (2001) Quantitative analysis of the stabilization by substrate of *Staphylococcus aureus* PC1 ß-lactamase. *Chemistry & Biology* **8**(8)**:** 831-842

Martinez JC, Elharrous M, Filimonov VV, Mateo PL, Fersht AR (1994) A calorimetric study of the thermal-stability of barnase and its interaction with 3'gmp. *Biochemistry* **33**(13)**:** 3919-3926

Matouschek A, Kellis JT, Serrano L, Fersht AR (1989) Mapping the transition state and pathway of protein folding by protein engineering. *Nature* **340**(6229)**:** 122-126

Matouschek A, Serrano L, Fersht AR (1992) The folding of an enzyme: IV. Structure of an intermediate in the refolding of barnase analyzed by a protein engineering procedure. *J Mol Biol* **224**(3)**:** 819-835

Mauguen Y, Hartley RW, Dodson EJ, Dodson GG, Bricogne G, Chothia C, Jack A (1982) Molecular structure of a new family of ribonucleases. *Nature* **297:** 162-164

McKenzie JL (2006) A Preliminary Investigation of the Application of MALDI-TOF Mass Spectrometry to Biological Systems. MSc Thesis, Biological Science, University of Waikato, Hamilton

Meiering EM, Bycroft M, Lubienski MJ, Fersht AR (1993) Structure and dynamics of barnase complexed with 3'-gmp studied by NMR-spectroscopy. *Biochemistry* **32**(41)**:** 10975-10987

Michaelis L, Menten ML (1913) *Biochemische Zeitschrift* **49:** 333

Miller BG, Wolfenden R (2002) Catalytic proficiency: The unusual case of OMP decarboxylase. *Annu Rev Biochem* **71:** 847-885

Mittermaier AK, Kay LE (2009) Observing biological dynamics at atomic resolution using NMR. *Trends BiochemSci* **34**(12)**:** 601-611

Mossakowska DE, Nyberg K, Fersht AR (1989) Kinetic characterization of the recombinant ribonuclease from *Bacillus amyloliquefaciens* (barnase) and investigation of key residues in catalysis by site-directed mutagenesis. *Biochemistry* **28**(9)**:** 3843-3850

Okorokov AL, Hartley RW, Panov KI (1994) An improved system for ribonuclease BA expression. *Protein Expr Purif* **5**(6)**:** 547-552

Paddon CJ, Vasantha N, Hartley RW (1989) Translation and processing of *Bacillus amyloliquefaciens* extracellular RNase. *J Bacteriol* **171**(2)**:** 1185-1187

Pauling L (1948) The nature of forces between large molecules of biological interest. *Nature* **161:** 707-709

Peterson ME (2005) Evidence for a third thermal parameter of enzymes. PhD Thesis, Biological Sciences, University of Waikato, Hamilton

Peterson ME, Daniel RM, Danson MJ, Eisenthal R (2007) The dependence of enzyme activity on temperature: determination and validation of parameters. *Biochem J* **402:** 331-337

Peterson ME, Eisenthal R, Danson MJ, Spence A, Daniel RM (2004) A new intrinsic thermal parameter for enzymes reveals true temperature optima. *J Biol Chem* **279**(20)**:** 20717-20722

Sali D, Bycroft M, Fersht AR (1988) Stabilization of protein structure by interaction of α-helix dipole with a charged side chain. *Nature* **335**(6192)**:** 740-743

Sambrook J, Russell DW (2001) *Molecular cloning: a laboratory manual*, Vol. 1, 3 edn. New York: Cold Spring Harbour Laboratory Press.

Sancho J, Fersht AR (1992) Dissection of an enzyme by protein engineering: The N-terminal and C-terminal fragments of barnase form a native-like complex with restored enzymatic activity. *J Mol Biol* **224**(3)**:** 741-747

Schanstra JP, Ridder A, Kingma J, Janssen DB (1997) Influence of mutations of Val226 on the catalytic rate of haloalkane dehalogenase. *Protein Eng* **10**(1)**:** 53-61

Serrano L, Matouschek A, Fersht AR (1992) The folding of an enzyme: VI. The folding pathway of Barnase: Comparison with theoretical models. *J Mol Biol* **224**(3)**:** 847-859

Sizer IW (1944) Temperature activation and inactivation of the crystalline catalase-hydrogen peroxide system. *J Biol Chem* **154:** 461-473

Stempfer G, Höll-Neugebauer B, Rudolph R (1996) Improved refolding of an immobilized fusion protein. *Nat Biotechnol* **14**(3)**:** 329-334

Thomas TM, Scopes RK (1998) The effects of temperature on the kinetics and stability of mesophilic and thermophilic 3-phosphoglycerate kinases. *Biochem J* **330:** 1087-1095

Tsou C-L (1995) Inactivation precedes overall molecular conformation changes during enzyme denaturation. *Biochimica et Biophysica Acta (BBA) - Protein Structure and Molecular Enzymology* **1253**(2)**:** 151-162

Wang T, Tomic S, Gabdoulline RR, Wade RC (2004) How optimal are the binding energetics of barnase and barstar? *Biophys J* **87**(3)**:** 1618-1630

Warshel A, Sharma PK, Kato M, Xiang Y, Liu H, Olsson MHM (2006) Electrostatic Basis for Enzyme Catalysis. *Chemical Reviews* **106**(8)**:** 3210-3235

Appendix A Reagents and Extra Methods

All percent values are in weight/volume unless noted otherwise. If noted, ingredients were filtered through a MiniSart 0.22 μm filter (Satorius AG, Germany) and solutions were filtered through Supor® 200 47 mm 0.2 μm filters (Pall Corporation, USA).

A.1 Buffers and Solutions

All buffers and solutions were made up using RO water and autoclaved, if noted, for at least 15 minutes at 121 °C.

Acetate buffer	5% (v/v) 0.1 M acetic acid, 95% 0.1 M sodium acetate, pH to 5.8 with 0.1 M acetic acid, all with DEPC water
Assay buffer	Mix together Pho buffers A:B in 932:68 ratio, check pH 8.0
Buffer A	20 mM tri-sodium citrate, pH 5.5 with 10 M HCl, 0.2 μm filtered
Buffer B	200 mM NaCl, 1.2 mL of 0.5 M KH_2PO_4, 18.8 mL of 0.5 M K_2HPO_4, pH 8.0 if needed, 0.2 μm filtered
Coomassie stain	0.05% coomassie blue R-250, 25% (v/v) isopropanol, 10% (v/v) acetic acid
DEPC water	0.1% (v/v) diethylpyrocarbonate is made up in 0.2 μm-filtered MQ water and incubated at 37 °C overnight, then autoclaved
Destain	10% acetic acid
FLD (2x)	80% (v/v) formamide, 5 mM EDTA, 0.1% bromophenol blue, 0.1% xylene cyanol FF made up with MQ water
GTE	50 mM glucose, 25 mM Tris-HCl pH 8.0, 10 mM EDTA pH 8.0
M9 salts	1.5% KH_2PO_4, 6.4% $Na_2HPO_4{\cdot}7H_2O$, 0.25% NaCl, 0.5% NH_4Cl, pH 7.2 and autoclaved (Note: $^{15}NH_4Cl$ used for NMR labelling)

Pho buffer A	0.355% Na_2HPO_4 (0.1 M) in DEPC water
Pho buffer B	0.390% $NaH_2PO_4 \cdot 2H_2O$ (0.1 M) in DEPC water
QX4	200 mM Tris-HCl pH 6.8, 8% SDS, 40% (v/v) glycerol, 0.4% bromophenol blue, 400 mM ß-mercaptoethanol
Resolving buffer	1.5 M Tris-HCl pH 8.8
Running buffer	25 mM Tris-HCl pH 6.8, 0.1% SDS, 190 mM glycine
Stacking buffer	0.5 M Tris-HCl pH 6.8
TBE (10x)	10.78% Tris base, 5.50% boric acid, 20 mM EDTA, made up with MQ water at pH 8.3
Tris	10 mM Tris-HCl, pH 8.0
100 mM Tris	100 mM Tris-HCl, pH 8.0

A.2 Growth Media

All media were made up with MQ water and sterilised via autoclaving at 121 °C for at least 15 minutes.

A.2.1 Solid Media

Agar was stored after autoclaving in a 55°C oven to preserve liquidity. Antibiotics were added at the desired concentration before pouring plates.

LB Agar	1% bactotryptone, 0.5% yeast extract, 0.5% NaCl, 1.2% agar

A.2.2 Liquid Media

LB	1% bactotryptone, 0.5% yeast extract, 1% NaCl, pH 7.0
M9	All v/v with no autoclaving: 20% M9 salts, 2% of 20% 0.22 μm-filtered D-glucose stock, 1% basal vitamins eagle media (Sigma-Adrich, USA), 0.2% pre-autoclaved 1 M $MgSO_4$, 0.01% pre-autoclaved 1 M $CaCl_2$
SOC	2% peptone from casein, 0.55% yeast extract, 10 mM NaCl, 2.5 mM KCl, the following ingredients were 0.22 μm-

filtered and added after autoclaving: 10 mM $MgCl_2$, 10 mM $MgSO_4$, 20 mM glucose

TB — Made up to 90% of volume and autoclaved: 1.2% bactotryptone, 2.4% yeast extract, 0.4% (v/v) glycerol. Made up to 10% of volume and autoclaved: 0.231% KH_2PO_4, 1.254% K_2HPO_4. The two solutions are combined using sterile techniques before use.

A.3 Antibiotics

The following antibiotics were made up as stocks, filtered through a MiniSart 0.22 μm filter (Satorius AG, Germany), and then used at one thousand-fold dilutions in all liquid media and agar plates:

Ampicillin — 100 mg/mL

Tetracycline — 25 mg/mL dissolved in 100% EtOH

A.4 PAGE Gels

A.4.1 15% SDS-PAGE Gels

Gels were made according to the following recipe and method, based on Sambrook et al. (Sambrook & Russell, 2001) which provides for 5 gels in a small multiple gel casting apparatus (Hoefer, USA). Note: 10% APS (ammonium persulphate) needs to be less than 1 week old.

Prepare the gel casting apparatus with 5 casts, then make up the following:

Resolving gel — 7.05 mL RO water, 15 mL 30% acrylamide, 7.5 mL resolving buffer, 300 μL 10% SDS (sodium dodecyl sulphate), 150 μL 10% APS, 15 μL TEMED (tetramethyl ethylene diamine)

This is gently mixed (inverted), added to the casts, then each individual gel is overlaid gently with 2 mL of isopropanol. Time to set is approximately 40 minutes. When set, the isolpropanol is drained away and the casts set upside down whilst the following is made up:

5% Stacking gel 8.5 mL RO water, 2.125 mL 30% acrylamide, 1.6 mL stacking buffer, 125 μL 10% SDS, 63 μL 10% APS, 6.3 μL TEMED

This is then added to each cast after gentle mixing, the combs inserted, and the whole apparatus is covered with a moist kitchen towel. Polymerisation takes approximately 30 minutes. Gels can be stored at 4 °C in a moist wrapping for up to two weeks.

A.4.2 5% Urea Denaturing PAGE Gels

As above, the following makes 5 gels in similar apparatus.

Gel mixture 12.6 g urea (final conc. 7 M), 20.6 mL RO water, 5 mL 30% acrylamide, 4.4 mL 10x TBE buffer and mix together at 55 °C until all is dissolved

130 μL 10% APS and 30 μL TEMED are added and gently mixed in before adding to the casting apparatus and inserting combs. At least an hour is needed to set and gels are very fragile.

A.5 Bacterial Strains and Preparations

A.5.1 *Escherichia Coli* DH5-α cells

Geneotype: F- φ80*lac*ZΔM15 Δ(*lac*ZYA-*arg*F) U169 *rec*A1 *end*A1 *hsd*R17 (rk-, mk+) *pho*A *sup*E44 λ- *thi*-1 *gyr*A96 *rel*A1

DH5-α cells were from Invitrogen (USA) (Catalogue #18258-012) and used for transformations of WT Barnase plasmids, expression and mini-preps.

A.5.2 *Escherichia Coli* XL1-blue cells

Geneotype: *rec*A1 *end*A1 *gyr*A96 *thi*-1 *hsd*R17 *sup*E44 *rel*A1 *lac* [F′ *proAB lacI*qZΔM15 Tn*10* (Tetr)]

XL1-blue cells were from Stratagene (USA) (Catalogue #200249) and used for transformations of mutant Barnase plasmids, expression and mini-preps.

A.5.3 Preparation of Electrocompetent XL1-blue Cells

Electrocompetent XL1-blue *E. coli* cells were prepared using a modified method based on the Gene Pulser™ operating manual (Bio-Rad Laboratories, USA, Catalogue #165-2098). 10 μL of XL1-blue cells (Section A.5.2) from the provided stock in the Stratagene QuikChange™ II-E kit (Section 2.3) was resuspended in 250 μL SOC media and incubated at 37 °C for 1 hour, then streaked on LB-agar plates with tetracycline at 25 μg/mL. The plate was incubated overnight at 37 °C. A single colony was used to inoculate an overnight 10 mL culture in LB media, shaken at 200 rpm at 37 °C. This starter culture was used to inoculate a 1 L culture of LB media incubated at 37 °C with 200 rpm shaking until at OD_{600} of 0.6.

This flask was chilled on ice for 30 minutes, then cells were pelleted at 4000 x g and 4 °C for 15 minutes in 750 mL centrifuge bottles. The supernatant was poured off and cells gently resuspended in 1 L of ice-cold, sterile, 10% glycerol. Cells were similarly centrifuged and resuspended in 500 mL then 20 mL of the 10% glycerol, decreasing the volume whilst increasing the concentration of cells. Pelleting and resuspension in 2 mL of the 10% glycerol gives a stock that can be aliquotted and snap-frozen at -80 °C using an EtOH slurry. The transformation efficiency of the cells was found to be $6x10^8$ cfu/μg of DNA for a pUC18 plasmid.

A.6 DNA Mini-prep Method (Alkaline Lysis)

The following is based on established methods (Sambrook & Russell, 2001): For plasmid sequencing, a 4 mL culture of TB media was inoculated with a single colony from an agar plate prepared as in Section 2.2.3.1. 3 μL ampicillin stock was added and the culture shaken at 200 rpm overnight in a 13 mL tube at 30 °C. Overnight culture was divided into two 1.5 mL centrifuge tubes and spun down at 13000 rpm in a MiniSpin™ Plus centrifuge (Eppendorf, Germany) for 2 minutes at room temperature. The remaining 1 mL was used for glycerol cell stocks (Section 0). Each cell pellet was then treated as follows: 200 μL GTE buffer kept at 4 °C was added for resuspension. 300 μL room temperature 0.2 M NaOH/1% SDS was mixed in gently with a pipette and left for 5 minutes. 300 μL 3.0 M

potassium acetate solution (pH 4.8) was added and the resulting solution left on ice for 10 minutes.

This solution was spun down similarly for 10 minutes, the supernatant transferred to a new tube with 1 μL 20 mg/mL RNAse A (Invitrogen, USA), and incubated at 37 °C for 20 minutes. 500 μL chloroform was mixed in and spun down for 1 minute to separate the phases. After transferring the aqueous layer to another 1.5 mL tube, the chloroform extraction was repeated. Removing the aqueous layer to another 1.5 mL tube, DNA was precipitated by addition of an equal volume of isopropanol, and spun down for 10 minutes.

The pellet of DNA was washed with 500 μL 70% EtOH and left to air dry. The dry pellet was dissolved in 64 μL MQ water and transferred to a new 1.5 mL tube, the old tube being washed out with 32 μL MQ water and pooled with the main volume. 24 μL 4 M NaCl and 120 μL autoclaved polyethylene glycol (PEG 8000) were mixed in thoroughly, then incubated on ice for 20 minutes. The mixture was spun similarly, but at 4 °C for 25 minutes, and the supernatant carefully removed. 400 μL 70% EtOH was used to wash the pellet, then it was air dried and resuspended in Tris buffer for storage at -20 °C.

A.7 Rotavirus RNA Synthesis

All reagents not listed in Appendix A.1 were from Joanna McKenzie (The University of Waikato).

A ~3-cm square portion of 14.6 mm diameter Spectra/Por® 6-8 kDa cut-off dialysis membrane tube (Spectrum Laboratories, USA) was pre-wet in 100 mM Tris buffer. 21 μL Rotavirus DLPs were placed into a 20 μL dialysis button covered with the membrane. In 50 mL of 100 mM Tris, the button was shaken gently on an orbital mixer for 2 hours, then in fresh buffer overnight. A small hole was made in the membrane with a sterile scalpel and 15 μL of the solution added to a 1.5 mL centrifuge tube (~ 0.1 μg/mL). 20 μL 1 M Tris (pH 8.0), 20 μL 10 mM rNTPs, 12 μL 100 mM $MgCl_2$ and 133 μL 0.22 μm-filtered MQ water were added and incubated at 37 °C for 1 hour, shaken at 300 rpm.

100 μL 7.5 M ammonium acetate and 500 μL 100 % EtOH were mixed in well and the solution incubated at -80 °C for 1-24 hours depending on available time. The slurry was then spun down at 13000 rpm at 4 °C for 25 minutes on a Biofuge Fresco™ centrifuge (Thermofisher Scientific, USA). The supernatant was carefully removed and the pellet air-dried for 30 minutes then resuspended in 20 μL 0.22 μm-filtered DEPC water. The concentration of RNA was determined as in Section 2.2.2, usually 1-5 μg/μL, and the solution stored at 4 °C.

A.8 Thermocouple Calibration

Thermocouples A and B, both H1 93530 thermocouple probes (Hanna Instruments, USA), were equilibrated in a water bath along with a NIST-traceable high resolution glass thermometer (Cole-Parmer, USA), the temperature increased in 5 °C increments and the readings from the thermometer plotted against those from the thermocouples. A linear relationship (R^2 >0.9999) was then used to convert thermocouple readings to accurate temperatures in assays.

Appendix B Derivations of Model Equations

B.1 Original Equilibrium Model

See section 1.2.2 for the reasoning behind derivations and explanations of terms. **Bold** equation numbers represent a final equation.

B.1.1 Original Model Species

$$E_{act} \underset{\longleftarrow}{\overset{K_{eq}}{\longrightarrow}} E_{inact} \xrightarrow{k_{inact}} X$$

B.1.2 General Definitions

$$V_{max} = k_{cat} \cdot [E_{act}] \tag{1.}$$

$$[E_0] = [E_{act}] + [E_{inact}] + [X] \tag{2.}$$

$$K_{eq} = \exp\left(\frac{\Delta H_{eq}}{R} \cdot \left(\frac{1}{T_{eq}} - \frac{1}{T}\right)\right) \quad \text{and} \quad K_{eq} = \frac{[E_{inact}]}{[E_{act}]} \tag{3. a\&b}$$

$$k_{cat} = \frac{k_B \cdot T}{h_P} \cdot \exp\left(\frac{-\Delta G^{\ddagger}_{cat}}{R \cdot T}\right) \tag{4.}$$

$$k_{inact} = \frac{k_B \cdot T}{h_P} \cdot \exp\left(\frac{-\Delta G^{\ddagger}_{inact}}{R \cdot T}\right) \tag{5.}$$

B.1.3 Derivations from General Definitions

$$[E_{act}] = \frac{[E_0] - [X]}{1 + K_{eq}} \quad \text{via (2) and (3b)} \tag{6.}$$

$$[E_{inact}] = \frac{[E_0] - [X]}{1 + 1/K_{eq}} \quad \text{via (2) and (3b)} \tag{7.}$$

$$V_{max} = k_{cat} \cdot \frac{[E_0] - [X]}{1 + K_{eq}} \quad \text{via (1) and (6)} \tag{8.}$$

B.1.4 Original Model Manipulations

$$\frac{d[X]}{dt} = k_{inact} \cdot [E_{inact}] \tag{9.}$$

$$\frac{d[X]}{dt} = \frac{k_{inact}}{1+1/K_{eq}} \cdot ([E_0]-[X]) \quad \text{via (7)} \tag{10.}$$

$$\frac{d[X]}{[E_0]-[X]} = \frac{k_{inact}}{1+1/K_{eq}}\, dt \tag{11.}$$

$$-\ln([E_0]-[X]) = \frac{k_{inact}}{1+1/K_{eq}} \cdot t + c \tag{12.}$$

$$[E_0]-[X] = \exp\left(\frac{-k_{inact} \cdot K_{eq} \cdot t}{1+K_{eq}}\right) \cdot \exp(c) \quad \text{(by multiplying through } K_{eq}\text{)} \tag{13.}$$

$$\begin{aligned} &\text{at } t = 0,\ [E_0]-[X] = \exp(c) \\ &\therefore \text{ if } [X]_0 = 0,\ [E_0] = \exp(c) \end{aligned} \tag{14.}$$

$$\therefore\ [E_0]-[X] = [E_0] \cdot \exp\left(\frac{-k_{inact} \cdot K_{eq} \cdot t}{1+K_{eq}}\right) \quad \text{via (14)} \tag{15.}$$

B.1.5 Original Model Rate Equation

$$V_{max} = \frac{k_{cat} \cdot [E_0]}{1+K_{eq}} \cdot \exp\left(\frac{-k_{inact} \cdot K_{eq} \cdot t}{1+K_{eq}}\right) \quad \text{via (8) and (15)} \tag{16.}$$

The above can be expanded to include $\Delta G^{\ddagger}$ terms via (4) & (5) and expanded to include ΔH_{eq} and T_{eq} terms via (3a).

B.1.6 Original Model Product Equation

The product equation is the integration of the rate equation with respect to time:

$$\frac{d[P]}{dt} = V_{max} \ \therefore\ [P] = \int \frac{k_{cat} \cdot [E_0]}{1+K_{eq}} \cdot \exp\left(\frac{-k_{inact} \cdot K_{eq} \cdot t}{1+K_{eq}}\right) dt \quad \text{via (16)} \tag{17.}$$

$$\therefore\ [P] = \frac{k_{cat} \cdot [E_0]}{k_{inact} \cdot K_{eq}} \cdot \left(1 - \exp\left(\frac{-k_{inact} \cdot K_{eq} \cdot t}{1+K_{eq}}\right)\right) \tag{18.}$$

The product equation can be expanded to include $\Delta G^{\ddagger}$, ΔH_{eq} and T_{eq} terms also.

B.1.7 Original Model Species Concentration Equations

$$[E_{act}] = \frac{[E_0]}{1+K_{eq}} \cdot \exp\left(\frac{-k_{inact} \cdot K_{eq} \cdot t}{1+K_{eq}}\right) \quad \text{via (6) and (15)} \quad \textbf{(19.)}$$

$$[E_{inact}] = \frac{[E_0]}{1+1/K_{eq}} \cdot \exp\left(\frac{-k_{inact} \cdot K_{eq} \cdot t}{1+K_{eq}}\right) \quad \text{via (7) and (15)} \quad \textbf{(20.)}$$

$$[X] = [E_0] - [E_0] \cdot \exp\left(\frac{-k_{inact} \cdot K_{eq} \cdot t}{1+K_{eq}}\right) \quad \text{via (15)} \quad (21.)$$

$$[X] = [E_0] \cdot \left(1 - \exp\left(\frac{-k_{inact} \cdot K_{eq} \cdot t}{1+K_{eq}}\right)\right) \quad \textbf{(22.)}$$

B.2 Model "M"

B.2.1 Model "M" Species

$$\left[E_{act} \overset{K_{eq}}{\rightleftharpoons} E_{inact}\right] \xrightarrow{k_{inact}} X$$

B.2.2 New Manipulations for Model "M"

$$\frac{d[X]}{dt} = k_{inact} \cdot \left([E_{act}] + [E_{inact}]\right) \quad (23.)$$

$$\frac{d[X]}{dt} = k_{inact} \cdot \left([E_0] - [X]\right) \quad \text{via (2)} \quad (24.)$$

$$\frac{d[X]}{[E_0] - [X]} = k_{inact}\, dt \quad (25.)$$

$$-\ln\left([E_0] - [X]\right) = k_{inact} \cdot t + c \quad (26.)$$

$$[E_0] - [X] = \exp\left(-k_{inact} \cdot t\right) \cdot \exp(c) \quad (27.)$$

$$\therefore\ [E_0] - [X] = [E_0] \cdot \exp\left(-k_{inact} \cdot t\right) \quad \text{via (14)} \quad (28.)$$

B.2.3 Model "M" Rate Equation

$$V_{max} = \frac{k_{cat} \cdot [E_0]}{1+K_{eq}} \cdot \exp\left(-k_{inact} \cdot t\right) \quad \text{via (8) and (28)} \quad \textbf{(29.)}$$

The above equation can be expanded as in Section B.1.5.

B.2.4 Model "M" Product Equation

The product equation is the integration of the rate equation with respect to time:

$$\frac{d[P]}{dt} = V_{max} \;\therefore\; [P] = \int \frac{k_{cat} \cdot [E_0]}{1 + K_{eq}} \cdot \exp\left(-k_{inact} \cdot t\right) dt \qquad \text{via (29)} \tag{30.}$$

$$\therefore\; [P] = \frac{k_{cat} \cdot [E_0]}{k_{inact} \cdot \left(1 + K_{eq}\right)} \cdot \left(1 - \exp\left(-k_{inact} \cdot t\right)\right) \tag{31.}$$

The above equation can be expanded as in Section B.1.5.

B.2.5 Model "M" Species Concentration Equations

$$[E_{act}] = \frac{[E_0]}{1 + K_{eq}} \cdot \exp\left(-k_{inact} \cdot t\right) \qquad \text{via (6) and (28)} \tag{32.}$$

$$[E_{inact}] = \frac{[E_0]}{1 + 1/K_{eq}} \cdot \exp\left(-k_{inact} \cdot t\right) \qquad \text{via (7) and (28)} \tag{33.}$$

$$[X] = [E_0] - [E_0] \cdot \exp\left(-k_{inact} \cdot t\right) \qquad \text{via (28)} \tag{34.}$$

$$[X] = [E_0] \cdot \left(1 - \exp\left(-k_{inact} \cdot t\right)\right) \tag{35.}$$

B.3 Reversible Denaturation Models (N & Q)

For these models, it is not possible to separate ([E_0] – [X]) from the time-independent rate variables (as in (25.)) and then directly integrate both sides with respect to X and t independently. Hence, a general method for solving linear differential equations is required:

For equations of the form: $$\frac{d[X]}{dt} + A \cdot [X](t) = B \tag{36.}$$

it can be shown that: $$[X](t) = \frac{\int B \cdot \exp\left(A \cdot t\right) dt}{\exp\left(A \cdot t\right)} + \frac{C}{\exp\left(A \cdot t\right)} \tag{37.}$$

where C is a constant. That simplifies to:

$$[X](t) = \frac{B}{A} + C \cdot \exp\left(-A \cdot t\right) \tag{38.}$$

if we let: $[X](0) = 0$ then $0 = \frac{B}{A} + C \cdot \exp\left(-A \cdot 0\right) = \frac{B}{A} + C$ (39. a&b)

$$\therefore\ C = -\frac{B}{A} \quad \text{and} \quad [X](t) = \frac{B}{A} - \frac{B}{A} \cdot \exp\left(-A \cdot t\right) \quad \text{simplifying to:} \tag{40.}$$

$$[X](t) = \frac{B}{A}\left(1 - \exp\left(-A \cdot t\right)\right) \tag{41.}$$

which can be substituted into (8) instead of the usual ([E_0] – [X]) term.

B.4 Model "N"

B.4.1 Model "N" Species

$$\left[E_{act} \underset{\longleftarrow}{\overset{K_{eq}}{\longrightarrow}} E_{inact} \right] \underset{k_{react}}{\overset{k_{inact}}{\rightleftharpoons}} X$$

B.4.2 New Definitions for Model "N"

$$k_{react} = \frac{k_B \cdot T}{h_P} \cdot \exp\left(\frac{-\Delta G^{\ddagger}_{react}}{R \cdot T}\right) \quad (k_{react} \text{ is the renaturation constant}) \tag{42.}$$

B.4.3 New Manipulations for Model "N"

$$\frac{d[X]}{dt} = k_{inact} \cdot \left([E_0] - [X]\right) - k_{react} \cdot [X] \quad \text{modifying (24)} \tag{43.}$$

$$\frac{d[X]}{dt} + \left(k_{inact} + k_{react}\right) \cdot [X] = k_{inact} \cdot [E_0] \tag{44.}$$

Model N must be solved as in Appendix Section B.3. We let:

$$A = k_{inact} + k_{react} \quad \text{and} \quad B = k_{inact} \cdot [E_0] \tag{45. a&b}$$

$$\therefore\ [X] = \frac{k_{inact} \cdot [E_0]}{k_{inact} + k_{react}} \cdot \left(1 - \exp\left(-\left(k_{inact} + k_{react}\right) \cdot t\right)\right) \quad \text{via (41)} \tag{46.}$$

This can be simplified using A (45 a):

$$[X] = \frac{k_{inact} \cdot [E_0]}{A} \cdot \left(1 - \exp\left(-A \cdot t\right)\right) \tag{47.}$$

B.4.4 Model "N" Rate Equation

$$V_{max} = \frac{k_{cat}}{1+K_{eq}} \cdot \left([E_0] - \frac{k_{inact} \cdot [E_0]}{A} \cdot \left(1 - \exp\left(-A \cdot t\right)\right) \right) \quad \text{via (8) and (47)} \quad (48.)$$

$$V_{max} = \frac{k_{cat} \cdot [E_0]}{1+K_{eq}} \cdot \left(1 - \frac{k_{inact}}{A} \cdot \left(1 - \exp\left(-A \cdot t\right)\right) \right) \quad \textbf{(49.)}$$

The above equation can be expanded as in Section B.1.5.

B.4.5 Model "N" Product Equation

The product equation is the integration of the rate equation with respect to time:

$$\frac{d[P]}{dt} = V_{max} \;\; \therefore \;\; [P] = \int \frac{k_{cat} \cdot [E_0]}{1+K_{eq}} \cdot \left(1 - \frac{k_{inact}}{A} \cdot \left(1 - \exp\left(-A \cdot t\right)\right) \right) dt \quad \text{via (49)} \quad (50.)$$

$$\therefore \;\; [P] = \frac{k_{cat} \cdot [E_0]}{1+K_{eq}} \cdot \left(t - \frac{k_{inact} \cdot \left(A \cdot t + \exp\left(-A \cdot t\right)\right)}{A^2} \right) \quad \textbf{(51.)}$$

The above equation can be expanded as in Section B.1.5.

B.4.6 Model "N" Species Concentration Equations

$$[E_{act}] = \frac{[E_0]}{1+K_{eq}} \cdot \left(1 - \frac{k_{inact}}{A} \cdot \left(1 - \exp\left(-A \cdot t\right)\right) \right) \quad \text{via (6) and (47)} \quad \textbf{(52.)}$$

$$[E_{inact}] = \frac{[E_0]}{1+1/K_{eq}} \cdot \left(1 - \frac{k_{inact}}{A} \cdot \left(1 - \exp\left(-A \cdot t\right)\right) \right) \quad \text{via (7) and (47)} \quad \textbf{(53.)}$$

[X] is defined above (47).

B.5 Model "O"

B.5.1 Model "O" Species

$$X \xleftarrow{k_{deact}} E_{act} \xrightleftharpoons{K_{eq}} E_{inact}$$

B.5.2 New Definitions for Model "O"

$$k_{deact} = \frac{k_B \cdot T}{h_P} \cdot \exp\left(\frac{-\Delta G^{\ddagger}_{deact}}{R \cdot T}\right) \quad (k_{deact} \text{ is the } E_{act} \text{ denaturation constant}) \quad (54.)$$

B.5.3 New Manipulations for Model "O"

$$\frac{d[X]}{dt} = k_{deact} \cdot [E_{act}] \quad (55.)$$

$$\frac{d[X]}{dt} = \frac{k_{deact}}{1 + K_{eq}} \cdot \left([E_0] - [X]\right) \quad \text{via (6)} \quad (56.)$$

$$\frac{d[X]}{[E_0] - [X]} = \frac{k_{deact}}{1 + K_{eq}}\, dt \quad (57.)$$

$$-\ln\left([E_0] - [X]\right) = \frac{k_{deact}}{1 + K_{eq}} \cdot t + c \quad (58.)$$

$$[E_0] - [X] = \exp\left(\frac{-k_{deact} \cdot t}{1 + K_{eq}}\right) \cdot \exp(c) \quad (59.)$$

$$\therefore\ [E_0] - [X] = [E_0] \cdot \exp\left(\frac{-k_{deact} \cdot t}{1 + K_{eq}}\right) \quad \text{via (14)} \quad (60.)$$

B.5.4 Model "O" Rate Equation

$$V_{max} = \frac{k_{cat} \cdot [E_0]}{1 + K_{eq}} \cdot \exp\left(\frac{-k_{deact} \cdot t}{1 + K_{eq}}\right) \quad \text{via (8) and (60)} \quad \mathbf{(61.)}$$

The above equation can be expanded as in Section B.1.5.

B.5.5 Model "O" Product Equation

The product equation is the integration of the rate equation with respect to time:

$$\frac{d[P]}{dt} = V_{max} \ \therefore\ [P] = \int \frac{k_{cat} \cdot [E_0]}{1 + K_{eq}} \cdot \exp\left(\frac{-k_{deact} \cdot t}{1 + K_{eq}}\right) dt \quad \text{via (61)} \quad (62.)$$

$$\therefore\ [P] = \frac{k_{cat} \cdot [E_0]}{k_{inact}} \cdot \left(1 - \exp\left(\frac{-k_{deact} \cdot t}{1 + K_{eq}}\right)\right) \quad \mathbf{(63.)}$$

The above equation can be expanded as in Section B.1.5.

B.5.6 Model "O" Species Concentration Equations

$$[E_{act}] = \frac{[E_0]}{1+K_{eq}} \cdot \exp\left(\frac{-k_{deact} \cdot t}{1+K_{eq}}\right) \quad \text{via (6) and (60)} \quad \textbf{(64.)}$$

$$[E_{inact}] = \frac{[E_0]}{1+1/K_{eq}} \cdot \exp\left(\frac{-k_{deact} \cdot t}{1+K_{eq}}\right) \quad \text{via (7) and (60)} \quad \textbf{(65.)}$$

$$[X] = [E_0] - [E_0] \cdot \exp\left(\frac{-k_{deact} \cdot t}{1+K_{eq}}\right) \quad \text{via (60)} \quad (66.)$$

$$[X] = [E_0] \cdot \left(1 - \exp\left(\frac{-k_{deact} \cdot t}{1+K_{eq}}\right)\right) \quad \textbf{(67.)}$$

B.6 Model "P"

B.6.1 Model "P" Species

$$X \xleftarrow{k_{deact}} E_{act} \xrightleftharpoons{K_{eq}} E_{inact} \xrightarrow{k_{inact}} X$$

B.6.2 New Manipulations for Model "P"

$$\frac{d[X]}{dt} = k_{inact} \cdot [E_{inact}] + k_{deact} \cdot [E_{act}] \quad (68.)$$

$$\frac{d[X]}{dt} = k_{inact} \cdot \frac{[E_0]-[X]}{1+1/K_{eq}} + k_{deact} \cdot \frac{[E_0]-[X]}{1+K_{eq}} \quad \text{via (6) and (7)} \quad (69.)$$

$$\frac{d[X]}{dt} = ([E_0]-[X]) \cdot \left(\frac{k_{inact} \cdot K_{eq} + k_{deact}}{1+K_{eq}}\right) \quad \text{(by multiplying through } K_{eq}\text{)} \quad (70.)$$

$$\frac{d[X]}{[E_0]-[X]} = \frac{k_{inact} \cdot K_{eq} + k_{deact}}{1+K_{eq}}\, dt \quad (71.)$$

$$-\ln([E_0]-[X]) = \frac{k_{inact} \cdot K_{eq} + k_{deact}}{1+K_{eq}} \cdot t + c \quad (72.)$$

$$[E_0]-[X] = \exp\left(\frac{-(k_{inact} \cdot K_{eq} + k_{deact}) \cdot t}{1+K_{eq}}\right) \cdot \exp(c) \quad (73.)$$

$$\therefore\ [E_0]-[X]=[E_0]\cdot\exp\left(\frac{-\left(k_{inact}\cdot K_{eq}+k_{deact}\right)\cdot t}{1+K_{eq}}\right)\quad \text{via (14)} \qquad (74.)$$

B.6.3 Model "P" Rate Equation

$$V_{max}=\frac{k_{cat}\cdot[E_0]}{1+K_{eq}}\cdot\exp\left(\frac{-\left(k_{inact}\cdot K_{eq}+k_{deact}\right)\cdot t}{1+K_{eq}}\right)\quad \text{via (8) and (74)} \qquad \textbf{(75.)}$$

The above equation can be expanded as in Section B.1.5.

B.6.4 Model "P" Product Equation

The product equation is the integration of the rate equation with respect to time:

$$\frac{d[P]}{dt}=V_{max}\ \therefore\ [P]=\int\frac{k_{cat}\cdot[E_0]}{1+K_{eq}}\cdot\exp\left(\frac{-\left(k_{inact}\cdot K_{eq}+k_{deact}\right)\cdot t}{1+K_{eq}}\right)dt\quad \text{via (75)} \qquad (76.)$$

$$\therefore\ [P]=\frac{k_{cat}\cdot[E_0]}{k_{inact}\cdot K_{eq}+k_{deact}}\cdot\left(1-\exp\left(\frac{-\left(k_{inact}\cdot K_{eq}+k_{deact}\right)\cdot t}{1+K_{eq}}\right)\right) \qquad \textbf{(77.)}$$

The above equation can be expanded as in Section B.1.5.

B.6.5 Model "P" Species Concentration Equations

$$[E_{act}]=\frac{[E_0]}{1+K_{eq}}\cdot\exp\left(\frac{-\left(k_{inact}\cdot K_{eq}+k_{deact}\right)\cdot t}{1+K_{eq}}\right)\quad \text{via (6) and (74)} \qquad \textbf{(78.)}$$

$$[E_{inact}]=\frac{[E_0]}{1+1/K_{eq}}\cdot\exp\left(\frac{-\left(k_{inact}\cdot K_{eq}+k_{deact}\right)\cdot t}{1+K_{eq}}\right)\quad \text{via (7) and (74)} \qquad \textbf{(79.)}$$

$$[X]=[E_0]-[E_0]\cdot\exp\left(\frac{-\left(k_{inact}\cdot K_{eq}+k_{deact}\right)\cdot t}{1+K_{eq}}\right)\quad \text{via (74)} \qquad (80.)$$

$$[X]=[E_0]\cdot\left(1-\exp\left(\frac{-\left(k_{inact}\cdot K_{eq}+k_{deact}\right)\cdot t}{1+K_{eq}}\right)\right) \qquad \textbf{(81.)}$$

B.7 Model "Q"

B.7.1 Model "Q" Species

$$X \underset{k_a}{\overset{k_{-a}}{\rightleftharpoons}} E_{act} \overset{K_{eq}}{\rightleftharpoons} E_{inact} \underset{k_{-i}}{\overset{k_i}{\rightleftharpoons}} X$$

B.7.2 New Definitions for Model "Q"

$k_i = k_{inact}$ as previously (5)

$k_a = k_{deact}$ as previously (51)

With associated $\Delta G^{\ddagger}$ values as output parameters, named appropriately.

$$k_{-i} = \frac{k_b \cdot T}{h_p} \cdot \exp\left(\frac{-\Delta G^{\ddagger}_{-i}}{R \cdot T}\right) \quad (k_{-i} \text{ is the } E_{inact} \text{ renaturation constant}) \qquad (82.)$$

$$k_{-a} = \frac{k_b \cdot T}{h_p} \cdot \exp\left(\frac{-\Delta G^{\ddagger}_{-a}}{R \cdot T}\right) \quad (k_{-a} \text{ is the } E_{act} \text{ renaturation constant}) \qquad (83.)$$

B.7.3 New Manipulations for Model "Q"

$$\frac{d[X]}{dt} = k_a \cdot [E_{act}] - k_{-a} \cdot [X] + k_i \cdot [E_{inact}] - k_{-i} \cdot [X] \qquad (84.)$$

$$\frac{d[X]}{dt} = k_a \cdot [E_{act}] + k_i \cdot [E_{inact}] - [X] \cdot \left(k_{-a} + k_{-i}\right) \qquad (85.)$$

$$\frac{d[X]}{dt} = \left([E_0] - [X]\right) \cdot \left(\frac{k_a + k_i \cdot K_{eq}}{1 + K_{eq}}\right) - [X] \cdot \left(k_{-a} + k_{-i}\right) \quad \text{via (6) and (7)} \qquad (86.)$$

$$\frac{d[X]}{dt} + \left(\frac{k_a + k_i \cdot K_{eq}}{1 + K_{eq}} + k_{-a} + k_{-i}\right) \cdot [X] = \left(\frac{k_a + k_i \cdot K_{eq}}{1 + K_{eq}}\right) \cdot [E_0] \qquad (87.)$$

Model Q must be solved as in Appendix Section B.3. We let:

$$A = \frac{k_a + k_i \cdot K_{eq}}{1 + K_{eq}} + k_{-a} + k_{-i} \quad \text{and} \quad B = \left(\frac{k_a + k_i \cdot K_{eq}}{1 + K_{eq}}\right) \cdot [E_0] \qquad (88.\ a\&b)$$

$$\therefore\ [X]=\frac{\left(\frac{k_a+k_i\cdot K_{eq}}{1+K_{eq}}\right)\cdot[E_0]}{\frac{k_a+k_i\cdot K_{eq}}{1+K_{eq}}+k_{-a}+k_{-i}}\cdot\left(1-\exp\left(-\left(\frac{k_a+k_i\cdot K_{eq}}{1+K_{eq}}+k_{-a}+k_{-i}\right)\cdot t\right)\right)\text{ via (41) (89.)}$$

This can be simplified into compound terms D (where $D = B/[E_0]$) and A:

$$D=\frac{k_a+k_i\cdot K_{eq}}{1+K_{eq}} \qquad (90.)$$

$$[X]=\frac{D\cdot[E_0]}{A}\cdot\left(1-\exp\left(-A\cdot t\right)\right) \qquad \textbf{(91.)}$$

This holds for all reversible models; N,Q and R.

B.7.4 Model "Q" Rate Equation

$$V_{max}=\frac{k_{cat}}{1+K_{eq}}\cdot\left([E_0]-\frac{D\cdot[E_0]}{A}\cdot\left(1-\exp\left(-A\cdot t\right)\right)\right)\quad\text{via (8) and (91)} \qquad (92.)$$

$$V_{max}=\frac{k_{cat}\cdot[E_0]}{1+K_{eq}}\cdot\left(1-\frac{D}{A}\cdot\left(1-\exp\left(-A\cdot t\right)\right)\right) \qquad \textbf{(93.)}$$

The above equation can be expanded as in Section B.1.5.

B.7.5 Model "Q" Product Equation

The product equation is the integration of the rate equation with respect to time:

$$\frac{d[P]}{dt}=V_{max}\ \therefore\ [P]=\int\frac{k_{cat}\cdot[E_0]}{1+K_{eq}}\cdot\left(1-\frac{D}{A}\cdot\left(1-\exp\left(-A\cdot t\right)\right)\right)dt\quad\text{via (93.)} \qquad (94.)$$

$$\therefore\ [P]=\frac{k_{cat}\cdot[E_0]}{1+K_{eq}}\cdot\left(t-\frac{D\cdot\left(A\cdot t+\exp\left(-A\cdot t\right)\right)}{A^2}\right) \qquad \textbf{(95.)}$$

The above equation can be expanded as in Section B.1.5.

B.7.6 Model "Q" Species Concentration Equations

$$[E_{act}]=\frac{[E_0]}{1+K_{eq}}\cdot\left(1-\frac{D}{A}\cdot\left(1-\exp\left(-A\cdot t\right)\right)\right)\quad\text{via (6) and (91)} \qquad \textbf{(96.)}$$

$$[E_{inact}] = \frac{[E_0]}{1+1/K_{eq}} \cdot \left(1 - \frac{D}{A} \cdot \left(1 - \exp\left(-A \cdot t\right)\right)\right) \quad \text{via (7) and (91)} \qquad \textbf{(97.)}$$

$[X]$ is defined above (91).

B.8 Model "R"

B.8.1 Model "R" Species

$$E_{act} \underset{}{\overset{K_{eq}}{\rightleftharpoons}} E_{inact} \underset{k_{react}}{\overset{k_{inact}}{\rightleftharpoons}} X$$

B.8.2 New Manipulations for Model "R"

$$\frac{d[X]}{dt} = k_{inact} \cdot [E_{inact}] - k_{react} \cdot [X] \qquad (98.)$$

$$\frac{d[X]}{dt} = \frac{k_{inact}}{1+1/K_{eq}} \cdot \left([E_0] - [X]\right) - k_{react} \cdot [X] \quad \text{via (6) and (7)} \qquad (99.)$$

$$\frac{d[X]}{dt} + \left(\frac{k_{inact} \cdot K_{eq}}{1+K_{eq}} + k_{react}\right) \cdot [X] = \frac{k_{inact} \cdot K_{eq} \cdot [E_0]}{1+K_{eq}} \qquad (100.)$$

Model R must be solved as in Appendix Section B.3. We let:

$$A = \frac{k_{inact} \cdot K_{eq}}{1+K_{eq}} + k_{react} \quad \text{and} \quad B = \frac{k_{inact} \cdot K_{eq} \cdot [E_0]}{1+K_{eq}} \qquad (101.\ a\&b)$$

$$\therefore\ [X] = \frac{\left(\frac{k_{inact} \cdot K_{eq} \cdot [E_0]}{1+K_{eq}}\right)}{A} \cdot \left(1 - \exp\left(-A \cdot t\right)\right) \quad \text{via (41)} \qquad (102.)$$

This can be simplified via the compound term D (where $D = B/[E_0]$):

$$D = \frac{k_{inact} \cdot K_{eq}}{1+K_{eq}} \qquad (103.)$$

$$[X] = \frac{D \cdot [E_0]}{A} \cdot \left(1 - \exp\left(-A \cdot t\right)\right) \qquad \textbf{(104.)}$$

B.8.3 Model "R" Rate Equation

$$V_{max} = \frac{k_{cat}}{1+K_{eq}} \cdot \left([E_0] - \frac{D \cdot [E_0]}{A} \cdot \left(1 - \exp\left(-A \cdot t\right)\right) \right) \quad \text{via (8) and (104)} \qquad (105.)$$

$$V_{max} = \frac{k_{cat} \cdot [E_0]}{1+K_{eq}} \cdot \left(1 - \frac{D}{A} \cdot \left(1 - \exp\left(-A \cdot t\right)\right) \right) \qquad \textbf{(106.)}$$

The above equation can be expanded as in Section B.1.5.

B.8.4 Model "R" Product Equation

The product equation is the integration of the rate equation with respect to time:

$$\frac{d[P]}{dt} = V_{max} \;\; \therefore \;\; [P] = \int \frac{k_{cat} \cdot [E_0]}{1+K_{eq}} \cdot \left(1 - \frac{D}{A} \cdot \left(1 - \exp\left(-A \cdot t\right)\right) \right) dt \quad \text{via (93.)} \qquad (107.)$$

$$\therefore \;\; [P] = \frac{k_{cat} \cdot [E_0]}{1+K_{eq}} \cdot \left(t - \frac{D \cdot \left(A \cdot t + \exp\left(-A \cdot t\right)\right)}{A^2} \right) \qquad \textbf{(108.)}$$

The above equation can be expanded as in Section B.1.5.

B.8.5 Model "R" Species Concentration Equations

$$[E_{act}] = \frac{[E_0]}{1+K_{eq}} \cdot \left(1 - \frac{D}{A} \cdot \left(1 - \exp\left(-A \cdot t\right)\right) \right) \quad \text{via (6) and (104)} \qquad \textbf{(109.)}$$

$$[E_{inact}] = \frac{[E_0]}{1+1/K_{eq}} \cdot \left(1 - \frac{D}{A} \cdot \left(1 - \exp\left(-A \cdot t\right)\right) \right) \quad \text{via (7) and (104)} \qquad \textbf{(110.)}$$

[*X*] is defined above (104).

Appendix C Contents of Compact Disc

The contents of the supplementary compact disc included at the back of this thesis are listed below. **Bold** headings represent folder names.

C.1 Ashley Davys Easter MSc Thesis Waikato 2010

C.1.1 PyMol Session Files and Structures

PyMol (DeLano, 2002) .pse session files are given for the WT and mutant overlays from Section 1.3.3.2. High-resolution renderings of these files, as well as the overall barnase structures from Section 1.3.1 and Section 1.3.2, are also included.

C.1.2 MALDI-TOF MS Data and Settings

Raw data for the MS in this thesis (Section 3.2.1) is included, alongside the Bruker Daltonics Autoflex™ II settings files used for the work.

C.1.3 CD and DSC Raw Data and Fitting

The raw, worked-up and fitted data for the thermostability measurements summarised in Section 3.2.6 is given.

C.1.4 GpUp Worked-up Data and Fitting

The raw, worked-up and fitted data for the GpUp substrate is included alongside output statistics from fitting.exe.

C.1.5 FrG Worked-up Data and Fitting

As above, for the FrG substrate. Also has FittingTool files for the EM.

C.1.6 Alternative Models Data and Fitting

The data sets used in the fitting experiments are given, alongside MATLAB files used to perform the fitting. Results are also included.

C.1.7 Simulations of Alternative Models and Species

Interactive files used to simulate rate, product and species curves are included. Parameters may be changed to observe changes in plots. Files ending with ".gcx" require the program Grapher and may need the version included in Mac OS X 10.6.2 (Grapher version 2.1 (43), Apple Inc., USA).

Appendix D Sequencing Results

D.1 Sequence of pMT1002

The sequence of pMT1002 is shown below annotated. See Section 2.2.4.1.

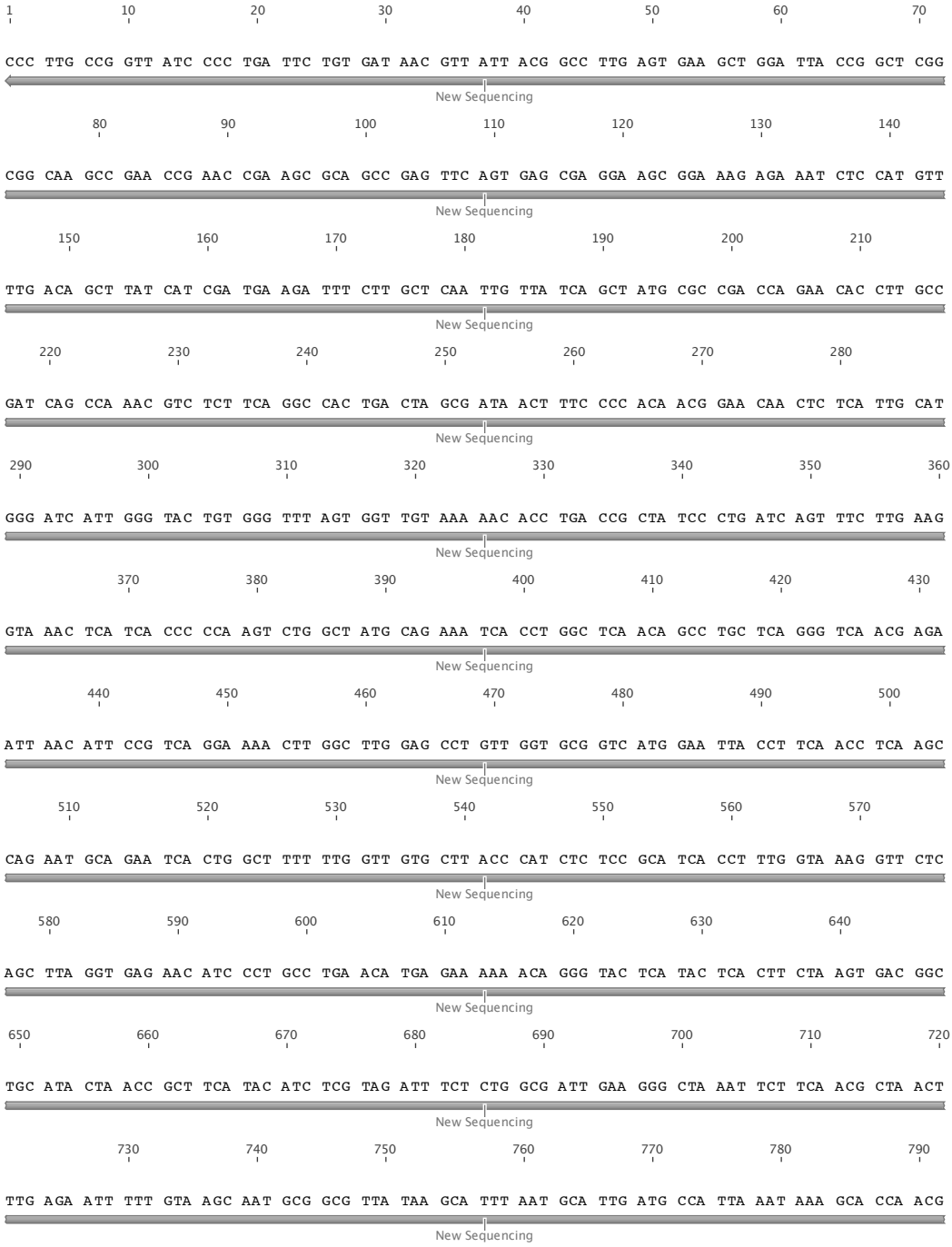


800 810 820 830 840 850 860
CCT GAC TGC CCC ATC CCC ATC TTG TCT GCG ACA GAT TCC TGG GAT AAG CCA AGT TCA TTT TTC TTT TTT TCA
New Sequencing
870 880 890 900 910 920 930
TAA ATT GCT TTA AGG CGA CGT GCG TCC TCA AGC TGC TCT TGT GTT AAT GGT TTC TTT TTT GTG CTC ATA CGT
New Sequencing
940 950 960 970 980 990 1,000
TAA ATC TAT CAC CGC AAG GGA TAA ATA TCT AAC ACC GTG CGT GTT GAC TAT TTT ACC TCT GGC GGT GAT AAT
New Sequencing
PR Promoter from Lambda Phage
RNA Polymerase Binding Site
1,010 1,020 1,030 1,040 1,050 1,060 1,070 1,080
Modified Addgene Sequence of pMT1002
GGT TGC ATG TAC TAA GGA GGT TGT ATG GAT CCG TGG AGA AAA TAA AGT GAA ACA AAG CAC TAT TGC ACT GGC
RNA Polymerase Binding Site
PR Promoter from Lambda Phage
New Sequencing
Forward Start Primer
1,090 1,100 1,110 1,120 1,130 1,140 1,150
Barnase
ACT CTT ACC GTT ACT GTT TAC CCC TGT GAC AAA AGC CGC ACA GGT TAT CAA CAC GTT TGA CGG GGT TGC GGA
Forward Start Primer
Modified Addgene Sequence of pMT1002
Reverse Start Primer
1,160 1,170 1,180 1,190 1,200 1,210 1,220
Barnase
TTA TCT TCA GAC ATA TCA TAA GCT ACC TGA TAA TTA CAT TAC AAA ATC AGA AGC ACA AGC CCT CGG CTG GGT
Reverse Start Primer
Modified Addgene Sequence of pMT1002
1,230 1,240 1,250 1,260 1,270 1,280 1,290
Barnase
GGC ATC AAA AGG GAA CCT TGC AGA CGT CGC TCC GGG GAA AAG CAT CGG CGG AGA CAT CTT CTC AAA CAG GGA
Modified Addgene Sequence of pMT1002
1,300 1,310 1,320 1,330 1,340 1,350 1,360
Barnase
AGG CAA ACT CCC GGG CAA AAG CGG ACG AAC ATG GCG TGA AGC GGA TAT TAA CTA TAC ATC AGG CTT CAG AAA
Modified Addgene Sequence of pMT1002
1,370 1,380 1,390 1,400 1,410 1,420 1,430 1,440
Barnase
TTC AGA CCG GAT TCT TTA CTC AAG CGA CTG GCT GAT TTA CAA AAC AAC GGA CCA TTA TCA GAC CTT TAC AAA
Modified Addgene Sequence of pMT1002
1,450 1,460 1,470 1,480 1,490 1,500 1,510
Barnase
AAT CAG ATA ACG AAA AAA ACG GCT TCC CTG CGG GAG GCC GTT TTT TTC AGC TTT ACA TAA AGT GTG TAA TAA
Modified Addgene Sequence of pMT1002
1,520 1,530 1,540 1,550 1,560 1,570 1,580
ATT TTT CTT CAA ACT CTG ATC GGT CAA TTT CAC TTT CCG GCT CTA GAG CTC TAG AGT CCG GTC CAA TCT GCA
Modified Addgene Sequence of pMT1002


1,590 1,600 1,610 1,620 1,630 1,640 1,650
GCC GTC CGA GAC AGG AGG ACA TCG TCC AGC TGA AAC CGG GGC AGA ATC CGG CCA TTT CTG AAG AGA AAA ATG
Modified Addgene Sequence of pMT1002
1,660 1,670 1,680 1,690 1,700 1,710 1,720
Barstar
GTA AAC TGA TAG AAT AAA ATC ATA AGA AAG GAG CCG CAC ATG AAA AAA GCA GTC ATT AAC GGG GAA CAA ATC
Modified Addgene Sequence of pMT1002
1,730 1,740 1,750 1,760 1,770 1,780 1,790 1,800
Barstar
AGA AGT ATC AGC GAC CTC CAC CAG ACA TTG AAA AAG GAG CTT GCC CTT CCG GAA TAC TAC GGT GAA AAC CTG
Modified Addgene Sequence of pMT1002
1,810 1,820 1,830 1,840 1,850 1,860 1,870
Barstar
GAC GCT TTA TGG GAT TGT CTG ACC GGA TGG GTG GAG TAC CCG CTC GTT TTG GAA TGG AGG CAG TTT GAA CAA
Modified Addgene Sequence of pMT1002
1,880 1,890 1,900 1,910 1,920 1,930 1,940
Barstar
AGC AAG CAG CTG ACT GAA AAT GGC GCC GAG AGT GTG CTT CAG GTT TTC CGT GAA GCG AAA GCG GAA GGC TGC
Forward End Primer
Modified Addgene Sequence of pMT1002
1,950 1,960 1,970 1,980 1,990 2,000 2,010
Barstar
GAC ATC ACC ATC ATA CTT TCT TAA TAC GAT CAA TGG GAG ATG AAC AAT ATG GAA ACA CAA ACC CGC AAG CTT
Reverse End Primer
Modified Addgene Sequence of pMT1002
New Sequencing
2,020 2,030 2,040 2,050 2,060 2,070 2,080
GCA TTG AAA AAG GAA GAG TAT GAG TAT TCA ACA TTT CCG TGT CGC CCT TAT TCC CTT TTT TGC GGC ATT TTG
New Sequencing
ß-lactamase Gene
2,090 2,100 2,110 2,120 2,130 2,140 2,150 2,160
CCT TCC TGT TTT TGC TCA CCC AGA AAC GCT GGT GAA AGT AAA AGA TGC TGA AGA TCA GTT GGG TGC ACG AGT
ß-lactamase Gene
New Sequencing
2,170 2,180 2,190 2,200 2,210 2,220 2,230
GGG TTA CAT CGA ACT GGA TCT CAA CAG CGG TAA GAT CCT TGA GAG TTT TCG CCC CAA AGA ACG TTT TCC AAT
ß-lactamase Gene
New Sequencing
2,240 2,250 2,260 2,270 2,280 2,290 2,300
GAT GAG CAC TTT TAA AGT TCT GCT ATG TGG CGC GGT ATT ATC CCG TAT TGA CGC CGG GCA AGA GCA ACT CGG
ß-lactamase Gene
New Sequencing
2,310 2,320 2,330 2,340 2,350 2,360 2,370
TCG CCG CAT ACA CTA TTC TCA GAA TGA CTT GGT TGA GTA CTC ACC AGT CAC AGA AAA GCA TCT TAC GGA TGG
ß-lactamase Gene
New Sequencing

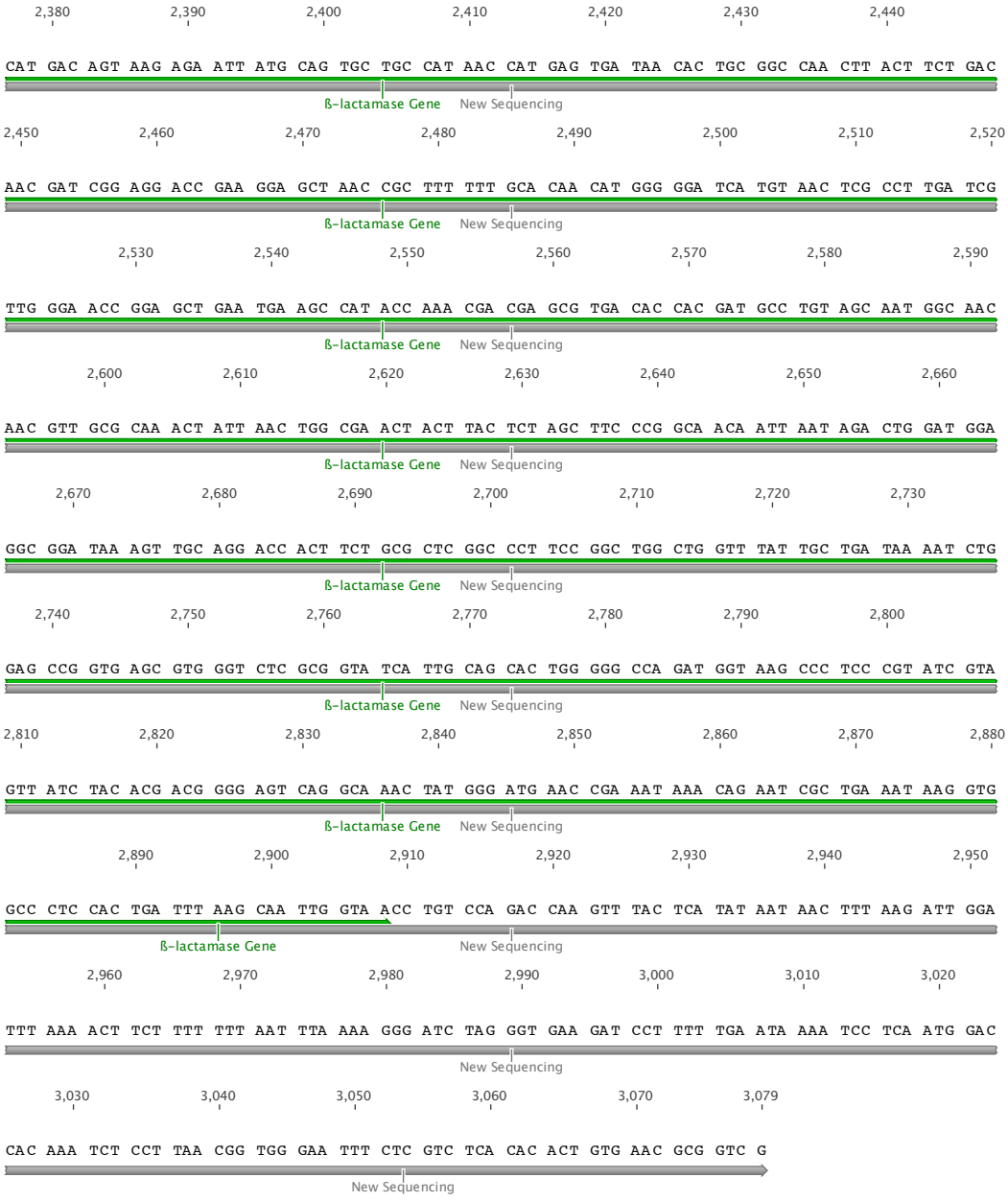

Figure D.1 – Sequence of pMT1002: Alignment of the modified Addgene sequencing (blue), additional new outward sequencing (grey), sequencing primers (brown) and other regions of interest (various)

Pr promoter is from λ phage (Okorokov et al., 1994) and is coloured in light green above. ß-lactamase is from *Citrobacter sp. CI157* and coloured in medium green.